559

Fermilab Library
0 1160 0038845 8

MIDWESTERN UNIVERSITIES RESEARCH ASSOCIATION

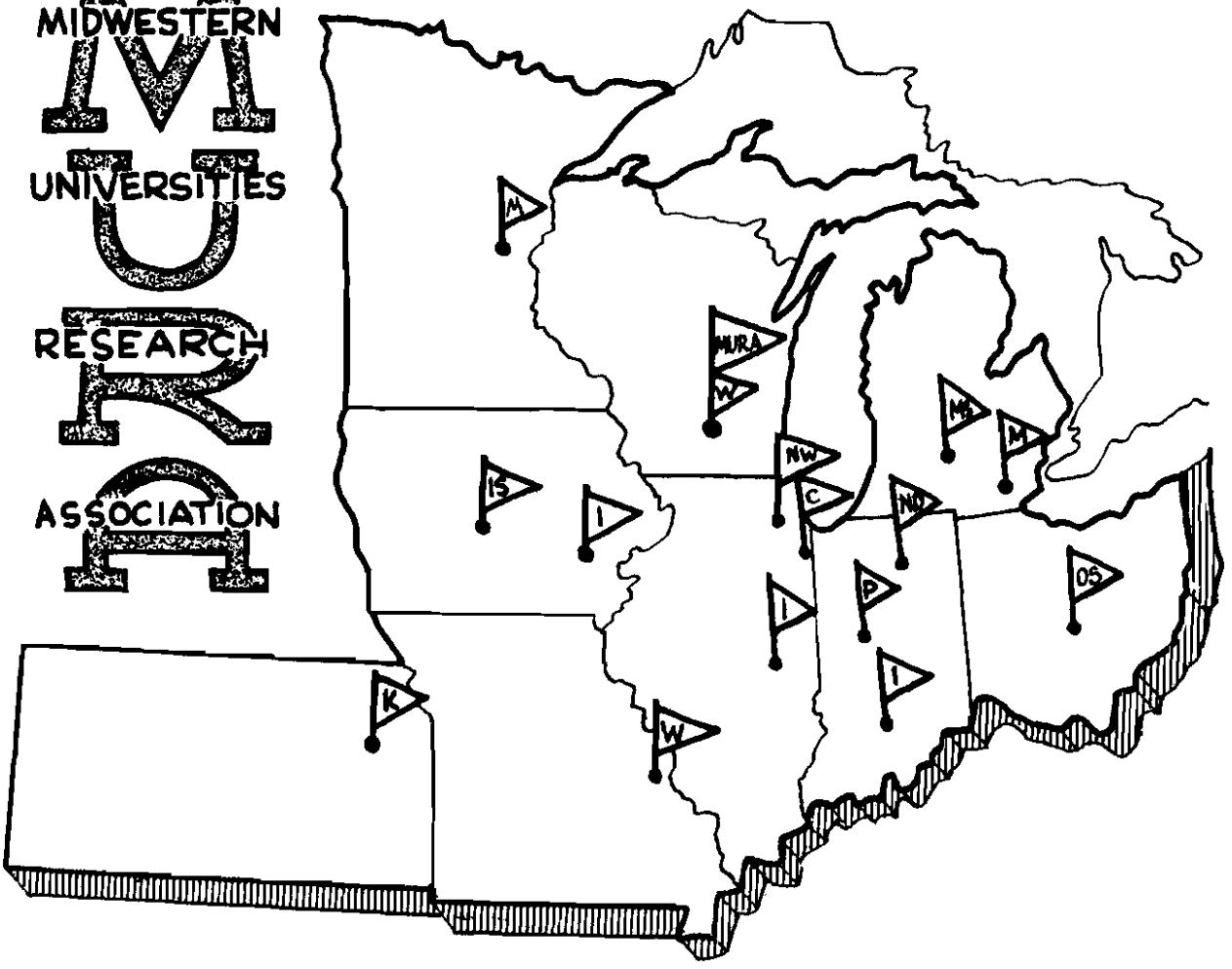

ELECTRON MODEL OF A SPIRAL SECTOR ACCELERATOR

D. W. Kerst, E. A. Day, H. J. Hausman, R. O. Haxby
L. J. Laslett, F. E. Mills, T. Ohkawa, F. L. Peterson, E. M. Rowe,
A. M. Sessler, J. N. Snyder, and W. A. Wallenmeyer

(To be submitted to The Review of Scientific Instruments)

REPORT **NUMBER** 559

Electron Model of a Spiral Sector Accelerator*

Short title: SPIRAL SECTOR ACCELERATOR

D. W. KERST[†], E. A. DAY[†], H. J. HAUSMAN[‡], R. O. HAXBY[§], L. J. LASLETT[‖], F. E. MILLS, T. OHKAWA[¶], F. L. PETERSON, E. M. ROWE, A. M. SESSLER[‡], J. N. SNYDER,** AND W. A. WALLENMEYER

Midwestern Universities Research Association, Madison, Wisconsin

---

*This work was supported by the U. S. Atomic Energy Commission, the National Science Foundation, and the Office of Naval Research.

[†] Present address: General Atomic Division of General Dynamics Corporation, San Diego, California.

[‡] The Ohio State University, Columbus, Ohio.

[§] On leave from Purdue University, Lafayette, Indiana.

[‖] Iowa State University, Ames, Iowa.

[¶] On leave from the University of Tokyo, Tokyo, Japan.

**University of Illinois, Urbana, Illinois

ABSTRACT

A six-sector spiral ridge FFAG accelerator has been constructed and successfully operated to accelerate electrons from 35 to 180 kev kinetic energy Acceleration was by betatron action, supplemented by radio-frequency acceleration when desired The design was based on magnetostatic and orbit computations performed with the Illiac digital computer, and the subsequent performance was found to be in good accord with these computations Tuning coils permitted variation of the basic parameters about the design values suggested by the computations, so that an experimental investigation could be made concerning the importance of near-by resonances. The theoretical basis of the computational work and the specific results obtained are first described, followed by a résumé of the constructional features and magnetostatic measurements. Tests with the operating model are then reported, comprising a resonance survey, injection studies, perturbation studies, and the use of radio-frequency acceleration The frequencies of radial and axial betatron oscillation at the nominal operating point were respectively $\nu_x = 1.40$ and $\nu_y = 1.12$, and the resonance survey indicated this operating point to be centrally located within a region of relatively large intensity which was bounded by the resonances $\nu_y = 1.0$, $\nu_x = 1.5$, and (less markedly) $2\nu_y - \nu_x = 1$. Injection from a deflector-structure with a thin septum permitted efficient injection to be achieved either by concomitant rapid acceleration of the injected electrons or,

alternatively, by use of a time-dependent radial electric field applied as a perturbation. Experiments with a protracted injection pulse permitted the observation of phenomena attributable to space-charge effects. A suitable frequency-modulation schedule permitted successful acceleration of a substantial fraction of stacked electrons through the transition energy. Appendices describe a modulator, with negative-feedback stabilization, to permit protracted injection; a magnetometer, used in the magnetic-field measurements; and the essentials of Parzen's theory of perturbations, which was found to account satisfactorily for the results of the perturbation experiments.

TABLE OF CONTENTS

ABSTRACT ii

I. INTRODUCTION 1

II. THEORY 6

A. The Potential Problem 7
B. The Dynamics Program 10
C. Computational Results 12

III. CONSTRUCTION 20

A. Magnets 20
B. Vacuum Chamber and Detectors 22
C. Accelerating System 25
D. Injector 27

IV. MEASUREMENT AND CORRECTION OF THE MAGNETIC FIELD 29

V. RESONANCE SURVEY AND STABILITY LIMITS 33

A. Method Employed in Resonance Survey 33
B. Results 35
C. Discussion 36
D. Stability Limits 38
E. The Resonance $\nu_x = 2\ \nu_y$ 40

VI. INJECTION METHODS 42

A. General Considerations 42
B. Methods Employed with Short-Pulse Injection 44
C. Long-Pulse Injection 46

VII. PERTURBATION STUDIES 51

A. General Description 51
B. Results of Perturbations at the Design Point 52
C. Results near the $\nu_x = 2\ \nu_y$ Resonance 55

VIII. STUDIES OF RADIO-FREQUENCY ACCELERATION 57

A. General Discussion 57
B. Experimental 59

IX. ACKNOWLEDGEMENTS 62

APPENDIX I. DESIGN OF THE LONG-PULSE INJECTOR 64

APPENDIX II. THE MAGNETOMETERS 71

APPENDIX III. PERTURBATION THEORY (by George Parzen) 75

CAPTIONS FOR FIGURES

FIG. 1. Overall view of the spiral sector model

FIG. 2. Resonance diagram for $N = 6$ Three possible operating points, for which detailed computations were made, are indicated by the letters A, B, and C

FIG 3 Cross section of magnet pole in the ξ η -plane, for operating point C. The pole contour is periodic in the variable ξ, with period 1. Azimuthal distances at constant radius are given by $2\pi r/N$ times the increment of ξ and axial distances by $2\pi r\left[(1/w)^2 + N^2\right]^{-1/2}$ times the increment of η. For the present structure $1/w = 6.25$ and these distances become $1.0472\, r\Delta\xi$ and $0.7252\, r\Delta\eta$, respectively

FIG. 4. Phase plot of limiting-amplitude stable radial motion obtained from computer results pertaining to $N\theta = 0$ (mod. 2π). The stable fixed point is designated by F P. and the four unstable fixed points by $\times$.

FIG 5. Matrix elements characterizing propagation of small-amplitude radial oscillations through one sector of the model, as a function of the starting point within the sector

FIG. 6. The parameter β_x for propagation of small-amplitude radial oscillations through one sector of the model.

FIG 7 Matrix elements characterizing propagation of small-amplitude axial oscillations through one sector of the model, as a function of the starting point within the sector

FIG. 8. The parameter β_y for propagation of small-amplitude axial oscillations through one sector of the model.

FIG. 9. Schematic drawing of one magnet sector.

FIG. 10. Exploded view, showing one of the main magnet coils above a magnet pole. The yoke, magnet pole, pole-face windings, and flutter-tuning coils are respectively denoted by a, b, c, and d.

FIG. 11. Exploded view of vacuum chamber. The current probe, scintillation detector, two vertical-scanning probes, plates for r-f excitation of betatron oscillations, and the ionization gauge are shown schematically at a, b, c, d, and e.

FIG. 12. Betatron core and excitation windings.

FIG. 13. Circuit and waveforms for pulsed excitation of betatron core.

FIG. 14. Block diagram of rf system.

FIG. 15. Injector assembly, with deflector. The cathode, shield, injector housing, deflector electrode, grounded septum, spherical bearing surface, and a typical equilibrium orbit are respectively shown at A, B, C, D, E, F, and G.

FIG. 16. Diagram of the null-reading flip coil arrangement used to determine the field-gradient index of the magnets.

FIG. 17. Beam intensity as a function of the flutter-tuning current, with no current in the k-tuning coils. The values of ν_x and ν_y, as measured by radio-frequency excitation of the betatron oscillations, are indicated above the curve. Points where certain resonances were crossed are also indicated.

FIG. 18. Beam intensity as determined in the resonance survey of the spiral sector model.

FIG. 19. Measured values of the revolution frequency and the betatron oscillation frequencies as a function of radius, without tuning currents. If the scaling condition were satisfied exactly, the oscillation frequencies ν_x and ν_y would be independent of radius.

FIG. 20. Measured variation of betatron oscillation frequencies with amplitude, without tuning currents.

FIG. 21. Semi-logarithmic plot illustrating growth of the amplitude of axial oscillations for operation near the $\nu_x = 2\ \nu_y$ resonance, as obtained by digital computation with $\nu_x = 1.25$ and $\nu_y = 0.62$. The number appended to each individual curve denotes the initial radial displacement for that run. Y_t denotes the semi-aperture of the vacuum chamber at the injection radius.

FIG. 22. Observed apparent radial stability limits as a function of the limitations imposed on the axial motion, for operation near the $\nu_x = 2\ \nu_y$ resonance with $\nu_x \cong 1.46$. The number appended to each individual curve denotes the value of $2\ \nu_y - \nu_x$ for that curve.

FIG. 23. Perturbation of the equilibrium orbit by an azimuthally-localized radial electric field, illustrated for $\nu_x = 1.40$ with the unperturbed equilibrium orbit drawn as a straight line and ignoring the scalloping which arises from the alternating gradient structure. Insert: Cross-sectional shape of electrode, intended to produce a region of substantially-constant field.

FIG. 24. Oscillograms to illustrate phenomena observed with long-pulse injection: (a) betatron voltage; (b) injector voltage; (c) beam current to target when the injector is operated at low emission; and (d) beam current at high emission, showing effects attributable to space-charge and positive-ion neutralization.

FIG. 25. Sketch depicting the essential features of the beam current observed at high emission, as obtained from the oscillogram of Fig. 24(d).

FIG. 26. Effect of perturbations on the equilibrium orbit: (a) radial displacement of the equilibrium orbit as a result of a 7% field reduction in one magnet sector; (b) radial displacement of the equilibrium orbit as a result of raising the field-index, k, from 0.7 to 0.8 in one sector, the effect being regarded as chiefly attributable to the 3.5% increase of field at the detection radius of the perturbed sector; (c) axial displacement of the equilibrium orbit as a result of raising one magnet sector 1 mm; and (d) radial displacement of the equilibrium orbit as a result of rotating one sector approximately 1 deg about its front pin, the effect being regarded as chiefly the result of the accompanying 2 - 2.5% increase of field at any given radius within the perturbed sector. The solid lines represent computational results, the dashed lines are based on the perturbation theory summarized in Appendix III, and the circles connected by a dotted line in (d) are the observed displacements.

FIG. 27. Electron energy, E, and revolution frequency f, vs. radius. E_t and f_t denote, respectively, the transition energy and the associated revolution frequency.

FIG. 28. The parameter α_1, to which the bucket area is proportional, vs. the parameter η of the Symon-Sessler theory.[20]

FIG. 29. Regions of W, ϕ phase space, showing typical phase-stable areas, or "buckets", (a) above and (b) below the transition energy. The shaded areas represent the buckets and the curves indicate possible particle trajectories in W, ϕ space.

FIG. 30. Particle energy and orbit radius vs. time for three acceleration programs.

FIG. 31. Oscillograms of (α) the beam received at the detector, (β) the betatron voltage, and (γ) the envelope of the rf voltage in experiments designed to investigate acceleration through the transition energy. The first pair of traces (a) correspond to curve A of Fig. 30, for which no rf acceleration is employed. Traces (b) correspond to curve B, with rf acceleration up to the transition energy. In (c), corresponding to curve C, some of the stacked beam is seen to have been successfully accelerated through the transition energy. In this figure one horizontal division corresponds to 200 μsec and, on the lower member of each pair, one vertical division represents 5 v.

FIG. 32. Frequency of rf oscillator vs. time for three acceleration programs leading to different efficiencies for traversal of the transition energy. The efficiencies for curves A, B, and C were measured as 10, 50, and 10%, respectively.

FIG. 33. Schematic circuit of the output stage for the long-pulse amplifier.

FIG. 34. Amplifier circuit for the long-pulse modulator.

FIG. 35. Schematic diagram illustrating the principle of the magnetometers.

FIG. 36. Construction of the magnetometer transformer, containing a Mo permalloy core.

FIG. 37. Magnetometer arrangement employing a quadrupole coil to permit operation in strong magnetic fields.

FIG. 38. Magnetometer, with stabilized oscillator-amplifier, for measurement of weak magnetic fields.

I. INTRODUCTION

In fixed field alternating gradient (FFAG) accelerators[1, 2] particles

[1]Symon, Kerst, Jones, Laslett, and Terwilliger, Phys. Rev. 103, 1837 (1956).

[2]L. Jackson Laslett, Science 124, 781 (1956).

with a large range of momenta can be simultaneously accommodated within an annular magnet of limited radial extent, thus permitting a desirable flexibility in the methods of accelerating the particles and affording the promise of high beam intensities. The nature and general theory of FFAG accelerators have been described previously[1, 2] and the operation of a radial sector electron model reported.[3] The spiral sector type is an attractive

[3]Cole, Haxby, Jones, Pruett, and Terwilliger, Rev. Sci. Instr. 28, 403 (1957).

alternative form of a FFAG accelerator, since smaller circumference factors may be utilized than appear feasible with the radial sector type and a significant economy may thus be achieved in the magnet design. Non-linear features of the orbit dynamics, on the other hand, would be expected to be materially more prominent than for a comparable radial sector accelerator. The present article describes the design, construction, and operation of a model FFAG electron accelerator employing spiral sectors,[4] which was constructed to provide an empirical

[4]Preliminary accounts of this model have been given in the following references: (a) D. W. Kerst, et al., Rev. Sci. Instr. 28, 970 (1957);

(b) Laslett, Sessler, and Snyder, Bull. Amer. Phys. Soc. (II) 2, 337 (1957); (c) H. J. Hausman, et al., Bull. Amer. Phys. Soc. (II) 2, 337 (1957); (d) R. O. Haxby, et al., Bull. Amer. Phys. Soc. (II) 2, 337 (1957); (e) D. W. Kerst and F. E. Mills, Bull. Amer. Phys. Soc. (II) 2, 337 (1957); (f) Stump, Waldman, and Wallenmeyer, Bull. Amer. Phys. Soc. (II) 2, 337 (1957); (g) F. L. Peterson and W. A. Wallenmeyer, Bull. Amer. Phys. Soc. (II) 3, 168 (1958); (h) F. E. Mills and D. S. Roiseland, Bull. Amer. Phys. Soc. (II) 3, 168 (1958); (i) F. L. Peterson, Bull. Amer. Phys. Soc. (II) 3, 331 (1958); and (j) R. O. Haxby, et al., Experience with a Spiral Sector FFAG Electron Accelerator, Proceedings of the CERN Conference on High Energy Accelerators and Instrumentation (European Organization for Nuclear Research, Geneva, 1959).

---

test of theoretical predictions, to contribute further evidence of orbit stability over intervals longer than could be examined computationally or under conditions in which multi-particle effects are important, and to permit the acquisition of experience with various acceleration methods possible in accelerators of this type.

As in other FFAG designs the magnet was such as to provide a field whose average value varies with radius as r^k, and use of logarithmically spiralled poles permitted possible orbits of particles with different energies, or momenta, to be geometrically similar. A separated sector design,[2] employing separate spiral magnets, was used in the interests of simplifying construction. More significantly, a field with a large

azimuthal variation was thereby obtained, in an aperture not excessively limited, and larger stability limits could be expected. The flutter, or azimuthal variation of the field, was further enhanced by the use of guard edges or "ears", of zero magnetostatic potential, at the edges of the spiral sectors.[††] Initially the model was operated with betatron acceler-

---

[††] In addition to effecting a more rapid decrease of the magnetic field at the edges of each sector, the ears provide additional shielding from the magnetic field of the earth, which is not entirely negligible in comparison to the rather low field strengths employed in the electron model. The influence of the earth's field was further reduced by use of large compensation coils surrounding the accelerator, similar to Helmholtz pairs, and with a hexagonal shape employed for the pair intended to neutralize the vertical component.

---

ation, although in later work fairly extensive tests of radio-frequency acceleration methods were undertaken.

The design of the spiral sector model was based, as discussed in Sec. II, on computations performed with the electronic digital computer of the Graduate College of the University of Illinois (Illiac), corroborated and supplemented later by some computations with an IBM-704 computer in the MURA Laboratory at Madison. Constructional work was begun in the Physics Research Laboratory of the University of Illinois and completed in Madison, where magnetic field tests were made, the model put into operation, and a beam immediately obtained.

With the number of sectors (N) selected as 6, in the interests of a conservative design which would permit avoiding an excessive number of resonances, the remaining basic parameters characterizing the model were selected by digital computations pertaining to the magnetostatic problem and to the orbit dynamics in the resultant magnetic field. The computational work included study of the effect of misalignments and the values finally recommended for the basic parameters were taken as central design values about which adjustments could later be made to determine empirically the effect of possible harmful resonances.

The inner radius of the accelerator was determined by the need to accommodate the betatron core and for convenience of access to various ancillary components, while the associated injection energy (≅ 35 Kev) was dictated by the specifications of the injector, which was originally planned to be of the type used in the University of Illinois 80 Mev betatron.[5] From the field strength thus found to be appropriate at the inner

---

[5] D. W. Kerst, et al., Rev. Sci. Instr. 21, 462 (1950), esp. Fig. 12.

---

radius, and from the value of the field-index k suggested by the digital computations, the maximum radius obtainable with readily available forgings of Armco iron thus determined the maximum energy which could be attained in the model (≅ 180 Kev). With the dimensions selected in this way the model permitted study of beam behavior in the neighborhood of the transition energy (155 Kev), which was reached by particles moving in orbits situated an adequate distance within the outer wall of the vacuum chamber.

Figure 1 presents a general view of the accelerator. In the following sections we review the theoretical and computational design studies, summarize the constructional features and test program, and report the results of experiments made with the operating model to determine the effects of resonances and the characteristics of various acceleration methods.

II. THEORY

The general theory of fixed field accelerators, as well as that specific to the spiral sector design, has been discussed extensively elsewhere.[1, 2] Many of the approximate analytic techniques which have been developed[6] were of great value in the preliminary theoretical de-

---

[6]The linear orbit equations may be approximated by aid of the "smooth approximation" (see reference 1, p. 1842) or by use of tabulated solutions to a Hill's equation (see reference 1, footnote 9). Results for the non-linear orbit equations may be approximated by techniques developed independently by a number of workers [see, for example, L. J. Laslett and A. M. Sessler, Midwestern Universities Research Association report MURA-263 (1957, unpublished)].

---

sign studies. This work, however, is not essentially unique, whereas the methods used to design this model are distinct from those used to design any other particle accelerator in that, to the best of our knowledge, this is the first time that a digital computer was used to determine completely the essential parameters of an accelerator by computation of the performance which would result from various choices of magnet design.

There were two digital computer programs which were essential to the design of the model. The first program started with any chosen magnet contour (provided only that the pole "scales"[1, 2]) and calculated the magnetostatic potential at all points in the region between the poles. The second program constituted a <u>dynamics</u> program, as differentiated

from the aforementioned potential program, and served to calculate the trajectory of a monoenergetic particle in the fields resulting from the solution to the potential problem. In effect, by use of these programs, it was possible by digital computation to construct a large number of poles and study in detail the resulting magnetic fields or, more generally, to construct a large number of accelerators and study the consequent particle dynamics. It cannot be overemphasized that this is an essentially exact procedure, save for possible long-range dynamical instabilities which would not be exhibited in digital computer runs corresponding to particle trajectories carried through a few hundred revolutions or for possible many-particle effects such as the limitations due to space charge. Thus, provided the accelerator was assembled according to the specifications and tolerances obtained from the computer, there could be no real doubt that the accelerator would operate successfully.

The remainder of this section is devoted to a description of the digital computer programs mentioned above and to the various calculations which were performed in order to determine a suitable set of design parameters.

A. The Potential Problem

Fixed field accelerators must be designed so that the betatron oscillation frequencies are substantially independent of radius. This may be accomplished most directly by having the orbits and the fields themselves simply scaled replicas, possibly rotated, of the orbits and fields at any other radius. In the case that such scaling is maintained,

it is clear that the fields throughout the entire gap can be characterized by the fields on a two-dimensional surface (for example on a cylinder). Limiting our attention then to scaling fields, we can reduce a three-dimensional potential problem to a two-dimensional problem--namely to a problem which is quite tractable with present high-speed digital computers.

The median-plane field $[H_r(r, \phi, 0) = H_\phi(r, \phi, 0) = 0]$ in a spiral sector, scaling accelerator can be written

$$H_z(r, \phi, 0) = - H_o \left(\frac{r}{r_o}\right)^k F\left(\frac{1}{w} \ln \frac{r}{r_o} - N\phi\right), \tag{1}$$

where r is the radial coordinate, ϕ is the azimuthal angle, and F is a periodic function (period 2π) of average value unity. The constant H_o denotes the average magnetic field at the reference radius r_o. The parameter k represents the field index, the number of sectors is N, and the spiral ridge makes an angle $\xi = \cot^{-1}(Nw)$ with a radius vector.

From Eq. (1) the magnetic scalar potential V may be written as

$$V = \left(\frac{r}{r_o}\right)^{k+1} G\left(\frac{1}{w} \ln \frac{r}{r_o} - N\phi, \frac{z}{r}\right), \tag{2}$$

where G is a periodic function (of period 2π) with respect to its first argument, r is the radial coordinate in a cylindrical coordinate system, and z is the vertical coordinate. If we define a new function by the equation

$$\Omega(\xi, \eta) = \frac{V}{H_o r_o (r/r_o)^{k+1}} \tag{3}$$

where

$$\xi = \frac{1}{2\pi}\left[\frac{1}{w} \ln \frac{r}{r_o} - N\phi\right] \tag{4a}$$

$$\eta = \frac{\left[(1/w)^2 + N^2\right]^{1/2}}{2\pi} \frac{z}{r}, \tag{4b}$$

$\Omega(\xi,\eta)$ is periodic with the period unity with respect to ξ and it becomes evident that the fields can be expressed in terms of the two variables ξ and η.

In terms of the function $\Omega(\xi,\eta)$, Laplace's equation in three dimensions reduces to the following partial differential equation with two independent variables:

$$\frac{\partial^2\Omega}{\partial\xi^2} + \left[1 + \frac{4\pi^2\eta^2}{(1/w)^2 + N^2}\right]\frac{\partial^2\Omega}{\partial\eta^2} - \frac{4\pi(1/w)}{(1/w)^2 + N^2}\,\eta\,\frac{\partial^2\Omega}{\partial\xi\,\partial\eta}$$

$$+ \frac{4\pi(k+1)/w}{(1/w)^2 + N^2}\frac{\partial\Omega}{\partial\xi} - \frac{4\pi^2(2k+1)}{(1/w)^2 + N^2}\,\eta\,\frac{\partial\Omega}{\partial\eta} + \frac{4\pi^2(k+1)^2}{(1/w)^2 + N^2}\,\Omega = 0, \quad (5)$$

in which Ω is an odd function of η, vanishing at $\eta = 0$, and is periodic in ξ with the period unity. The potential problem was accordingly solved with the Illiac digital computer through application of a relaxation method to Eq. (5), the input data being the parameters k, 1/w, N, and the values of Ω on a boundary curve.[7] For a typical

---

[7]A more complete description of this computational method is given by L. J. Laslett, Midwestern Universities Research Association report MURA-99 (1956, unpublished). The nature of a more elaborate program, subsequently prepared for an IBM-704 computer, is summarized by L. J. Laslett, Midwestern Universities Research Association report MURA-221 (1957, unpublished). The technical difficulties of constructing an efficient relaxation program which would fit the capacities of the Illiac were by no means trivial, but are not discussed here.

---

problem, the computation time required to obtain Ω with sufficient accuracy for studies of particle dynamics was of the order of one or two hours.

B. The Dynamics Program

The solution of the potential problem, Ω (or strictly Ω/η), was stored in the fast memory of the Illiac computer as $\frac{1}{2}$ - words so that a mesh of up to 2000 points was available. The fields which enter into the differential orbit equations were computed from these stored values by differentiation-interpolation[7] as needed during the course of the integration of the dynamical equations. The field components are given by

$$H_z = -\frac{H_o}{r_o}\,\frac{\left[(1/w)^2 + N^2\right]^{1/2}}{2\pi}\left(\frac{r}{r_o}\right)^k\left[\frac{\Omega}{\eta} + \eta\frac{\partial}{\partial\eta}\left(\frac{\Omega}{\eta}\right)\right] \tag{6a}$$

$$H_r = -\frac{H_o}{r_o}\left(\frac{r}{r_o}\right)^k\left[k\left(\frac{\Omega}{\eta}\right) + \frac{1}{2\pi w}\frac{\partial}{\partial\xi}\left(\frac{\Omega}{\eta}\right) - \eta\frac{\partial}{\partial\eta}\left(\frac{\Omega}{\eta}\right)\right] \tag{6b}$$

$$H_\phi = \frac{H_o}{r_o}\,\frac{N}{2\pi}\left(\frac{r}{r_o}\right)^k\eta\frac{\partial}{\partial\xi}\left(\frac{\Omega}{\eta}\right), \tag{6c}$$

and the dynamical equations, employing these field components, are

$$dx/d\phi = (1 + x)\,p_x\,(1 - p_x^2 - p_y^2)^{-\frac{1}{2}} \tag{7a}$$

$$dy/d\phi = (1 + x)\,p_y\,(1 - p_x^2 - p_y^2)^{-\frac{1}{2}} \tag{7b}$$

$$dp_x/d\phi = (1 - p_x^2 - p_y^2)^{-\frac{1}{2}} + \frac{1}{H_o}(1 + x)\left[H_z - p_y(1 - p_x^2 - p_y^2)^{-\frac{1}{2}}H_\phi\right] \tag{7c}$$

$$dp_y/d\phi = \frac{1}{H_o}(1 + x)\left[p_x\,(1 - p_x^2 - p_y^2)^{-\frac{1}{2}}H_\phi - H_r\right] \tag{7d}$$

in terms of the dependent variables $y \equiv z/r_o$ and $x \equiv (r - r_o)/r_o$.[8]

---

[8] Actually the program worked with the variables S and T, rather than x and y, where $S \equiv \ln(1 + x)$ and $T \equiv y/(1 + x)$. This procedure avoided the use of a logarithm routine in the computational program and thus provided memory capacity for a more detailed representation of

the field For details concerning this feature, the interpolation and differentiation algorisms (which are constructed to provide field components which were continuous from one cell of the mesh to another), and for other details of the computational method see L. J. Laslett, Midwestern Universities Research Association report MURA-99 (1956, unpublished). A description of a similar program subsequently written for an IBM-704 computer is given by L. J. Laslett, Midwestern Universities Research Association report MURA-222 (1957, unpublished).

In order to study the effects of misalignments and field imperfections for the purpose of obtaining tolerances for construction of the model, the dynamics program was arranged so that certain simple algebraic transformations could be inserted periodically. Such transformations, which are called "bumps", were of the following types:

(1) Axially-displaced sector bump. At the entrance to some chosen sector the following transformation was introduced to relate the initial values (x_i, etc.) of the orbit variables to the values (x_f, etc.) which result from application of the transformation.

$$\begin{aligned} x_f &= x_i & y_f &= y_i - \Delta y \\ p_{xf} &= p_{xi} & p_{yf} &= p_{yi} \end{aligned} \tag{8}$$

The program then proceeded with the integration until the end of the sector, at which point the transformation

$$\begin{aligned} x_f &= x_i & y_f &= y_i + \Delta y \\ p_{xf} &= p_{xi} & p_{yf} &= p_{yi} \end{aligned} \tag{9}$$

was introduced. This same bump was then used repetitively on each revolution.

(2) Radially-displaced sector bump. The transformation used to simulate a radially displaced sector was identical to that used for a vertical displacement, except that the displacement was made in the x coordinate rather than in y.

(3) Rotated sector bump. At the entrance to a chosen sector the transformation

$$\begin{aligned} x_f &= x_i - \frac{\pi}{N}(\Delta\theta) & y_f &= y_i \\ p_{xf} &= p_{xi} + \Delta\theta & p_{yf} &= p_{yi} \end{aligned} \tag{10}$$

was made. The transformation was then followed, at the end of the sector, by

$$\begin{aligned} x_f &= x_i - \frac{\pi}{N}(\Delta\theta) & y_f &= y_i \\ p_{xf} &= p_{xi} - \Delta\theta & p_{yf} &= p_{yi} \end{aligned} \tag{11}$$

As with the other bumps, this series of transformations was repeated on each revolution of the particle.

C. Computational Results

Figure 2 depicts the operating region of interest, in terms of the quantities $\sigma_x/\pi = 2\,\nu_x/N$ and $\sigma_y/\pi = 2\,\nu_y/N$, where ν_x and ν_y denote the number of radial or axial betatron oscillations per revolution. The important intrinsic resonances have been indicated on Fig. 2, as well as imperfection resonances through third order. On the basis of linear theory, and guided by the theory of imperfections for the linear problem,[1, 3, 6] three possible operating points were selected for detailed study. For each of these operating points, indicated on Fig. 2 by the letters A, B, and C, a realistic pole profile and gap were selected and suitable values of the parameters k and 1/w determined

computationally to give the desired frequencies for small-amplitude betatron oscillations. In Table I we list the parameters which correspond to the three operating points and in Fig. 3 we show a cross section,

TABLE I. Parameters for the three operating points studied computationally.

Parameter	Point A	Point B	Point C
k	1.62	1.65	0.70
1/w	6.65	6.00	6.25
N	6	6	6
$f_{eff.}$ [a]	1.083	1.085	1.087
σ_x	0.597π	0.595π	0.466π
σ_y	0.225π	0.129π	0.375π
ν_x	1.791	1.785	1.398
ν_y	0.675	0.387	1.125

[a] $f_{eff.}$ denotes the effective flutter, defined as

$$f_{eff.} = \left[2\left(\langle H^2\rangle - \langle H\rangle^2\right)/\langle H\rangle^2\right]^{\frac{1}{2}}$$

$$= \left[2\left\langle (H - \langle H\rangle)^2\right\rangle / \langle H\rangle^2\right]^{\frac{1}{2}} .$$

in the ξ, η -plane, of the pole shape used for point C. It may be noted that a pole profile, depicted in this way in the ξ, η -plane, represents a section taken at constant r, but with unequal scale factors in the azimuthal and axial directions. The outline represents more truly a cross section perpendicular to the spiral, save that the general increase of all linear dimensions with radius is not depicted.

The results of a computational study of orbit dynamics for the three operating points are summarized in Table II, wherein we include some refined estimates of radial stability limits determined with the MURA IBM-704 in Madison To insure that the computations would not ignore the possibility of strong coupling, between radial and axial motion at certain operating points, the Illiac searches for radial stability limits were made with a small initial axial displacement ($y_o = 10^{-5}$) in cases which otherwise would have been entirely free of axial motion, and likewise, the subsequent IBM-704 studies of radial motion included searches made with an initial axial displacement which was about 12% of the corresponding axial stability limit. Despite the relatively short duration of the individual computer runs for the estimation of stability limits, the introduction of this modest amount of initial axial motion led to substantially reduced, but it is believed more realistic, radial limits for operation at points A and B. For point C, however, the radial stability limits were found to be substantially independent of the presence of such axial motion. Although the data of Table II may be subject to some sampling errors, a significant trend seems unmistakable which served as a helpful guide in selection of a suitable operating point for the model.

The radial stability limits for point A appeared undesirably low when even small amounts of axial motion were present This result, attributed to proximity to the $\nu_x = 2\ \nu_y$ resonance, motivated the investigation of point B, situated somewhat further from this coupling

TABLE II. Summary of the dynamics studies for the three operating points A, B, and C. The numbers in the body of the table give the magnitudes of the limiting amplitudes, for the free betatron oscillations, in units of the radius. Save where otherwise indicated, the amplitudes refer to the center of a radially-focusing region. The threshold for y-growth denotes the amplitude of radial oscillation above which coupling results in a marked (exponential) increase in the amplitude of initially-small axial oscillations. Approximate magnitudes of the various sector displacements are given in mm for a nominal radius of 30 cm.

Perturbation	Length of Individual Run	Point A Radial Ampl.[a]	Point A Axial Ampl.	Point B Radial Ampl.[a]	Point B Axial Ampl.	Point C Radial Ampl.[a]	Point C Axial Ampl.
Unperturbed							
	30 sectors	0.088[b]		0.117[b]		0.106[b]	
		0.028[c]		0.052[c]		0.106[c]	
	80 sectors		0.029		0.033		0.036
	Max. ampl., stable[d]		0.073		0.072		0.075
Threshold							
	90 sectors, growth	0.032		0.049		0.092	
	no growth	0.027		0.031		0.074	
Axially Displaced Sector							
$\Delta y = 0.00351$ ($\Delta z \cong 1$ mm)	90 sectors	0.019[c]	0.029	0.036[c]	0.033	0.099[b,c]	0.040
$\Delta y = 0.00702$ ($\Delta z \cong 2$ mm)		0.019[c]	0.028	0.030[c]	0.035	0.077[b,c]	0.033
Radially Displaced Sector							
$\Delta x = 0.00351$ ($\Delta r \cong 1$ mm)	90 sectors	0.026[c]	0.025	0.037[c]	0.032	0.100[b,c]	0.036
$\Delta x = 0.00702$ ($\Delta r \cong 2$ mm)		0.023[c]	0.020	0.034[c]	0.029	0.097[b,c]	0.036
Rotated Sector							
$\Delta\theta = 0.0015$	90 sectors, unstable	0.032[c]	0.032	0.060[c]	0.034	0.126[b,c]	0.039
	stable	0.023[c]	0.029	0.042[c]	0.030	0.100[b,c]	0.034
$\Delta\theta = 0.0060$	unstable	0.036[c]	0.027	0.065[c]	0.030	0.104[b,c]	0.044
	stable	0.023[c]	0.025	0.046[c]	0.028	0.078[b,c]	0.039

[a]Amplitude to left of stable fixed point when p_x has the value corresponding to the fixed point.
[b]With no axial amplitude present.
[c]With a small amount of axial amplitude introduced initially.
[d]Amplitude at center of axially-focusing region.

resonance. As is seen from Table II, the stability limits, although significantly greater than for point A, were still rather small and, in view of the low value of ν_y associated with point B, the useable volume of phase space was again regarded as undesirably small.

Attention was therefore finally directed to point C, lying a considerable distance above the $\nu_x = 2\ \nu_y$ resonance. Here the stability region was found to be materially greater than for points A and B, and the axial oscillation frequency was also comparatively large. Most important, moreover, coupling effects were no longer apparent and the sensitivity to misalignments did not appear to be pronounced.

On the basis of the Illiac computations included in Table II, which incidentally were obtained with a total of approximately 200 hours of computer time,[9] it accordingly was decided to proceed with the construction of the model at operating point C. It was, of course, planned to be able to tune the model, but the central design parameters

---

[9]This estimate does not include code checking, various simplified problems which were studied to test the programs, or checks of internal consistency used to confirm that the results were substantially independent of mesh size. Some tests of the effect of mesh size are described in reference 10.

were taken as those associated with point C. It is encouraging to note that the subsequent performance of the model, reported in Sec. V, indicated that point C fell within a region of maximum beam intensity.

Following initiation of construction of the model, further digital computation was performed on the MURA IBM-704 at Madison. This work proved to be completely consistent with all the results described above, but, because the pressure to obtain a satisfactory design point was no longer present, the opportunity presented itself to obtain a more complete description of the accelerator represented by point C.[10]

---

[10] A more complete description of this work is given by L. J. Laslett, Midwestern Universities Research Association report MURA-213 (1957, unpublished).

Some of these supplementary results are described below.

(1) Median-plane field. A Fourier analysis was obtained for the magnetic field in the median plane, with the results given in Table III.

TABLE III. The prominent Fourier components of the normalized magnetic field for operating point C.

m	f_m(the coeff. of sin $2\pi m \xi$)	g_m(the coeff. of cos $2\pi m \xi$)
0		1 (normalized)
1	1.0688	-0.1312
2	-0.0258	-0.0875
3	0.0742	-0.0357
4	-0.0087	-0.0122
$f_{eff.}$	1.084	

(2) Large-amplitude radial oscillations. A phase plot for large-amplitude radial oscillations is illustrated in Fig. 4 for the model free of imperfections.

(3) Small-amplitude radial oscillations. The small-amplitude betatron oscillations occur about an equilibrium orbit for which the major terms in its Fourier representation were found to be

$$x_f \cong -0.0211 \; -0.0290 \sin N\theta \; - 0.0071 \cos N\theta \; - 0.0011 \cos 2 N\theta \; -0.0001 \sin 3 N\theta - 0.0002 \cos 3 N\theta \; . \qquad (12)$$

The elements of the matrix $\begin{pmatrix} A & B \\ C & D \end{pmatrix}$ which serves to carry the vector $(x - x_f, \; p_x - p_{xf})$, characterizing a small-amplitude betatron oscillation, through one sector also were computed. These elements, as a function of the starting point within the sector, are plotted in Fig. 5. The parameter β , defined as $B/\sin\sigma$, has been introduced by Courant and

Snyder[11] for convenience in treating the response of an orbit to scatter-

[11] E. D. Courant and H. S. Snyder, Annals of Physics 3, 1 (1958).

ing and other disturbances. For the present structure β_x varies between about 0.43 and 1.29, as can be seen from Fig. 6, and the value at the reference point used in the earlier work ($N\theta = 0$, mod. 2π) is about 1.12.

(4) Small-amplitude axial oscillations. Corresponding results for axial motion in the model are plotted in Fig. 7 and 8. The values of β_y at $N\theta = 0$ and $N\theta = \pi$ (mod. 2π) are respectively 0.62 and 1.40.

Motivated by the unexpected comparative behavior of three Illiac runs, 22 runs, each of 400 sectors duration, were made with the IBM-704. None of these runs gave evidence of instability and many gave reasonably definite p_y vs. y phase plots, of which some were characterized by a rotation number close to $2\pi/5$. The initial conditions for the axial motion were varied over a considerable range within the stability limits quoted in Table II, while the initial values for the radial motion were the coordinates of the fixed point which characterizes the equilibrium orbit.[10]

A careful study[12] was made of the effect of k assuming in one sector

[12] L. J. Laslett, Midwestern Universities Research Association report MURA-257, (1957, unpublished).

the value 0.8, while in the remaining sectors it retained its design value 0.7. It was found that there were no notable effects attributable to the

decrease of periodicity of the structure, but only a partial decrease of the radial phase space available for stable oscillations which was similar to the larger decrease found when k was increased in all sectors.

III. CONSTRUCTION

A. Magnets

As mentioned previously, it was the intention that the accelerator design should scale and accordingly that all annular rings of the magnet should be similar, with the dimensions increasing in direct proportion to the radius. In addition the edges, and other equivalent points of each magnet sector, should progress radially outward along a logarithmic spiral which makes an angle $\xi = \cot^{-1}(Nw) = 46$ deg with a radius vector. With such a design, computations made for one radius in the accelerator should be immediately applicable to other radii.

It was appropriate, therefore, to cut the magnet poles from a surface having the correct conical angle to satisfy the scaling requirements of the machine. The sectors were made from forgings of Armco iron, $1\frac{1}{4}$ - in. thick, from which annular rings of 25 cm inner radius and 61 cm outer radius were flame cut. These annular rings were then placed upon a template, pressed into the desired conical shape, and subsequently annealed.

The individual magnet pole pieces were cut from the conical rings, mounted on a turntable, and machined to the final conical surface. Grooves were machined in the pole surfaces, near the sector edges, to carry the magnetizing windings and tuning coils. The rim of iron remaining beyond the coils could thus be regarded as remaining at zero

magnetostatic potential, thereby increasing the effective flutter of the resultant magnetic field by effecting a more abrupt fall-off and serving to provide additional shielding against external magnetic fields. The back leg and pole faces of each magnet sector were finally assembled on a jig and pinned by dowels in the final position. Figure 9 illustrates an assembled sector, prior to winding.

Since the magnet gap increases in direct proportion to the radius, and the magnetic field as $r^{0.7}$, the magnetostatic potential of the pole face must vary as $r^{1.7}$. It was therefore necessary to use distributed pole-face windings. These were so designed that a single layer of wire gave the requisite field dependence if infinite permeability were assumed for the iron. Current densities in the wires were kept below 2000 amp/in^2, thus obviating the need for water cooling. The coil configuration is shown in Fig. 10.

The main pole-face windings were formed of No. 16 Formex-insulated wire and employed 110 turns on each pole, of which 86 were distributed across the pole face, on circular arcs concentric with the accelerator. The wires crossing the pole were secured with polystyrene cement into grooves machined in a lucite form $\frac{1}{8}$ - in. thick. The return copper bundles were then rigidly formed to fit into the edge slots and were carefully mounted on the magnet faces, using fish paper and varnished cambric for insulation.

To provide a desirable flexibility in the operation of the model, both k-tuning coils and flutter-tuning coils were provided for adjusting the operating point of the accelerator. From an expansion of the desired

magnetic field through terms of first order in Δk,

$$H(k + \Delta k) \cong H_o (r/r_o)^k + H_o (r/r_o)^k \ln (r/r_o) \Delta k , \qquad (13)$$

one is led to a distribution of a single layer of supplemental pole-face windings adequate to produce a suitable change in k with no more than a small non-scaling error. These distributed windings were fabricated in the same way as the main field coils. They were wound with 97 turns of No. 22 Formex-insulated wire, following a schedule similar to that for the main coils, and the return copper bundles were also buried in the edge slots. The flutter-tuning coils were wound on thin lucite strips which then were secured to the guard edges of each pole so that the edges could be adjusted to magnetostatic potentials different from zero. During the installation of all the coils, the resistances were continually monitored and great care taken to avoid short circuits or grounds.

The main coils were all connected in series, so that they carried the same current ($\cong$ 3.4 amp). The k-tuning coils had their own series circuit with an adjustable current supply and the flutter-tuning coils were similarly in series with a separate control. Power for these currents was provided by a stabilized Nobatron power supply. A current of $\pm$ 1 amp in the k-tuning coils produced a change in k of $\pm$ 40%, and $\pm$ 1 amp in the flutter-tuning coils effected a $\pm$ 30% change of the effective flutter. It should be noted, however, that if both types of tuning coils are simultaneously employed, a significant departure from the desired scaling property of the magnetic field will result.

B. Vacuum Chamber and Detectors

(1) The vacuum chamber. The vacuum chamber was designed to permit utilization of as much of the magnet gap as possible, this consideration

being of particular importance at the injection radius where the largest oscillation amplitudes occur, and to afford a flexibility which would permit modifications of the experimental arrangements to be made readily. It was necessary to provide at least one insulated gap across which accelerating voltages could be placed when required, and several access ports for the insertion of probes and detectors were considered desirable For adequate beam lifetime, ultimate pressures in the neighborhood of 10^{-6} mm Hg were considered appropriate and an operating pressure of 2×10^{-6} mm Hg was typical for most of the tests described in the following sections.

The chamber, Fig. 11, was constructed as two hollow semi-circular annuli, sealed together by means of a $\frac{1}{8}$ - in. flat rubber gasket compressed by insulated bolts. The rubber gasket was located behnind a metal shoulder, which served to shield the insulating gasket from the beam and assisted in assembly of the chamber. The inner and outer chamber walls were formed by brass rings, $\frac{5}{8}$ - in. thick, to which the top and bottom plates of $\frac{1}{2}$ - in. brass were brazed to form a chamber with an interior height of $1\frac{1}{2}$ - in. The top and bottom exterior surfaces were chamfered, on the inner portion, to fit closely between the magnet poles.

The chamber was pumped continuously through two of eight 4 - in. holes in the bottom plate, selection of the particular holes to be used being determined by the desired azimuthal location of the chamber with respect to the magnet sectors. Two Consolidated Electrodynamics Type MCF-300 oil diffusion pumps, trapped by baffles which were freon cooled to -40° C, evacuated the chamber through 4 - in. gate valves. The fore-

vacuum was provided by a Welch Type 1397 rotary pump which, by a suitable system of ball-valves and use of ballast tanks, also served as a roughing pump. Pressures in the high vacuum system were measured with Consolidated Electrodynamics VG-1A ionization gauges and fore-pressures by thermocouple gauges. Gauges of the latter type also served to actuate protective vacuum interlocks.

(2) Detectors. For direct detection and analysis of the accelerated electron beam a scintillation detector was constructed for insertion into the vacuum chamber. The scintillator proper consisted of a 1 - in. dia. cylinder of Sintilon plastic, attached to the end of a brass tube which passed through an O-ring sliding seal at the vacuum chamber wall. The scintillator was covered on its front surface by an evaporated aluminum layer which was light-tight and yet sufficiently thin to permit electrons to strike the plastic. Electrical pulses were then obtained from an RCA Type 6342 photomultiplier situated at the end of the brass tube and were either viewed directly on an oscilloscope or integrated to give a signal indicative of the total beam striking the scintillator.

In moving the scintillator radially within the vacuum chamber, it necessarily crosses the spirals of the magnet structure and in consequence presents a variable aspect to the scalloped particle orbits. To avoid variations in the geometrical acceptance it was therefore necessary to make the front of the scintillator chisel-shaped.

A second detector consisted of a current probe, constructed to provide an absolute measurement of beam intensity. This probe was in the form of a Mo flag $\frac{5}{8}$ - in. high, $\frac{3}{8}$ - in. wide, and 0.010 in. thick. Tests

indicated that secondary emission caused no detectable error in measurements made with this probe. An additional type of probe carried an offset 0.040 - in. Mo wire which, through rotation of the probe, served to measure the vertical location of the equilibrium orbit, to indicate the amplitudes of vertical oscillations, and to limit these amplitudes when desirable.

For accurate measurement of the betatron oscillation frequencies and of the revolution frequency in tests of the operating model, it was planned to use destructive radio-frequency excitation of the betatron motion.[3,13] For this purpose a pair of plates was introduced near the

---

[13]Hammer, Pidd, and Terwilliger, Rev. Sci. Instr. 26, 555 (1955).

---

upper and lower surfaces of the vacuum chamber. These electrodes consisted of 0.010 - in. Mo, $\frac{1}{2}$ - in. wide, 2 - in. long, separated vertically by 1 in. They were electrically insulated, both from each other and from the chamber wall, and, by exciting them either in opposition or together, suitable vertical or radial electric fields could be placed in resonance with the corresponding betatron oscillations. An additional electrode of $\frac{1}{16}$ - in. Cu, 6 - in. long and $\frac{27}{32}$ - in. high, was also provided to permit application of a radial electric field near the injection radius.

C. Accelerating System

Betatron acceleration alone was used when the model was first put into operation, and later supplemented the radio-frequency fields employed in the series of experiments described in Sec. VIII. The dimen-

sions and windings of the betatron core, which was constructed of 0.014 -in. transformer laminations, are illustrated in Fig. 12. The four butt joints were surrounded, as shown, by separate windings connected in parallel with the main distributed windings and the resultant flux-forcing served to reduce the leakage flux. Measurements made at the center of the betatron-core window, before insertion of the vacuum chamber, indicated a leakage flux-density of approximately 1 gauss and a residual field of about 1/7 gauss from the core--the $\frac{1}{2}$ - in. brass plates of the vacuum chamber would be expected, of course, to effect a further reduction of stray time-varying fields.

At the time the core was designed the final basic parameters of the model had not been selected and it was believed desirable to provide an induction field of as much as 50 v/turn with continuous operation from a 500-cps alternator. In practice, however, it proved convenient to operate the core from a pulsed power supply, for which the circuits and resultant wave-forms are illustrated by Fig. 13. By use of this circuit electrons could be accelerated in two stages, first being carried to an intermediate radius and then, after a short interval, further accelerated to the final energy. During this interval experiments on radio-frequency acceleration could be performed.

The radio-frequency system is illustrated by the block diagram of Fig. 14. Since the required frequency change was small for the radio-frequency experiments with the model, a 6CL6 reactance tube was used to modulate the 6C4 oscillator. A 6CL6 gated buffer drove the 829-B final stage, which was then coupled to one of the insulated gaps of the

vacuum chamber. Since at 60 Mc the gap presents a reactance of very low Q, it was feasible to connect it to a tuning coil to provide a broad-band resonant circuit. The frequency-modulation function generator used to control the reactance tube was sufficiently versatile to control, independently, the initial radio-frequency program as well as the program in the neighborhood of the transtion[1] energy.

D. Injector

Although it was possible to employ as an injector a simple gun of the type customarily used for injection into betatrons,[5] it was considered preferable in the model tests to use an injection system with a very narrow septum so that one could inject into a region as small as several millimeters. To avoid voltage limitations within the injector assembly it proved convenient to employ an auxiliary deflector which permitted a septum as thin as 0.005 in. to direct the beam emerging from the injector.

The injector assembly is shown in Fig. 15. The electron optics of the gun itself were determined by a rubber dam method, leading to a design in which the focus was several millimeters in front of the gun save for space-charge effects which would displace this focus toward the deflector system. The deflector was constructed to bend the electrons through 15 deg, so that they would emerge through a slit 0.080 - in. wide and effectively 0.365 - in. high. The electric fields of the deflector were shielded by a box, of which the 0.005 - in. septum formed the grounded wall, in order to preclude disturbance of the electron orbits within the accelerator. This deflector system provided a small amount

of radial focusing and substantially no vertical focusing. When changing injectors, the mounting and alignment provisions permitted a pretested assembly to be inserted and a beam obtained within 20 min.

Tests of the injector in a separate vacuum system indicated an emittance of 0.2 mm·radian horizontally (± 1 mm, ± 0.05 rad) and 2 mm·radian vertically ($\pm$ 5 mm, $\pm$ 0.1 rad). The emergent intensity, amounting to about $\frac{1}{5}$ the total emission from the tungsten filament, was typically 25 to 50 ma at operating conditions which would insure a filament life of at least 600 hr. The radial admittance[11] of the accelerator at the point where the injector was located, as determined by the digital computations for the design point C, was expected to be 18 mm·radian (Fig. 4) and the axial admittance (as limited by the vacuum chamber) about 2.6 mm·radian, so that multi-turn injection radially warranted consideration. The injector was normally located at the center of a vertically-focusing sector, where the envelope of vertical oscillation is greatest.

Two distinct pulse circuits were constructed for the injector, to permit operation with short or protracted pulses, as desired. In the short-pulse circuit an artificial delay line was discharged, by a 5C22 hydrogen thyratron, through the primary winding of a 7.5:1 iron-cored, oil-insulated pulse transformer. The secondary of the transformer was connected to the injector and used a bifilar winding to provide power for the filament transformer. Resonant charging of the delay line was provided through a choke and high-vacuum rectifier circuit. An inverse diode served to clip overshoot and to prevent continuous conduction by the thyratron. The output impedance of this pulse supply was sufficiently low that variation

of the load through its entire range caused no measurable voltage change. Pulses up to 40 kv in height and 4 μsec duration were available from this circuit, with a flat top which was achieved by careful adjustment of matching resistors provided at the primary of the pulse transformer and by adjustment of the lengths of the individual delay-line sections.

The detailed construction of the modulator designed to produce long pulses is described in Appendix I. It could provide pulses up to 45 kv in height and 1 msec duration, with a rise time of 8 μsec By negative feedback the output was stabilized to 0.1%.

IV. MEASUREMENT AND CORRECTION OF THE MAGNETIC FIELD

To insure that the model would operate in the manner suggested by the computational work, and to make it effective for quantitative performance studies, it was necessary to measure the magnetic field carefully throughout the entire aperture of the machine. The numerical value and constancy of the field-index, k, the nature of the azimuthal variation of the magnetic field, and the character of the median plane were examined. Adjustments were then made so that magnetic fields could be obtained which were substantially the same as those used in the orbit computations. The measurements were made difficult by the low value of the magnetic field, the maximum value being 60 gauss, and by the complication of the spiral geometry. Following an initial investigation, it was found that the original magnet surfaces differed 2 or 3 mm from a conical shape and would have required corrective pole-face windings over the entire pole surface. Accordingly, the poles

were carefully remachined before making the final set of measurements and adjustments.

For most of the magnetic measurements small flip coils about 1 cm in length and diameter were used. To measure k three coils were used in an arrangement similar to that previously described.[3] The coils were mounted on an arm which was rotatable about the center of the accelerator and could be changed in radius. The radial and azimuthal positions were determined by suitable scales (to an accuracy of a few tenths of a mm in radius and a few tenths of a degree in azimuth). The end two coils were equally spaced from the center coil and were located along an axis, intersecting the axis of the center coil, which made an angle of 46 deg with the radius so as to be tangent to the central spiral locus of the magnet-sector (Fig. 16). The three coils could be flipped simultaneously, through 180 deg, about this axis.

The arrangement just described was only satisfactory for measuring k along the central spiral of each magnet (shown as a broken line in Fig. 16), since a large error results in regions where the field varies rapidly at right angles to the rotation axis and the error is greatly enhanced if the magnetic axes of the coils do not intersect this line accurately. Despite this limitation, however, the results obtained with the aforementioned method were found to be adequate when taken in conjunction with measurements of the average value of k by means to be described later.

Preliminary measurements indicated a value of k which was low and varied with radius. With the remachined poles the addition of a suitable number of back-leg turns in series with the main magnet windings made

it possible to hold k constant within 5% at low and intermediate radii--i.e., out to about 48 cm. In order to keep k constant at large radii, it was found necessary to distribute the main forward windings and the extra back-leg turns very carefully across the inside surface of the back legs. It will be noted from Fig. 9 that, for these larger radii, the region in which a good field is desired is as close to the back legs as to the pole-face windings.

Measurements of the magnetic field dependence on azimuth were first made using a single flip coil (the center coils of the three-coil arrangement), connected directly to a General Electric flux-meter. Some of the later measurements were taken with a peaker-strip magnetometer (Appendix II), which was constructed and kindly made available to us by Dr. Joseph Ballam of Michigan State University. These measurements were analyzed in the form of a Fourier series, using the IBM-704 computer. The program calculated both the Fourier components of the field and also the "effective flutter," $f_{eff} = \left[2\left(\langle H^2\rangle - \langle H\rangle^2\right)/\langle H\rangle^2\right]^{\frac{1}{2}}$. From the average values of the field at different radii, the average value of k could be computed. From the components of the Fourier analysis it was possible to determine which magnets had too large or too small a field. It was found that the effective flutter was slightly lower than desired, even when the vertical component of the earth's magnetic field was removed by means of a large

hexagonal Helmholtz coil pair placed around the accelerator, but final adjustments of course could be made by use of the flutter-tuning coils described in Sec. III A. In addition to the hexagonal coil pair just mentioned, a second set of coils was installed to remove the horizontal component of the earth's field.

In order to measure the horizontal component of field in the geometric median plane of the model, a piece of plate glass was carefully leveled and adjusted so that its top surface was parallel to and below the geometric median plane of the magnets. A peaker-strip magnetometer (Appendix II), sensitive to small fields, was connected to a zero-center meter and set on this glass plate so that its axis was at the height of the median plane. By moving the magnetometer about on this surface it was found that there were fairly large and random horizontal fields of magntitudes up to more than one gauss. Since the radial component of the horizontal field was felt to be the more harmful, attempts were made to reduce this as much as possible. To this end the magnets were raised or lowered, and tipped, and it was also necessary to wind turns properly positioned about the poles of the magnets, forward on one pole and backward on the other. In some cases it also was necessary to provide "plaster" coils on the inside of the back legs of the magnets. With these various adjustments it was possible to reduce the horizontal field to a maximum of about 10 milligauss at all radii less than about 52 cm. Beyond this radius, the many back-leg windings seemed to make the attempt excessively difficult.

When the flutter coils were added to the edges of the magnets, it was found necessary to adjust their feeder-windings carefully along the slots

to reduce their effect on the horizontal field. Careful adjustments were made until the horizontal field was no more than 20 milligauss when the coils were excited sufficiently to change the effective flutter by $\pm$ 40 %.

V. RESONANCE SURVEY AND STABILITY LIMITS

A. Method Employed in Resonance Survey

A detailed measurement of the variation in beam intensity over a large part of the ν_x, ν_y stability region of the model was made[4f, 14, 15]

---

[14] R. Stump and B. Waldman, Midwestern Universities Research Association report MURA-361 (1957, unpublished).

[15] W. A. Wallenmeyer, Midwestern Universities Research Association report MURA-407 (1958, unpublished).

---

in order to study the effects of various resonances on the operation of the accelerator. The field index was varied within the range 0.20 to 1.16 by the k-tuning coils (Sec. III A) and the flutter from 0.57 to 1.60 by the flutter-tuning coils. The measurements were chiefly made at a radius of 37 cm, which was as close to the injection radius as it was possible to operate and still clearly differentiate the accelerated beam from newly-injected electrons. The beam intensity was obtained from the integrated signal of the plastic scintillation detector (Sec. III B 2). During the intensity survey the injector filament current was kept low and constant; likewise the betatron core voltage, the gas pressure, and the injection timing were held fixed.

To correlate the measurements of beam intensity vs. tuning currents with the betatron-oscillation frequencies, the method[3, 13] of radio-frequency

resonant enhancement of the betatron oscillations was employed. Enhancement of the axial oscillations was detected by loss of beam due to interception by the vertical-scanning probe (Sec. III B 2) or by the walls of the vacuum chamber, while enhancement of the radial oscillations was identified by a shift in the time of arrival of the beam at the detector. The frequencies at which such resonances are observed are related to the betatron-oscillation frequencies by a relation of the form[3]

$$f_{rf} = \left| p \ \nu_x \pm q \ \nu_y \pm m \right| \ f_o \ , \tag{14}$$

where f_o is the revolution frequency of the particles and p q, and m are integers. The radio-frequency oscillator used for these measurements covered a range from 12 to 74 Mc, while the frequency of revolution at the 37 cm radius varied from 42 to 58 Mc as the tuning was changed within the range of interest. A typical set of frequency measurements, assignments, and results is given in Table IV. In order to make the correct assignments and thus determine the oscillation frequencies, approximate values for these frequencies of course should be known by other means.

TABLE IV Determination of ν_x and ν_y from resonant radio frequencies at the central operating point (tuning coils de-energized).

Measured Frequency (Mc)	Character of Resonance	f_o (Mc)	$\frac{f_{rf}}{f_{o,\ av.}}$	Assignment (f_{rf}/f_o)	Result
50.53	y, strong	49.25	1.025	ν_y	$\nu_y = 1.025$
47.96	y, strong		0.974	$2 - \nu_y$	1.026
27.48	y medium	49.24	0.558	$3 - (\nu_x + \nu_y)$	$\nu_x + \nu_y = 2.442$
21.76	y, strong		0.442	$(\nu_x + \nu_y) - 2$	2.442
29.74	y, medium	49.40	0.604	$1 - (\nu_x - \nu_y)$	$\nu_x - \nu_y = 0.396$
19.66	y, strong		0.399	$\nu_x - \nu_y$	0.399
49.27		49.27	1.000	1	
70.23	x, very strong	49.43	1.426	ν_x	$\nu_x = 1.426$
28.63	x, very strong	49.43	0.581	$2 - \nu_x$	1.419
20.80	x, very strong		0.422	$\nu_x - 1$	1.422
41.13	x, strong	49.26	0.835	$2\nu_x - 2$	$2\nu_x = 2.835$
57.38	x, medium		1.163	$4 - 2\nu_x$	2.837
46.40	x, medium		0.941	$3 - 2\nu_y$	$2\nu_y = 2.059$
Average		49.3			$\nu_x = 1.420$
					$\nu_y = 1.026$

B. Results

The intensity survey as a function of the tuning currents was taken in a series of runs where one of the tuning currents was kept constant (generally that for the k-tuning coils) and the other was varied over most of its range in order to determine most of the maxima and minima of

intensity. A typical plot obtained by this procedure is shown in Fig. 17 This plot shows the relative beam intensity measured by the scintillation detector as a function of the current in the flutter-tuning coils for the case where there was no current in the k-tuning coils The experimentally-measured flutter at three points is also indicated on the abscissa. Values of the axial and radial betatron oscillation frequencies are indicated above the curve, as are also the locations of certain significant resonances. By measuring the betatron-oscillation frequencies as a function of the tuning currents, interpolation graphs were prepared which permitted the results of the intensity survey to be replotted in terms of these frequencies. The resonance diagram which resulted is shown in Fig. 18, in which the increasing width of the resonances at points further from the center of the diagram is chiefly attributed to the increasing non-scaling of the field as the tuning currents are increased (Sec. III A). An indication of the degree to which the untuned fields satisfy the scaling condition is provided by Fig. 19, in which the measured frequencies are shown as a function of radius.

C. Discussion

Interpretation of the results just reported is subject to some uncertainty due to incomplete control of the betatron-oscillation amplitudes In the intensity survey the injector and deflector potentials were adjusted for each point so as to obtain maximum intensity and the amplitudes of the radial oscillations necessarily increased or decreased with the injection energy. The amplitudes of the axial oscillations, moreover were limited during the intensity measurements only by the upper and lower

walls of the vacuum chamber In the measurements of the betatron-oscillation frequencies by the radio-frequency resonance method however, no quantitative attempt was made to return to the injection conditions previously used except that adjustments were again made to attain maximum intensity Also the axial amplitudes were here deliberately limited, by the vertical-scanning probe in the interests of observing a sharp radio-frequency resonance with the axial oscillations The observed frequencies of the betatron oscillations as a function of oscillation amplitude are shown in Fig 20 for the central operating point of the model. It is seen that although the variation of ν_x with amplitude is small the variation of ν_y is considerable and presents some uncertainty in the values determined for ν_y in the intensity survey (Fig 18) It should also be mentioned that the radio-frequency resonance method is difficult when operation is near one of the intensity minima of Fig. 18 and that reliance must be placed in such cases, on interpolation from results obtained in regions of good beam intensity This fact, the amplitude dependence of the oscillation frequencies, and the non-scaling character of the magnetic field when substantial tuning currents are applied may account for the observation that the positions of the resonance lines drawn on Fig 18 do not coincide exactly with the observed positions of minimum intensity

It may be noted that the betatron-oscillation frequencies observed in the model (Table IV), without current in the tuning coils were close to the values resulting from the digital computations[5b 10] (Table I) and that a small current in the flutter-tuning coils sufficient to raise f_{eff} to its design value of 1 087 raised ν_y from 1 025 to the predicted value

of 1.12 (cf. Fig. 17). A sizable region of maximum intensity was found to occur centered about the design point in Fig. 18. The resonance diagram indicates the importance of several resonances in the region accessible by the tuning controls. Although the computer studies summarized in Table I suggested that the coupling resonance $\nu_x = 2 \nu_y$ could affect the intensity markedly in the neighborhood of operating point A, the specific influence of this resonance on beam intensity, when no misalignments were deliberately introduced, was less clearly marked in the results of the intensity survey illustrated by Fig. 18. An additional investigation, reported in Sec. V E, was therefore directed toward the examination of effects associated with operation near the accessible portion of this resonance line.

D. Stability Limits

Experimental measurements were made of the axial and radial stability limits at the design point of the model. At a given working point there is a range of energies at which electrons will be accepted into stable orbits in the accelerator. If one assumes that the minimum-energy particles are injected onto an equilibrium orbit which just misses the injector and that the maximum-energy particles oscillate about an equilibrium orbit which is situated a distance from the injector corresponding to the radial stability limit, it is possible to obtain a measurement of the radial stability limit.

In one method it is convenient to apply a long pulse (Appendix I) to the injector, modified to give a wave form having a linearly-falling portion and with the maximum injector voltage set above the high voltage limit

for injection of a beam into the accelerator. By suddenly dropping the deflector potential to zero at a time which is adjustable with respect to the wave form applied to the injector, the time interval over which injection occurs may be measured. From the rate of decrease of the injector voltage the acceptable energy range for injection may then be computed and hence the corresponding radial displacements of the injected particles from their respective equilibrium orbits. In a second method a long rectangular pulse which drops rapidly to zero (Appendix I) is applied to the injector, so that injection occurs over a quite short interval of time, and the time interval over which the accelerated beam is received at the target is measured. In this case electrons injected with a higher energy, and undergoing larger betatron oscillations, will arrive at the target earlier than electrons injected onto an equilibrium orbit which just misses the injector. From the known properties of the accelerator, in particular the value of the betatron accelerating voltage, the radial stability limit may again be evaluated. The adiabatic damping of the radial betatron oscillations must be taken into account, of course, in this calculation.

Axial stability limits are conveniently obtained by use of the vertical-scanning probe (Sec. III B 2). For all these measurements, where the injector, detector, and vertical-scanning probe were at different azimuthal and radial locations, some adjustments had to be made to the measured values so as to have the radial and axial limits refer to the same value of ξ. These adjustments could be made with the aid of the curves of β vs. $N\theta$ (Sec. II C; Figs. 6 and 8) for small-amplitude oscillations,

taking the betatron oscillation amplitude as proportional to $\beta^{1/2}$,[11] or by use of similar computer information pertaining to larger-amplitude oscillations.

A measurement of the radial stability limit by the second of the methods described led to a value at the azimuth of the injector given by $\pm(0.058 \pm 0.006)r$, or $\pm$ 1.75 cm, for the design point. This result corresponds to a limit of approximately $\pm$ 0.08 r at the azimuth to which Table II applies (cf. Fig. 6) and is in reasonable agreement with the value of approximately $\pm$ 0.09 r found computationally. The measured value for the axial stability limit similarly was $\pm$ (0.045 $\pm$ 0.006) r. This result is somewhat smaller than the maximum amplitude which would be permitted by the internal dimension of the vacuum chamber, as would necessarily be the case if the magnetic median plane were not quite centrally located within the vacuum chamber, while the computational result given in Table II suggests a dynamical limit at the injector somewhat greater than the available aperture.

E. The Resonance $\nu_x = 2\ \nu_y$

The design point for the model was deliberately chosen (Sec. II) to be far from the difference resonance $\nu_x = 2\ \nu_y$. As noted in Fig. 18, however, it was possible with the tuning controls to reach operating points in the vicinity of this resonance line, although the accessible portion was of somewhat limited extent and fell in a region where other important resonances were also present. It is apparent from Fig. 18 that the beam intensities in the neighborhood of the $\nu_x = 2\ \nu_y$ resonance are generally low, although no pronounced decrease of beam intensity is unambiguously attributable to this particular resonance. For this reason, and because

of the general interest in the $\nu_x = 2\ \nu_y$ resonance, additional information was sought experimentally for operation near this resonance, with $\nu_x \cong 1.46$, and the interpretation was guided by the results of digital computations made specifically for the point $\nu_x = 1.25$, $\nu_y = 0.62$.

From the computations it appeared that the radial motion, if present alone, would have very generous stability limits but, as is typical of performance on a coupling resonance,[16, 17] a very small amount of radial

---

[16] L. J. Laslett and K. R. Symon, Proceedings of the CERN Symposium on High Energy Accelerators and Pion Physics (European Organization for Nuclear Research, Geneva, 1956), Vol. 1, p. 279.

[17] L. Jackson Laslett and A. M. Sessler, Midwestern Universities Research Association report MURA-263 (1957, unpublished).

---

oscillation would be accompanied by a marked growth of the axial oscillations. This growth of axial oscillation-amplitude is shown in the semi-logarithmic plot of Fig. 21, wherein it is evident that a radial amplitude in excess of about 0.022 r, or about 0.7 cm measured at the injector, will carry the axial motion to amplitudes in excess of 0.06 r (1.9 cm) and result in interception of the beam by the chamber wall. If the wall were not present, however this physical limitation would not occur and stable motion with axial amplitudes up to about 0.1 r might then be considered possible.

Experimental measurement of the radial stability limit at the operating point assumed in the computations, using the methods described in Sec. V D, led to an effective limit of 0.51 cm and, as was the case for

the design point, axial amplitudes in excess of 1.3 cm were found. In a more detailed set of measurements, made with $\nu_x \cong 1.46$, results were obtained to suggest that the effective radial limit was indeed decreased if the axial amplitudes were restricted, the effect becoming more pronounced when operating close to the resonance line (Fig. 22). In summary, it is felt that the empirical measurements, when recognition is given to possible small departures of the magnetic median plane from the mid-plane of the vacuum chamber, are consistent with the computational results and that the growth of axial amplitude associated with operation near the $\nu_x = 2 \nu_y$ coupling resonance can effect a pronounced loss of intensity.

VI. INJECTION METHODS

A. General Considerations

It is impossible to trap particles in a static field, since particles injected externally ultimately will re-emerge and those injected from a source in the field eventually will return to strike the source. The imposition of secularly-changing fields, the presence of gas-scattering, or the use of time-varying fields arising from the particles themselves therefore is essential for injection. It frequently may be convenient, however, to analyze such injection methods by a study of the equilibrium orbit and the oscillations about it for a static field, followed by corrections for the secular changes which are necessarily present. With this procedure one can determine, for example, the time required before a particle injected with particular initial conditions from a source in the static field will return to strike the injector. Attention can then be

directed to effecting a modification of the equilibrium orbit, or a damping of the betatron oscillations, sufficient to move the orbits away from the deflector structure.

For efficient injection it is also necessary, of course, that the injected particles be sufficiently limited in their initial positions and directions that they can be contained within the stable region of phase space for particles in the accelerator. If the emittance of the injector is substantially smaller than the corresponding admittance of the accelerator, however, it may then be profitable to inject many turns successively. When many particles are present, their mutual interactions may cause a shift of the betatron-oscillation frequencies by such an amount that the effect of one or more resonances (possibly due to imperfections) is materially enhanced and thereby particles are lost from the beam. The limit to beam density which results from such space-charge effects will impose a less serious limit on the total current which it is possible to contain within the accelerator if the area utilized by the beam can be increased. An increase of the intensity of the injected beam at the expense of increased energy spread may be a chimerical gain, however, if beams ultimately are to be stacked by a repetitive acceleration system. Similarly, arranging a rapid energy change, in an effort to move the equilibrium orbit away from the injector and to suppress space-charge effects by increasing the beam area, may augment the amplitude of the betatron oscillations appreciably and somewhat reduce the effectiveness of this injection method.

B. Methods Employed with Short-Pulse Injection

In the spiral sector model one method of injection undertook to accelerate the electrons rapidly, but under conditions such that the amplitudes of the radial betatron oscillations remained smaller than the radial width of the beam due to energy spread. Under these circumstances, it is to be expected that the total number of particles successfully injected will be proportional to the radial width of the beam and that this, in turn, will be proportional to the energy gain per turn. With an acceleration voltage of 150 v/turn, successful injection for a 4 μsec interval was accomplished and led to individual beam pulses containing in excess of 10^{10} electrons. The electron density in this case was estimated as 3×10^6 cm^{-3}, which may be compared with the calculated limit[18] of 10^7 cm^{-3} at which space-

---

[18] L. Jackson Laslett, Midwestern Universities Research Association report MURA-14 (1954, unpublished). Our present estimate is one-half the value which would follow from the formulas of this reference, since in place of a toroidal beam we here consider a beam which is significantly more extended radially than in the axial direction.

---

charge effects would induce beam loss from the $\nu_y = 1$ resonance.

A second method which was successfully applied to the model did not require acceleration of the electrons but employed an azimuthally-localized, time-dependent radial electric field. This electric field, by producing a forced oscillation, resulted in a perturbation of the equilibrium orbit (Fig. 23). The injection conditions were chosen so that,

with the perturbation present, the betatron oscillations of the accelerated electrons were of small amplitude. Presuming that the strength of the perturbation is decreased to zero adiabatically, the orbits of these electrons will follow the changing equilibrium orbit with little change of oscillation amplitude, thus, in effect, being pulled away from the injector structure. Electrons injected somewhat later also can be accepted, with somewhat larger amplitudes of oscillation, and they too would be removed from the region of the injector as the perturbation was turned off. Despite the objective that the perturbation be removed adiabatically, it is necessary, of course, that the radial motion of the equilibrium orbit in the neighborhood of the injector be sufficiently rapid to preclude interception of the beam by some portion of the injector structure. If the vertical admittance of the accelerator were considerably larger than the vertical emittance of the injector, the injection structure could be displaced from the median plane, the perturbation could be turned off more slowly, and an improved utilization of phase space in this way might be possible. In the spiral sector model, however, the vertical emittance was not such as to permit such use of the vertical motion to assist in injection.

The perturbation was applied by a radial electric field, from an electrode inserted into the vacuum chamber. The electrode was shaped, as shown on Fig. 23, to produce a field of fairly constant strength throughout a region of several centimeters radial extent, and modulation provided by discharge of a capacitor with a thyratron. When injection with large-amplitude betatron oscillations was attempted, the electric field apparently effected a coupling between radial and axial motion which resulted in beam

loss; the system otherwise appeared to work well, however, permitting multi-turn injection to be achieved and leading to beam densities of approximately one-sixth the space-charge limit.

C. Long-Pulse Injection

One of the desirable possibilities[1, 2] for use of fixed-field accelerators is that in which a large betatron core might be employed in conjunction with a fixed-field magnet structure in such a way that particles may be injected and accelerated to the target or extractor with a duty cycle approaching 30 or 40 %. Use of the long-pulse modulator (Appendix I) permitted the injection of high-intensity beams into the spiral sector model for times as long as the 500-cps flux-wave in the betatron core could accelerate them and enabled a study to be made of ionization phenomena which would be unnoticeable with a short-pulse injection system.

The accelerating voltage was provided by the positive half of the 500-cps sinusoidal excitation of the betatron core and usually amounted to about 20 v/turn. Electrons could be accelerated thereby from the injection energy (30 kev) to the target, situated at a 45 cm radius (80 kev), in approximately 80 μsec. The equilibrium orbits of individual electrons thus moved outward at a rate of roughly 2×10^5 cm/sec during the course of acceleration. Injection could be maintained for periods as long as several msec, but usually occupied only 400 μsec at the peak of the accelerating-voltage wave, during which time the accelerating voltage was comparatively constant. Injection conditions otherwise were as described in Sec. III D.

Space-charge forces limit the density of electrons at injection to about 10^7 cm^{-3} (Sec. VIB).[††] The injector can supply more electrons

---

[††]The change of the oscillation frequency $\nu_y \equiv N\,\sigma_y/2\pi$ may be estimated readily for the simplified case of a beam of uniform density in a constant-gradient field (cf. ref. 18, in which a toroidal beam is considered). With the particle density denoted by n_e for the electrons, of velocity βc, and by n_i for the singly-charged stationary positive ions, one obtains

$$\delta(\nu_y^2) = -4\pi r_o R_o^2 \beta^{-2} (1-\beta^2)^{1/2} \left[n_e (1-\beta^2) - n_i \right] ,$$

in which r_o denotes the classical electron radius and R_o represents the radius of the accelerator. It is seen that the space-charge effect of the electron density is to decrease the oscillation frequency, by an amount which depends on $1 - \beta^2$ because of the partial cancellation of electrostatic defocusing by magnetic focusing effects, but that the accumulation of positive ions can reduce this decrease and ultimately lead to a net increase of the oscillation frequency.

---

than are required to reach this density and in consequence we would expect that the frequencies of betatron oscillations would decrease significantly as a result of space-charge, possibly to be limited by the nearest lower resonance. In the course of time during the injection pulse, ions formed by interaction of the beam with the residual gas in the vacuum chamber should collect in the beam and begin to neutralize the space-charge forces due to the electrons themselves. The initial value of the potential well which acts to trap these ions is of the order of several ev

and this process may be aided to some extent by the configuration of the applied magnetic field. The ions would not, in general, gain enough energy to escape the potential well of the beam and one accordingly visualizes a sheet of charge, originally some 2 cm thick, whose density is limited initially by the space-charge forces at injection and within which ions are being formed and trapped to neutralize these forces. It may be supposed, finally, that the accumulated ion density will serve to increase the frequencies of the electron betatron oscillations, possibly until the stability limitations imposed by the nearest resonance of higher frequency begin to affect the beam.

When the injector is operated at low emission currents with a good vacuum in the chamber, one observes a current at the target such as that shown in Fig. 24 (c). This current is quite uniform with respect to time and only becomes more intense when the betatron voltage is increased. The current is proportional to the emission from the injector and no effects of space charge or of ionization are observed. As the emission from the injector is increased, however, several more complicated phenomena are seen to occur. In this case the output current presents a time dependence shown in Fig. 24 (d), of which the essential features are sketched in Fig. 25. The time dependence is extremely reproducible from pulse to pulse, as is illustrated by the several hundred pulses contributing to the oscillogram of Fig. 24 (d).

The initial current, I_0 (Fig. 25), is found to be directly proportional to emission when this latter current is small and to reach a constant value at high emission currents. At high currents, I_0 is directly proportional

to the betatron voltage--i.e., upon the rate of progression of the equilibrium orbits away from the injector--and is independent of gas pressure, save for single-scattering losses estimable by other means The electron density corresponding to I_o, when calculated from dr/dt and the other known parameters of the accelerator, is approximately 2×10^6 cm^{-3}, so that this limiting value of the output current evidently may be related to the space-charge limit mentioned in Sec. VIB.

Following attainment of the current-value I_o, but depending on the particular operating point chosen, the output current may or may not undergo a further rise to reach a plateau value, I_{max} (Fig. 25). At a time T_1 the output current drops to zero and is restored only after an interval T_d. At the time T_2 the current again drops to zero and from then on the phenomenon reproduces itself in the manner indicated. It is found that T_1 is inversely proportional to the product of vacuum-chamber pressure and emission current, while the interval T_d is generally slightly less than the time required to accelerate electrons from the injector to the target and appears to be relatively independent of emission current. Evidently at time T_1 the sheet of charge extending from the injector to the target becomes unstable and is lost. Specifically it was found that when the operating point lay just below an axial resonance a probe situated above or below the beam would receive a large amount of charge at the time T_1, whereas when operating just below a radial resonance a probe inserted near the inner or outer radii would receive a burst of charge at T_1. The instability usually appeared

to begin at the injection radius and proceed outward to the target radius, taking approximately 5 μsec to do so.

Since the slope dI/dt (Fig. 25) and I_{max} are each proportional to emission current and T_1 varies inversely with pressure and emission, the phenomena appear attributable to ionization of the gas in the vacuum chamber. The initial space-charge limited current, I_o, can increase as ions are formed and collected in the beam until the current I_{max} is reached, which may represent the maximum current available from the injector. As additional ions are collected, the oscillation frequencies increase to approach a resonant value, whereupon, at T_1, the beam is lost. Following this, after a sufficient number of ions have migrated to the chamber walls, injected electrons may once again build up a new sheet of charge, commencing at the injection radius, and the phenomena then repeat themselves as long as the emission and accelerating voltage are both present. Radio-frequency measurements of the betatron oscillation frequencies,[3, 13] made at various times during the acceleration process, confirmed that with high emission currents the initial oscillation frequencies are lowered, as expected, and that at later times the frequencies increased to values which were above those obtained with low emission and which approached a half-integral resonance (e.g. $\nu_x = 1.5$). Once the operating point enters a stop-band and some electrons become quickly lost, the ions remaining behind may be expected to drive the operating point further into the stop-band and the beam must necessarily be lost very rapidly.

Although the foregoing explanation in terms of beam neutralization by ionization of residual gas appears to account for the phenomena described above, additional phenomena involving the collective motion of particles undoubtedly occur. Thus, for example, a strong rf electromagnetic field was found to arise from the beam, with frequencies which usually were half-integral multiples of the electron revolution frequency at the injector radius. The strength, frequency spectrum, and duration of this electromagnetic field depended quite markedly on the operating point of the accelerator. Since the intensity usually was particularly strong just prior to the time at which the beam was lost, the radiation may, at least in part, have been due to coherent motion of the charges as the operating point entered a stop-band. In one instance, moreover, it appeared that the current which arrived at the target was bunched at the revolution frequency of the electrons.

VII. PERTURBATION STUDIES

A. General Description

It was of interest to obtain experimental information concerning the effects of misalignments on the operation of the model to permit a comparison with computational and analytic results and to provide information concerning constructional tolerances for an accelerator of the spiral type. Four types of perturbations were specifically studied in turn: (1) the magnetic field in one of the six sectors was reduced 7 % by reducing the currents in the main field coils which produced the excitation for that sector; (2) the field index, k, in a sector was raised from 0.7 to 0.8 by adjustment of the current in the k-tuning coils for that sector;

(3) a sector was raised by 1 mm with respect to the remaining five sectors; and (4) a sector was rotated approximately 2 deg about a pin on its inner radius. For each such perturbation, measurements were made of, (1) the resultant radial and axial displacements of the equilibrium orbit, (2) changes in the frequencies of radial and axial betatron oscillations, and (3) changes in the radial and axial stability limits.

B. Results of Perturbations at the Design Point

The radial displacement of the equilibrium orbit which resulted from lowering the field by 7 % in one of the sectors is shown by the points in Fig. 26a. The solid line of Fig. 26a represents the displacement predicted by digital computation with the IBM-704, using the measured values of the magnetic field at a given radius together with the design values for k and w, while the dotted line represents the result predicted by Parzen[19] from an analytic treatment of this problem where

---

[19]The results of an analytic treatment by G. Parzen of the effect of perturbations in a spiral ridge accelerator are given in Appendix III. The authors are very grateful to Dr. Parzen for his courtesy in permitting this material to be included in the present paper.

---

the indicated shape is obtained from the addition of a $\cos\theta$ first harmonic term and a negative $\cos 2\theta$ second harmonic term. As expected, no significant vertical movement of the equilibrium orbit arose from this type of perturbation. As a result of this perturbation, the frequencies and amplitudes of the betatron oscillations were changed by the amounts

listed in Table V

A perturbation in which the field index k is raised from 0.7 to 0.8 in a sector has the effect of leaving the field unchanged at a radius of 25 cm but strengthens the field by increasing amounts at larger radii within the perturbed sector (cf. Sec. IIIA). The effect of such a perturbation on the equilibrium orbit appears[19] to be essentially due to the associated increase of the field strength at the radius of interest. The shift of the radial position of the equilibrium orbit as obtained experimentally at a radius of 37 cm is indicated by the points plotted in Fig 26b together with computational and analytic results obtained by considering only the increased field strength within the perturbed sector Again, as expected, no vertical movement of the equilibrium orbit was found to occur. The change in the field strength at 37 cm as a result of the change in k is about half that which was produced by the preceding field perturbation and in the opposite sense. Changes in the frequencies of the betatron oscillations and the stability limits which were observed to occur from the perturbation of k and the resulting field perturbation are summarized in Table V. Also included are the results of computations[12] made with the IBM-704 prior to operation of the model As noted previously (Sec. IIC), the main effect of this perturbation appears to be a partial decrease of the phase space available for stable oscillations similar to the larger decrease found when k was increased in all sectors.

TABLE V. Effect of Perturbations on the Oscillation Frequencies and Stability Limits at the Design Point.

Perturbation	Item	Theory[a]	Computer	Experiment
Unperturbed	ν_x	1.32	1.40	1.41
	ν_y	1.15	1.12	1.12
	A_x		$0.097\ ^{+0.005}_{-0.000}$	0.058 ± 0.006
	A_y		$0.058\ ^{+0.005}_{-0.000}$	0.045 ± 0.006
Field Decreased 7% in One Sector	$\Delta\nu_x$		0 ± 0.001	$+0.006 \pm 0.003$
	$\Delta\nu_y$		-0.002 ± 0.0005	-0.006 ± 0.005
	$\Delta A_x/A_x$		-0.18 ± 0.05	-0.25 ± 0.08
	$\Delta A_y/A_y$		-0.31 ± 0.05	-0.22 ± 0.08
Field Index, k, Changed from 0.7 to 0.8 in ne Sector	$\Delta\nu_x$		$+0.01 \pm 0.001$	$+0.011 + 0.003$[b]
	$\Delta\nu_y$		-0.01 ± 0.001	-0.015 ± 0.005[b]
	$\Delta A_x/A_x$			-0.20 ± 0.08[b]
	$\Delta A_y/A_y$			-0.23 ± 0.08[b]
Axially Displaced Sector (raised 1 mm)	$\Delta\nu_x$			$+0.001 \pm 0.004$
	$\Delta\nu_y$			$+0.002 \pm 0.006$
	$\Delta A_x/A_x$			-0.20 ± 0.10
	$\Delta A_y/A_y$			-0.08 ± 0.10
Rotated Sector (approx 2°)	$\Delta\nu_x$			$+0.004 \pm 0.006$
	$\Delta\nu_y$			$+0.003 \pm 0.007$
	$\Delta A_x/A_x$			0.0 ± 0.15
	$\Delta A_y/A_y$			0.0 ± 0.15

[a]Theoretical results from Appendix III.

[b]The experimental values for the perturbation in k also include the effect of the field being increased by about 3 1/2% at the detection radius in the perturbed sector.

The vertical movement of a sector by 1 mm resulted in an equilibrium orbit displaced from the median plane by amounts shown in Fig 26c and produced no detectable change in the radial position. The effects on the betatron oscillation frequencies and on the limiting stable amplitudes are summarized in Table V, together with computer results obtained by means of the Illiac prior to construction of the model.

Clockwise rotation of a sector, through 2 deg about a vertical axis at its inner radius, will necessarily increase somewhat the field strength at a given radius--in the present case by about 2 $\frac{1}{2}$ %. The change in the equilibrium orbit which results from this perturbation is shown in Fig. 26d and is believed to arise primarily from the increase of field strength associated with rotation of the sector. The changes produces in the betatron oscillation frequencies and the stability limits appear to be small.

C. Results Near the $\nu_x = 2\ \nu_y$ Resonance

To supplement the results just reported it was considered of interest to obtain information concerning the effect of perturbations applied to the model when operating in the neighborhood of the difference resonance $\nu_x = 2\ \nu_y$. Unfortunately, as noted in Sec. V, the accessible portion of this resonance line was of somewhat limited extent and fell in a region where other important resonances were also present. The computer results obtained for the operating points A and B considered in Sec. II C indicated that the radial stability limits were very greatly reduced in the neighborhood of the $\nu_x = 2\ \nu_y$ resonance when even small amounts

of axial motion were introduced, and misalignments of course were found to effect a further reduction of these stability limits. In practice, the pronounced exchange of amplitude between radial and axial oscillations which occurs when operating near a coupling resonance presents a complication in making it difficult to distinguish experimentally motions in these two degrees of freedom.

Two types of perturbations were studied at a point near the $\nu_x = 2\,\nu_y$ resonance; (1) the magnetic field was lowered by 5 % in a sector and (2) a sector was raised 1 mm. The same measurements were made as at the design point. The radial displacement of the equilibrium orbit which resulted from lowering the magnetic field by 5 % was about the same as at the design point with the exception that the negative $\cos 2\theta$ part had less of an effect here, as expected [19] The changes in the betatron oscillation frequencies and the stability limits were less than the indeterminancies of the measurements. The vertical displacement of a sector caused a small vertical displacement of the equilibrium orbit and no detectable radial displacement. The observed changes in the betatron frequencies and stability limits were again very small. Computer studies made specifically for $\nu_x = 1.25$, $\nu_y = 0.62$ appeared to confirm the result that little further reduction of the radial stability limit would occur at this operating point with an axial sector displacement of 1 mm.

VIII. STUDIES OF RADIO-FREQUENCY ACCELERATION

A. General Discussion

The objective of the radio-frequency acceleration experiments reported here for the spiral ridge model was to determine empirically the frequency-modulation programs which could most successfully be applied to accelerate particles through the transition energy. The magnet excitation and the injector voltage were adjusted so that the transition radius was 49 cm. This allowed electrons to be accelerated through the transition to at least a 52 cm radius before edge effects in the magnets reduced the beam. Figure 27 shows the energy and revolution frequency as a function of radius under these operating conditions. The energy was calculated on the basis of field measurements and the known value k, while the frequency was measured by radio-frequency excitation of betatron oscillations (Secs. III B and V)[3, 13] and by the more accurate method which we now describe. The first of two successive betatron acceleration pulses (Sec. III C) was adjusted so that practically all the electrons were taken out to the target. The remaining electrons could be assumed to have extremely small betatron oscillations and could be observed striking the target at the start of the second betatron pulse. In the interval between these betatron pulses radio-frequency power was applied to the vacuum chamber at a constant frequency close to the revolution frequency and tuned to bring these electrons with small oscillation amplitudes onto the target, possibly by exciting synchrotron oscillations. In this way the frequency could be determined quite accurately as a function of radius.

The transition energy for fixed-field alternating-gradient accelerators is given by[1]

$$E_t = E_o (k + 1)^{\frac{1}{2}} \tag{15}$$

and the transition radius, in cm, by

$$r_t = \left[\frac{E_o^2 \; k \; r_o^{2k} \; 10^8}{9 \; H_o^2}\right]^{\frac{1}{2k+2}} , \tag{16}$$

where E_o = electron rest energy in Mev, E_t = transition energy (including rest energy) in Mev, k = mean field index, and H_o is the average field in gauss at r_o cm.

In discussing radio-frequency acceleration methods, reference is made to the electrical phase angle, ϕ, at which a particle crosses the acceleration gap; the peak value, V, of the voltage applied to the gap; the phase angle, ϕ_s, for an equilibrium particle; and the gap voltage, V_s, appearing across the gap at the time of transit of the equilibrium particle. It is convenient to introduce the quantity Γ, defined by

$$\Gamma \equiv \sin \phi_s = V_s/V , \tag{17}$$

and to note that

$$V_s = \frac{df/dt}{f \, df/dE} , \tag{18}$$

where f denotes the revolution frequency of a particle in the given magnetic field (Fig. 27).

The Symon-Sessler theory[20] of radio-frequency acceleration in

---

[20]K. R. Symon and A. M. Sessler, Proceedings of the CERN Symposium on High Energy Accelerators and Pion Physics (European Organization for Nuclear Research, Geneva, 1956) Vol. 1, p. 44.

fixed field alternating-gradient accelerators further employs the variable W, shown to be canonically-conjugate to ϕ, defined by

$$W = \int_{E_o}^{E} dE/f(E) \quad . \tag{19}$$

The stable area in W, ϕ phase space, within which stable synchrotron oscillations may occur, is termed a "bucket." For a given machine and a constant radio-frequency voltage, the bucket area is proportional to a quantity α_1, which is given by the Symon-Sessler theory[20] in terms of a parameter η. The latter quantity is proportional to $1 - f/f_t$ and α_1 approaches zero as the revolution frequency f approaches the transition frequency f_t, in the manner illustrated by Fig. 28.

Typical buckets above and below the transition energy are shown in Fig. 29. As a bucket approaches the transition energy the stable area approaches zero and, in passing to operation above the transition frequency, particles may be expected to be deposited in a band lying just above the transition energy in the W, ϕ plane. If, however, the frequency is modulated non-adiabatically to a value slightly greater than the transition frequency and then decreased, it is possible to pick up some particles from this region and accelerate them further. This procedure requires a carefully scheduled program of frequency modulation so that, in effect, the correct phase slip required to continue acceleration above the transition energy is introduced.

B. Experimental

In the experimental work ϕ_s was normally between 11 and 55 deg when operating below the transition energy, with Γ correspondingly

between 0.2 and 0.8; in going through the transition energy, Γ, of course, became greater than unity; and, finally, in the operation above the transition energy ϕ_s typically approached the value 150 deg. The frequency-modulation program in the neighborhood of the transition energy was then adjusted empirically to obtain effectively the optimum phase slip and thereby achieve the most efficient transfer of electrons to states of stable synchrotron motion above the transition energy.

The effectiveness of the various frequency-modulation programs was determined by a method which paralleled that used in similar studies[21]

---

[21] Terwilliger, Jones, and Pruett, Rev. Sci. Instr. 28, 987 (1957).

---

with the radial sector model.[3] Figure 30 illustrates this method schematically. With curve A no radio-frequency acceleration is provided, so that electrons are accelerated by an initial betatron pulse to an energy of about 118 kev and to a radius of 45.5 cm, to remain at that radius for about 1230 μsec before being further accelerated by a second betatron pulse which carries them to the scintillation detector at a radius of 52 cm. In the case depicted by curve B the radio-frequency voltage is used to carry the electrons, which have been stacked at the intermediate radius of 45.5 cm, up to the transition energy and the voltage is then turned off. In this case the electrons are once again brought to the detector by the further acceleration provided by the second betatron pulse, but arrive 150 μsec earlier than with curve A. Finally, with curve C, the radio-frequency voltage is applied in accordance with a frequency-modulation schedule intended to provide acceleration through the transition

energy and electrons successfully accelerated in this way will appear at the detector at a time preceding onset of the second betatron pulse.

Typical results of the method just described are illustrated by the oscilloscope traces drawn in Fig. 31. The upper trace of each pair shows the beam received at the detector and the lower trace represents the rf voltage. In actuality the first betatron pulse had dropped to zero by the time the sweep started, but the second betatron pulse appeared on the trace and the radio-frequency voltage, when present, was also displayed. In the first pair of traces in Fig. 31 no radio-frequency voltage was used and the single beam pulse shown represents the electrons accelerated entirely by betatron action. In the second pair the radio-frequency voltage served to carry about 60 % of the stacked electrons to the neighborhood of the transition energy (155 kev) and these electrons gave rise to the earlier of the two pulses shown. Finally, the third set of traces illustrates the case in which some electrons were successfully accelerated through the transition energy to arrive at the detector prior to the onset of the second betatron pulse, while others were dropped at the transition energy and the remainder were not captured by the radio-frequency system at all. In the quantitative interpretation of results such as those illustrated by Fig. 31 it must be recognized that the true efficiency (50 %) is somewhat less than that indicated directly by the data (70 %), since the pressure in the vacuum chamber was of the order of 3×10^{-6} mm Hg at the time the experiments were performed and the consequent half-life of the beam due to gas scattering was approximately 400 μsec.

The adjustment of the frequency-modulation schedule to obtain efficient traversal of the transition energy is, of course, critical. This is illustrated by Fig. 32, in which three frequency schedules are shown, of which the second (denoted B) gave an efficiency approximately five times as great as with either of the other two.

IX. ACKNOWLEDGEMENTS

We would like to express our indebtedness to the several universities which, by granting leaves of absence, made it possible for many of the authors to contribute to the success of the model. We particularly appreciate the cooperation of the Graduate College of the University of Illinois in the arrangements permitting extensive use of the Illiac computer, the willingness of the Physics Research Laboratory to assume the burdens of initial construction, and the assistance of the mechanical engineering shop at the University of Illinois in making available a large press for initial shaping of the magnet poles.

Invaluable assitance in programming the digital computations was provided by Dr. R. F. King, Mrs. G. Belford, and Mr D. Hutchinson. Use of the computers was greatly facilitated by the cooperation of Drs. J. P. Nash and R. E. Meagher of the Digital Computer Laboratory, by Mr. Jess Anderson who prepared the individual problems for the computer, and by Mr. Melvin Storm who supervised some of the later work with the IBM-704 installation in Madison.

The initial construction was implemented by the administrative assistance of Mr. J. J. Cochrane and by the work of Mr. T. B. Elfe. The final assembly and portions of the test program received sub-

stantial contributions from Dr. Carl E. Nielsen, of the Ohio State University; Dr. R. Stump, of the University of Kansas; and Dr. F. T. Cole, of the State University of Iowa. Assistance was provided by G. F. Dell, of the Ohio State University; C. Bernhardt, G. E. Bush, and E. C. Weinberg, of Purdue University; C. W. Owen, D. S. Roiseland, D. Schroeder, and M. G. Silbert, of the University of Wisconsin; and by J. D. Hogan, E. S. Kennedy, J. Mulady, and C. A. Radmer, of the MURA Laboratory.

The cooperation of Dr. Joseph Ballam of Michigan State University in providing a field magnetometer was very helpful in facilitating the magnetic measurements and the contributions of Drs. E. S. Akeley, F. T. Cole, G. Parzen, and K. R. Symon to the basic theory are also gratefully acknowledged.

APPENDIX I.

DESIGN OF THE LONG-PULSE MODULATOR

For the studies of stability limits and space-charge effects described in Secs. V and VI, it was necessary to inject electrons into the accelerator for relatively long periods of time. The long injection time and the required constancy of injection energy demanded by the specifications for the modulator (Table VI) precluded the use of conventional delay line and pulse transformer techniques for driving the injector. Fortunately, a power tetrode

TABLE VI. Specifications for the long-pulse modulator.

Pulse amplitude	Pulse current	Pulse length	Rise time	Flatness
-45 kv	250 ma	10^{-3} sec	10^{-5} sec	0.25 %

capable of withstanding 50-kv plate potentials became available at the time these experiments were being considered, so that the use of a plate-loaded amplifier for driving the injector appeared to be an attractive possibility. The problem then became one of constructing from available components an amplifier with adequate frequency response and output capability. This appendix describes briefly the design and performance of such an amplifier.

The values of pulse amplitude, current, and duration listed in Table VI represent, of course, maximum values and are much greater than necessary for the present purpose. It was felt, however, that the amplifier should be designed to make full use of the output stage. The characteristics of the output tube (Eimac type X556) are given in Table VII.

TABLE VII. Characteristics of Eimac type X556 power tetrode.

DC plate voltage	50 kv max.
Pulse cathode current	6 amperes max.
Average control grid dissipation	5 watts max.
Average screen grid dissipation	25 watts max.
Average plate dissipation	250 watts max.
Transconductance (estimated)[a]	6000 μmho
Grid bias for 10 μamp anode current[b]	-450 volts

[a]Screen potential = 1 kv, anode current = 1 amp.

[b]Anode potential = 50 kv, screen potential = 1 kv.

A simplified circuit diagram of the amplifier output stage is shown in Fig. 33, wherein C_s denotes the parasitic capacitance of the output circuit, including the injector, and R_L represents the resistive load presented by the injector. Because the output of the amplifier is to be a moderately fast pulse at high potential, the choice of the coupling capacitor is severely limited with respect to its capacitance. The largest commercially-available capacitance in the 50-kv range with reasonable physical size and electrical properties seems, in fact, to be about 0.1 μfd. With the output tube specified, the design of the amplifier then must start with the coupling capacitor since it alone will determine the flatness of the output pulse under the assumption that all other time constants ahead of the output stage may be made long compared to 10^{-3} sec.

The injector operates in the emission-limited region and consequently the expression

$$\Delta V = (I_L/C_c)\,\Delta t \tag{20}$$

is exact. Taking C_c to be 0.1 μfd, I_L to be 250 ma, and Δt to be 10^{-3} sec, ΔV is found to be 2.5×10^3 v and a 20-kv output pulse of 1 ms duration thus would be expected to drop by 12.5 % as a result of the capacitative coupling. An amplitude of 20-kv was chosen for this calculation because it corresponds to the minimum pulse amplitude that will be required of the amplifier and therefore gives the maximum percentage drop for a given output current. Moreover, even if it were possible to increase the size of C_c without limit to obtain the required flatness of the output pulse, there will be variations in the output level due to shifts in the 50-kv power supply, which is not regulated. These latter variations might be as large as $\pm$ 5 % and would appear in the output because the dynamic plate impedance of the X556 tetrode is fairly low. It was considered essential, therefore, to incorporate a feedback loop to stabilize the gain of the amplifier and to decrease the drop of the output pulse to the required 0.25 %.

Before calculating the value of the loop gain, βA_o, necessary for the required degree of stability, the rest of the amplifier must be considered. The output stage requires a driving signal of at least 500 v peak from a low-impedance source in order that it can conduct heavily during the rise of the pulse. The heavy conduction is necessary to discharge the parasitic capacitance C_s, which was estimated to be as high as 150 $\mu\mu$fd. In order for this discharge to occur in approximately

5 μsec for a 45-kv pulse, a current at least as large as that given by

$$I_p = C_s (\Delta V / \Delta t) = 1.2 \text{ amp} \tag{21}$$

must pass through the tube. This requires that the output tube be driven into the region of grid conduction. A cathode follower using a high-powered tube such as a 3E29 dual beam power tube would be expected to prove satisfactory as a driver. It furthermore seems reasonable to expect that a two-stage amplifier ahead of the cathode follower then could supply the necessary 500 - 600 v signal.

If the arbitrary assumption is made that the gains of the first two amplifier stages and of the output stage may change in the course of time by $\pm$ 10 % due to aging of components, power supply variations, etc., then the loop gain will vary by $\pm$ 33 %. The cathode follower is not included in this estimate since it is a degenerative device. The necessary value of loop gain, βA_o, would then follow from the relation[22]

---

[22] Duncan MacRae, Jr. in Vacuum Tube Amplifiers, edited by G. E. Valley, Jr. and H. Wallmann (McGraw-Hill Book Co., New York, 1948), Mass. Inst. of Tech. Radiation Laboratory Series, Vol. 18, Ch. 9, p. 366, Eq. (45).

$$\frac{1}{\beta A_o} \cdot \frac{1}{2} \left(\frac{1}{0.67} - \frac{1}{1.33} \right) \leq 0.0025 , \tag{22a}$$

whence

$$\beta A_o \cong 150 . \tag{22b}$$

It can be seen that this value of βA_o is considerably greater than that necessary to reduce the 12.5 % drop of the output pulse to the required 0.25 %. It now remains only to pick a reasonable closed-loop gain in

order to calculate the required overall gain of the amplifier. Taking the closed-loop gain to be 10^3, the necessary overall gain is then $A_o = 10^3 \times 1.5 \times 10^2 = 1.5 \times 10^5$. This value may seem excessive for three stages until it is recalled that the transconductance of the output stage is 6000 μmho. For a plate-load resistance of 50 kΩ this gives a gain of 300 for this stage alone and the preceding two stages should be able to provide a gain of 500 quite easily.

The seemingly arbitrary choice in the previous paragraph for the plate-load resistor in the output stage was actually motivated by consideration of the power dissipation in the output tube. It was expected that the duty cycle for the amplifier might be as high as 0.03. If 5-kv is assumed as the plate voltage during the pulse and 250 w as the maximum permissible plate dissipation, the pulse-plate current should be less than 1.7 amp. Since there is a significant contribution to plate dissipation during the rise of current at the beginning of the pulse when heavy conduction at high plate potential takes place, it seemed advisable to reduce the plate current to 1.25 amp and a value of 50 kΩ accordingly was selected for the plate resistor.

Figure 34 shows the circuit of the complete amplifier. The design of all stages is conventional and will not be discussed in any great detail. Feedback from the output to input is obtained from a capacitive voltage divider with a ratio of 1000:1. The first stage is a standard non-inverting amplifier with a gain of approximately 30. The second grid is used as a feedback terminal. The second stage is biased unsymmetrically to obtain a large positive pulse of short rise time. The cathode follower

is of low impedance since it must supply the grid current of the final stage as well as drive a rather high parasitic capacitance. Small resistors were included in the plate, grid, and cathode circuits of the cathode follower to serve as parasitic suppressors. The direct coupling used in the last two stages serves two purposes: first, it reduces the number of low-frequency phase-shifting networks in the loop and, second, it provides a convenient method of adjusting the bias on the final amplifier stage. The small capacitors in the cathode circuits of the first and second stages and the RC series circuit to ground from the plate of the first stage are networks required for stabilization of the feedback amplifiers.

The measured performance of the amplifier was rather close to the original specifications (Table VI). The closed-loop gain was 995 and the rise time was 8 μsec. A 4 μsec rise time could be obtained, in fact, at the expense of a single 5 % overshoot. The flatness of the output pulse was measured with a differential amplifier and oscilloscope. For a 1 ms 30-kv pulse applied to a 120 kΩ load the voltage drop was less than 0.1 %.

In summary, the modulator design reported here appeared to represent a straightforward method of generating long pulses of moderate rise time with a good constancy of amplitude at high voltage. There seem to be no complications arising from the high voltages that cannot be circumvented by the usual techniques. Faster rise and decay times undoubtedly may be obtained at the expense of pulse length as tubes with higher maximum plate current become available. Again, however, feedback could

be used to reduce the value of coupling capacitance necessary for good reproduction of the flat top of the pulse and this would appear to be of some advantage since the cost of increasing loop gain is much less than that of increasing the size of the coupling capacitor. Since the modulator is a linear amplifier, the output pulse is an accurate reproduction of the input pulse subject to the limitations of frequency response. In some of the stability-limit measurements described in the text (Secs. V D, E) the input pulse, which ordinarily was a square pulse of variable amplitude derived from a multi-vibrator circuit, was shaped so as to exhibit a region with a substantially-linear and moderately-slow decrease of potential.

APPENDIX II.

THE MAGNETOMETERS

The two magnetometers used in measuring the magnetic field and locating the median plane were basically of the same type. The operation of these instruments is based on the fact that if one excites a transformer wound on a ferromagnetic core with a sinusoidally-varying current, the magnetic field within the core and hence the secondary voltage may be represented by a series which involves only the fundamental and odd-order harmonics, provided the hysteresis loop of the core is symmetrical about the origin. If this symmetry is destroyed by the presence of a dc magnetic field which displaces the hysteresis loop along the H-axis, even harmonics will appear in the output. The amplitude of the even harmonic content of the output is, to a first approximation, proportional to the superimposed dc field. In principle, then, the magnitude of the superimposed field may be obtained from the amplitude of the second harmonic component. A block diagram of a magnetometer employing this method is shown in Fig. 35.

The core of the transformer consists of a single short, thin strip of material for which the hysteresis loop has a very steep slope. The primary and secondary windings each employ a few hundred turns wound on a bobbin, with the core in the geometrical center (Fig. 36). The assembly is then mounted in a suitable non-magnetic holder, which serves to protect the windings.

Since the amplitude of the second harmonic component in the output of the transformer not only depends on the strength of the external field

but also on that of the exciting field, the amplitude of the current in the primary must be kept constant. Moreover, because tuned amplifiers are used between the transformer output and the phase-sensitive detector, the excitation frequency must also be maintained constant. There are, in addition, other considerations that enter in the practical application of this method. For example, the shape and symmetry of the hysteresis loop are very dependent on the mechanical and magnetic history of the core. Also, since the magnetometers used with the spiral-sector model were required to give good spatial resolution in an inhomogeneous field, the active volume of the core had to be extremely small. This latter requirement led to considerable difficulty with heat dissipation in the primary winding, because it was necessary that the core be driven into saturation in both directions to avoid its taking a permanent "set."

As is understandable, the aforementioned problems could not all be overcome conveniently in any one instrument. Accordingly, two magnetometers were constructed--one for fairly large fields (1 - 300 gauss) and one for very small fields($\approx 10^{-2}$ gauss). The magnetometer for "large" fields incorporated a feed-back circuit that energized a quadrupole coil mounted coaxially with the core (Fig. 37), to insure that the core was never operated in a field of more than a few tenths of a gauss and thus reduce the driving power in the primary winding. This instrument was essentially a copy of the device described by Voelker and Leavitt[23, 24]

---

[23] F. Voelker and M. A. Leavitt, University of California Radiation Laboratory report UCRL-3084 (Berkeley, 1955, unpublished).

[24] F. Voelker, Electronics 31 (No. 11), 152 (March 14, 1958).

and was used in mapping the vertical component of the magnetic field in the region of the geometric median plane. The core was a 2 mm x 5 mm strip of Mo permalloy, 0.5 mils thick, mounted with its long axis parallel to the vertical component of the magnetic field. This magnetometer was entirely adequate for the use described, but suffered from two significant drawbacks which made it unsuitable for finding the magnetic median plane. The first such defect arose because the bias coil produced a small but not negligible external magnetic field at distances from the coil of as much as 3 cm (or half a gap width at the injection radius) and it was initially feared that in the magnet measurements (Sec. IV) the low-field ends of the magnets would be highly sensitive to external fields. Secondly, since the bias current was supplied by series vacuum tubes, the magnetometer could be used only in fields of one polarity, for otherwise the core might become saturated and thus take on a "set" which would give an appreciable error when measuring small fields. The situation just described could readily occur when making measurements in the fringing-field region with large currents in the flutter-tuning coils.

The "sensitive" magnetometer for measurement of weak fields is shown schematically in Fig. 38. The oscillator-amplifier circuit operated at 3500 cps and incorporated current feedback to stabilize the driving field. The reject filter was included to keep the fundamental component of the signal from overloading the tuned amplifier and thus generating a spurious second-harmonic component. The pickup transformer consisted of two,

twenty-turn windings of No. 40 B & S gauge Formvar-insulated wire wound directly on a 1 mm x 10 mm strip of Mo permalloy, 0.5 mil thick. This magnetometer was insensitive to transverse magnetic fields as great as 200 gauss, while showing good sensitivity for longitudinal fields of 10^{-2} gauss. Because of the small driving field, considerable care had to be exercised to keep the pickup transformer out of longitudinal fields in excess of 10 gauss. In practice, the magnetometer was not used to determine the magnitude of the horizontal field in the region of the median plane, but rather to implement adjustments directed toward reduction of the radial component of magnetic field in this plane.

APPENDIX III.

PERTURBATION THEORY

In this appendix theoretical results for the linear orbit properties and for effects of field perturbations will be presented. No derivations of the results will be given here.

We will first give some results for the linear orbit properties of a scaling FFAG accelerator. Somewhat more general and accurate results, and their derivations are available in MURA reports.[25]

---

[25] G. Parzen, Midwestern Universities Research Association reports MURA-454, 451, 397 (1959, 1958, unpublished).

We will write the magnetic field in the median plane as

$$H_z = -\left[H_0(r) + 2H_1(r)\cos(N\theta - \beta_1(r)) + 2H_2(r)\cos(2N\theta - \beta_2(r)) + \ldots\right] \tag{23a}$$

where

$$H_n(r) = -B_0(r/r_0)^K h_n, \tag{23b}$$

$$\beta_n(r) = (n/w)\ln(r/r_0) + \alpha_n. \tag{23c}$$

The average radius of the equilibrium orbit, R, and the momentum, p, are related by

$$p = eRH_{ef}/c, \tag{24a}$$

where H_{ef} the effective magnetic field is given by

$$H_{ef} = B_0(R/r_0)^K/b, \tag{24b}$$

$$b = \frac{2}{h_0 + [h_0^2 + 8h_1^2(K+\frac{3}{2})/N^2]^{1/2}} \quad . \tag{24c}$$

The equilibrium orbit is given by $r(\theta) = R(1+x(\theta))$ where

$$x(\theta) = (2bh_1/N^2)\cos(N\theta - (1/w)\ln(R/r_0) - \alpha_1) . \tag{25}$$

The radial tune, ν_x , is given by

$$\nu_x^2 = bh_0(K+2) - 1 + 4b^2h_1^2(K^2+3K+2)/N^2 . \tag{26}$$

The vertical tune, ν_y , is given by

$$\nu_y^2 = 2b^2(h_1^2 + h_2^2 + \ldots) - bh_0K + 2b^2h_1^2(2/w^2 + \tfrac{1}{4})/N^2 . \tag{27}$$

The beat factor, B_x , which gives the ratio of the largest amplitude of betatron oscillation to the smallest amplitude as one goes around the machine is related to β_x by

$$B_x = [\beta_{x,max}/\beta_{x,min}]^{\frac{1}{2}} . \tag{28}$$

B_x is given by

$$B_x = 1 + 4bh_1[(K+\tfrac{3}{2})^2 + 1/w^2]^{\frac{1}{2}}/(N^2 - 4\nu_x^2) . \tag{29}$$

The beat factor for the vertical betatron oscillations, B_y , is given by

$$B_y = 1 + 4bh_1[(K+\tfrac{1}{2})^2 + 1/w^2]^{\frac{1}{2}}/(N^2 - 4\nu_y^2) . \tag{30}$$

A comparison of the results given by the theory with results found by numerical integration of the equations is given in Table VIII for the tune and beat factors of the spiral sector model.

TABLE VIII. A comparison of the theoretical and computer results for the tune and beat factors of the spiral sector model.

	Computer	Theory
ν_x	1.40	1.32
ν_y	1.12	1.15
B_x	1.73	1.66
B_y	1.51	1.41

We will now give some theoretical results for the effects of field perturbations. No derivations of the results will be given here.

We assume that the magnetic field in the median plane for the unperturbed machine is written as

$$H_z = - \sum_{n = 0, \pm N, \pm 2N, \ldots} G_n(r) \exp(i n \theta) . \tag{31}$$

The harmonics $G_n(r)$ may also be written as

$$G_n(r) = H_n(r) \exp(-i \beta_n(r)) \tag{32}$$

where H_n and β_n are real. The effect of the perturbation on the median plane field is to change the field components by the amount ΔH_z, ΔH_r, ΔH_θ. We will first treat the case where only $\Delta H_z \neq 0$. This is a particularly important case as all deliberate perturbations like straight sections fall into this case.

We assume that the field perturbation ΔH_z is written as

$$\Delta H_z = -\sum_{n=-\infty}^{\infty} \Delta G_n(r) \exp(in\theta), \tag{33}$$

$$\Delta G_n(r) = \Delta H_n(r) \exp(-i\alpha_n(r)) \tag{34}$$

This field perturbation will affect the equilibrium orbit and the tune ν_x, ν_y. For the sake of simplicity, the results will not be presented in the most general or accurate form that has been obtained, but the results will be given for the particular case of the spiral sector model and for the perturbations that were introduced into this model. The following results should be accurate within about 20%.

The following assumptions will also be made. It will be assumed that the field gradient is large, which for the spiral sector machine means that $1/\nu \gg 1$. It will be assumed that the perturbing field does not shift the tune appreciably, that the unperturbed tune is not too close to the stop bands introduced by the perturbation, and that neither ν_x nor ν_y are close to $\frac{1}{2}N$.

We find the change in the equilibrium orbit. The effect of the perturbation on the equilibrium orbit can be broken down into two parts. There is the effect due to the harmonics of ΔH_z for $n = 0$, $\pm N$, $\pm 2N, \ldots$, and there is the effect due to the harmonics for which $n \neq 0$, $\pm N$, $\pm 2N, \ldots$. These two effects are calculated separately and the effect of the harmonics for $n = 0$, $\pm N$, $\pm 2N$ is treated first.

Let us consider an orbit of the unperturbed field which corresponds to the momentum p and the average radius R. p and R are related by

$$p = eRH_{ef}/c \tag{35a}$$

where H_{ef}, the effective field, is given by

$$H_{ef} = \frac{1}{2}\left[H_0 + \left(H_0^2 + 8H_N\left(RH_N' + \frac{3}{2}H_N\right)/N^2\right)^{1/2}\right] \tag{35b}$$

where H_0, H_N are evaluated at $r = R$ and the prime indicates differentiation with respect to r.

The equilibrium orbit corresponding to the particle momentum p is shifted by the amount $R\Delta x$, where R is the average radius of the equilibrium orbit of the unperturbed field.

We write $\Delta x(\theta)$ in Fourier series form as

$$\Delta x = \sum_n \Delta x_n \exp(in\theta). \tag{36}$$

The Δx_n for $n = 0, \pm N, \pm 2N \ldots$ are given by

$$\Delta x_n = (\Delta x_n)_1 + (\Delta x_n)_2, \tag{37a}$$

where

$$(\Delta x_0)_1 = -\frac{1}{\nu_x^2}\left\{\frac{eR}{pc}\Delta H_0 + 2\left(\frac{eR}{pc}\right)^2 \sum_{n>0}^{N} \frac{1}{n^2}\left(RH_n'\Delta H_n + R\Delta H_n' H_n + 3H_n\Delta H_n\right)\right\}, \tag{37b}$$

$$(\Delta \chi_n)_1 = \frac{eR}{pc} \frac{1}{n^2} \left[\Delta G_n + (R G_n' + 2G_n)(\Delta \chi_0)_1 \right], \tag{37c}$$

for $n = \pm N, \pm 2N \ldots$.

$$(\Delta \chi_n)_2 = \frac{1}{n^2 - \nu_\chi^2} \sum_m{}' \frac{\Delta G_{n+m}}{(m+n)^2 - \nu_\chi^2} (R \Delta G_{-m}' + 2 \Delta G_{-m}) \tag{37d}$$

$$+ \frac{1}{n^2 - \nu_\chi^2} \frac{1}{2} \sum_s^N \left[(R^2 G_s'' + 2 R G_s' + 2 G_s) \sum_m{}' \Delta \chi_m \Delta \chi_{-s-m} \right].$$

In Eqs. (37), $\sum_s^N$ signifies a sum over $s = 0, \pm N, \pm 2N \ldots$ and $\sum_m{}'$ signifies a sum over m but omitting $m = 0, \pm N, \pm 2N \ldots$ The $\Delta \chi_m$ for $m \neq 0, \pm N, \pm 2N$ are given below.

We may note that the $(\Delta \chi_n)_1$ are due to the harmonics ΔG_n for which $n = 0, \pm N, \ldots$ and the $(\Delta \chi_n)_2$ are due to the harmonics for which $n \neq 0, \pm N, \ldots$ The G_n and ΔG_n are to be evaluated at $r = R$.

For $n \neq 0, \pm N, \ldots$ we find

$$\Delta \chi_n = a_n - \sum_{s \neq 0}^N \frac{g_s}{s(-s+2n)} a_{n-s}, \tag{38a}$$

where

$$a_n = \frac{1}{n^2 - \nu_x^2}\Big[\frac{eR}{pc}\,\Delta G_n + \frac{eR}{pc}\sum_{s\neq 0}^{N} \chi_s \left(R\,\Delta G'_{n-s} + 2\,\Delta G_{n-s}\right) - \sum_{s\neq 0}^{N} \frac{eR}{pc}\,\Delta G_{n+s}\,\frac{g_{-s}}{s(s+2n)}\Big], \tag{38b}$$

$$g_s = -\frac{eR}{pc}\left(R\,G'_s + \frac{3}{2}\,G_s\right), \tag{38c}$$

$$\chi_s = \frac{1}{s^2}\,\frac{eR}{pc}\,G_s\,. \tag{38d}$$

Equation (38a) is not valid for $n = \frac{1}{2}N$, and we find for the case $n = \frac{1}{2}N$,

$$\Delta\chi_n = \frac{eR}{pc}\,\Delta G_n\,\exp[i(\gamma_N + \alpha_n)]\Big[\frac{\cos(\gamma_N + \alpha_n)}{n^2 - \nu_x^2 - |g_N|} - i\,\frac{\sin(\gamma_N + \alpha_n)}{n^2 - \nu_x^2 + |g_N|}\Big], \tag{38e}$$

where γ_N is the phase of the complex number g_N.

The second term in Eq. (38a) is usually of the order of 10% of the first term and may be neglected unless the first term is absent.

A somewhat simplified but useful expression for the oscillatory part of the equilibrium orbit is given by

$$\Delta\chi(\theta) = A\sum_n \frac{eR}{pc}\,\frac{1}{n^2 - \nu_x^2}\,\Delta G_n\,\exp(in\theta), \tag{39a}$$

$$A = 1 + |g_N|^2/(N^2 - 4\nu_x^2). \tag{39b}$$

We will now treat the general case where we have not only a ΔH_z but also a ΔH_r and ΔH_θ perturbations. Usually such perturbations are accidental and the exact form of the perturbation is not known. Also, the r and z motions are now coupled. Instead of having an r- tune and a z-tune, one now has two normal modes whose tunes we may still label as ν_x and ν_y since one mode is predominantly r - motion and the other is predominantly z-motion.

The equilibrium orbit corresponding to the particle momentum is shifted by the amount $R\Delta x$ and $R\Delta y$ The radial shift is given by Eqs (37), (38), and (39). The vertical shift is given by

$$\Delta y = -B \frac{ek}{p_c} \sum_n \frac{1}{n^2 - \nu_y^2} \Delta G_{r,n} \exp(in\theta), \tag{40a}$$

$$B = 1 + \frac{1}{1 - (2\nu_y/N)^2} \frac{|f_N|^2}{N^2}, \tag{40b}$$

$$f_N = \frac{eR}{p_c} \left| R G_N' + \frac{1}{2} G_N \right|, \tag{40c}$$

and we represent the perturbation ΔH_r as

$$\Delta H_r = -\sum_n G_{r,n}(r) \exp(in\theta). \tag{40d}$$

The above result for Δy holds if the perturbation does not change the tune very much in the same manner as was assumed in the case of a pure ΔH_z perturbation.

We will now apply the above theoretical results to the various field perturbations that were introduced into the spiral sector model.

Sector Bump

A bump that was applied to the radial sector model was to decrease the field in one sector by 7%. To apply the results given above we must first calculate the ΔG_n due to the perturbation. The ΔG_n are given by

$$\Delta G_n = \frac{1}{2\pi} \int_0^{2\pi} d\theta \, \exp(-in\theta) \, \Delta H_z(r, \theta) \, . \tag{41}$$

For the spiral sector model we may write the unperturbed field as

$$H_z = -B_0 (r/r_1)^K \; h(\theta, r) \, , \tag{42a}$$

$$h(\theta, r) = \sum_n h_n \exp\left[inN\left(\theta - (1/w-N)\ln(r/r_1)\right)\right] , \tag{42b}$$

and the perturbation may be written as

$$\Delta H_z = -B_0 (r/r_1)^K \; \Delta h(\theta, r) \, , \tag{43}$$

where Δh is different from zero in only one sector and reduces the field by 7% in that sector.

An approximate result for ΔG_n, valid for $n \ll N$, is

$$\Delta G_n = B_0 \left(\frac{r}{r_1}\right)^k \exp\left[-\frac{in}{wN} \ln \frac{r}{r_1}\right] \frac{(\Delta h)_{av}}{N}, \tag{44}$$

Δh_{av} being the average value of Δh over the sector where it is not zero.

One may also note that for this unperturbed machine

$$(eR/p_0) \simeq 1/G_0 \tag{45}$$

Using these results for ΔG_n one now computes the shift in the orbit and tune.

The change in the equilibrium orbit shown in Fig. 26 may be easily understood. Since the tune $\nu_x = 1.40$, the orbit shift is primarily due to the first and second harmonics of the perturbing field. The theoretical curve in Fig. 26 only takes into account the first and second harmonics, and including the higher harmonics would have improved the agreement with experiment Equation (39) was used to calculate the equilibrium orbit

ΔK Bump

In this bump, K was changed in one sector from $K = .7$ to $K = .8$. The value of the magnetic field was unchanged at $r = 25$ cms and the measurements were made at $r = 37$ cms.

We can write the unperturbed field as

$$H_z = -B_0 (r/r_1)^k \, h(\theta, r), \tag{46}$$

where $r_1 = 25$ cms. and the perturbed field as

$$\bar{H}_z = -B_1 (r/r_1)^{K'} h(\theta, r) , \tag{47}$$

where $K' = K + \Delta K$ and $\Delta K = .1$ in one sector, $\Delta K = 0$ in the other five sectors

The field perturbation $\Delta H_z = \bar{H}_z - H_z$ is then given by

$$\Delta H_z = -B_1 (r/r_1)^K \Delta K \ln(r/r_1) h(\theta, r) , \tag{48}$$

where we have expanded in powers of keeping just the lowest term

This perturbation ΔH_z has the same form as the perturbation for the 7% sector bump where $\Delta h(\theta, r)$ is given by

$$\Delta h(\theta, r) = \Delta K \ln(r/r_1) h(\theta, r) \tag{49}$$

This ΔK bump then shifts the equilibrium orbit in the same way as a sector bump where the field is changed by the fraction $\Delta K \ln(R/r_1)$ where R is the radial distance to the point of measurement.

Vertical Displacement Bump

In this bump a magnet was raised 1 mm. Raising a magnet introduces a radial component ΔH_r, in the magnetic field in the median plane ΔH_r is given by

$$\Delta H_r = - \left. \frac{\partial H_z}{\partial r} \right|_{z=0} \Delta z , \tag{50}$$

in the sector where the magnet is raised, and Δz is the distance the magnet is raised.

If we write the unperturbed field as

$$H_z = -B_0 (r/r_1)^K \; h(\theta, r), \tag{51a}$$

$$h(\theta, r) = 1 + f \cos(N\theta - (i/w) \ln(r/r_1)), \tag{51b}$$

then

$$\Delta H_r = \frac{\Delta z}{r} B_0 \left(\frac{r}{r_1}\right)^K \left\{ \frac{f}{w} \sin\left[N\theta - \frac{1}{w} \ln \frac{r}{r_1}\right] \right. \tag{52}$$

$$\left. + K \left(1 + f \cos\left[N\theta - \frac{1}{w} \ln \frac{r}{r_1}\right]\right) \right\}.$$

We find $\Delta G_{r,n}$ from

$$\Delta G_{r,n} = -\frac{1}{2\pi} \int_0^{2\pi} d\theta \; \exp(-in\theta) \Delta H_r . \tag{53}$$

An approximate result for $\Delta G_{r,n}$ is

$$\Delta G_{r,n} = -\frac{\Delta z}{r} B_0 \left(\frac{r}{r_1}\right)^K \left[\frac{K}{N} h_{av} \right. \tag{54a}$$

$$\left. - i \frac{n\pi}{2N^2} \left| \frac{\partial h}{\partial r} \right|_{av} \right] \exp\left[-\frac{i n}{wN} \ln \frac{r}{r_1}\right],$$

$$h_{av} \simeq \frac{2}{3} (1 + f), \tag{54b}$$

$$\left| \frac{\partial h}{\partial r} \right|_{av} \simeq \frac{2}{3} f/w . \tag{54c}$$

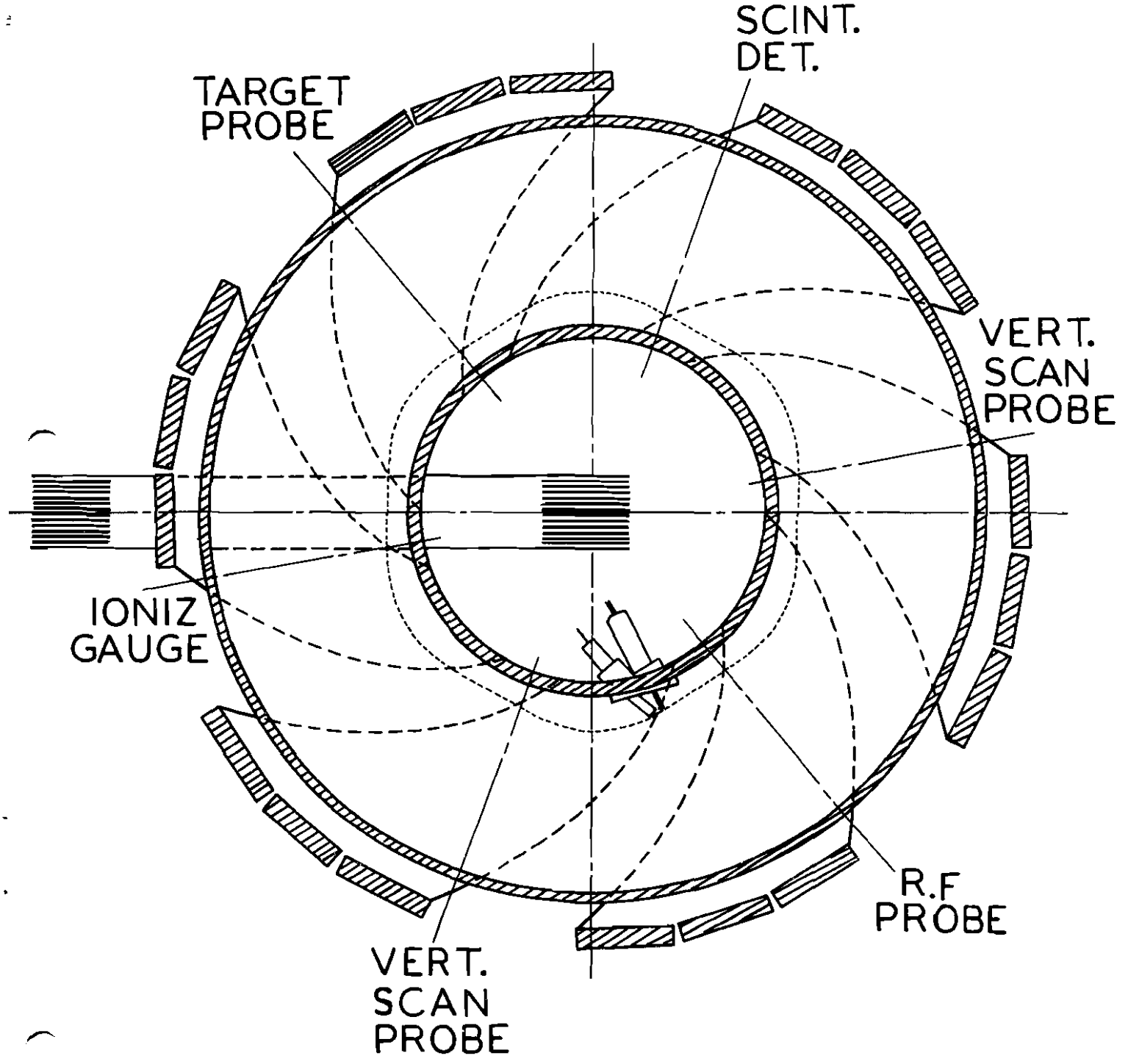
SCINT.
DET.
TARGET
PROBE
VERT.
SCAN
PROBE
IONIZ
GAUGE
R.F
PROBE
VERT.
SCAN
PROBE

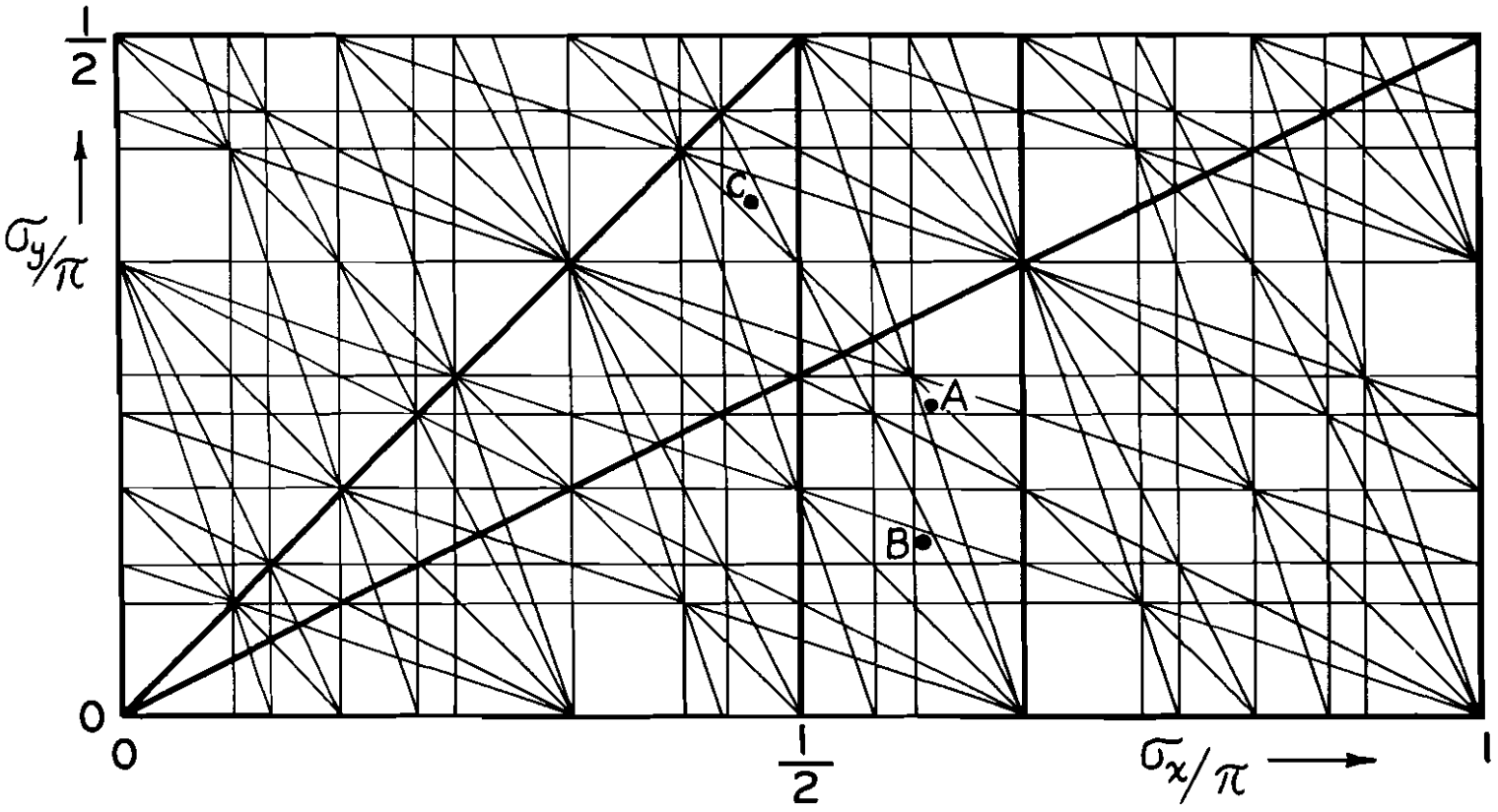
1/2
σy/π
0
0
1/2
σx/π
1
A
B
C

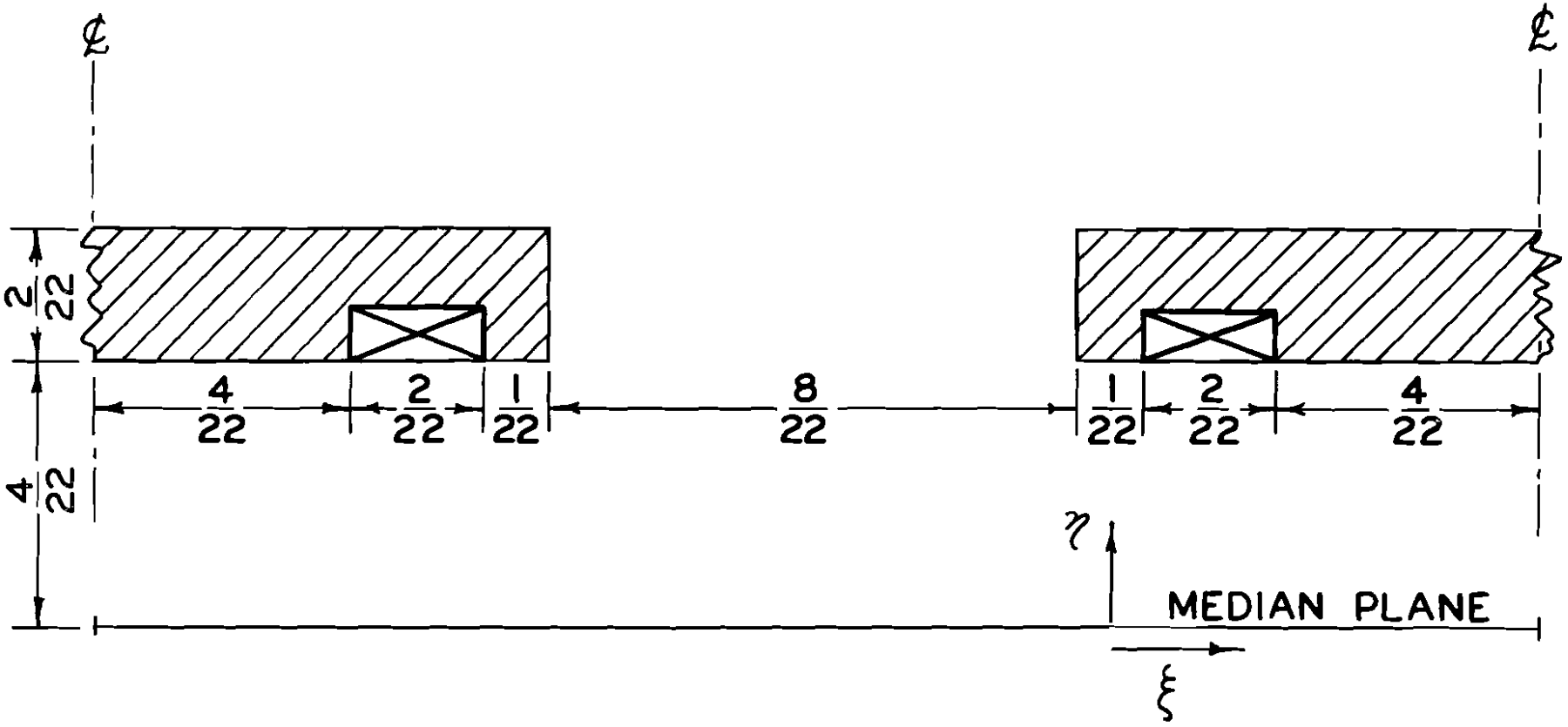
℄
℄
2/22
4/22
4/22
2/22
1/22
8/22
1/22
2/22
4/22
η
MEDIAN PLANE
ξ

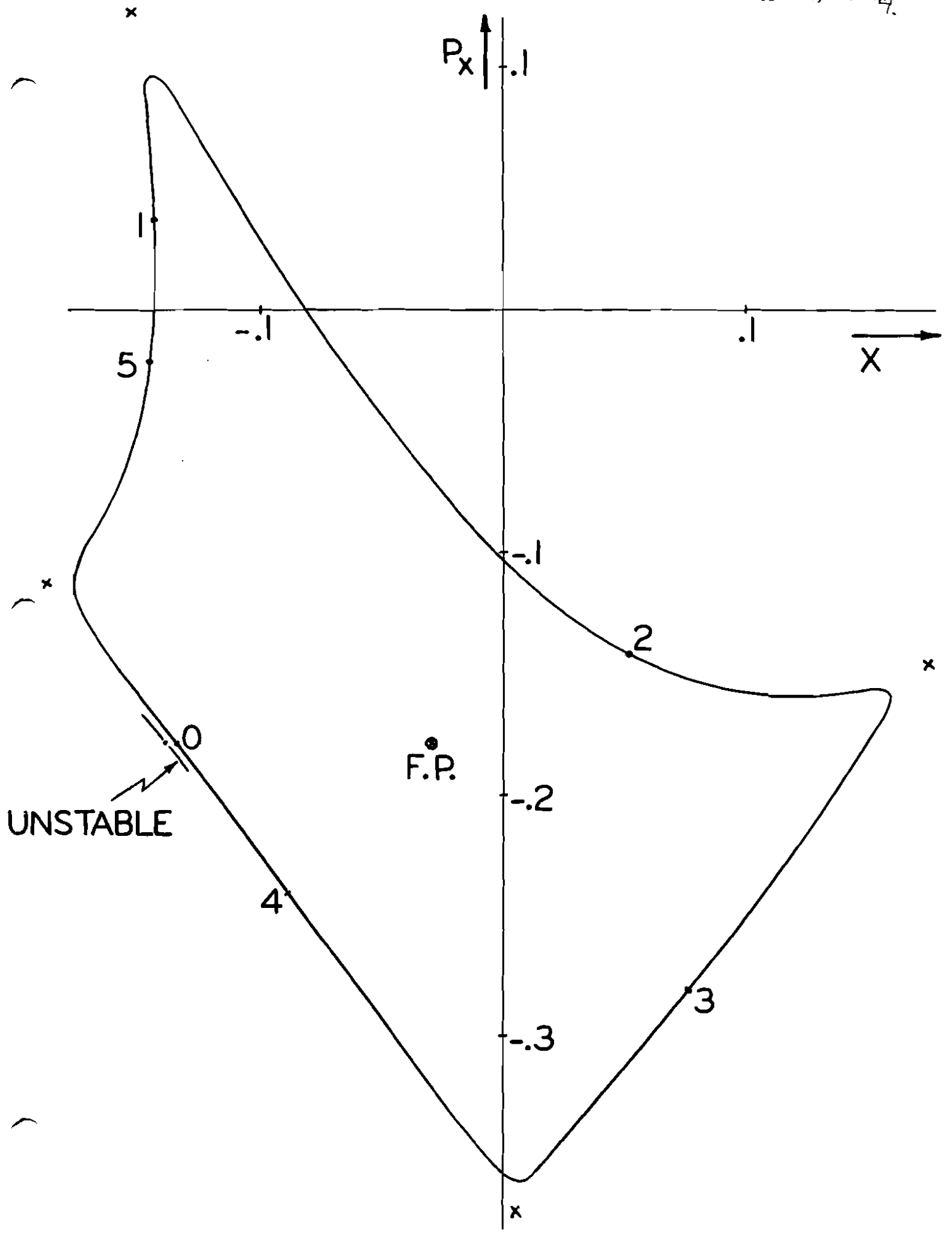
P_x
.1
1
-.1
.1
X
5
-.1
2
0
F.P.
-.2
UNSTABLE
4
3
-.3

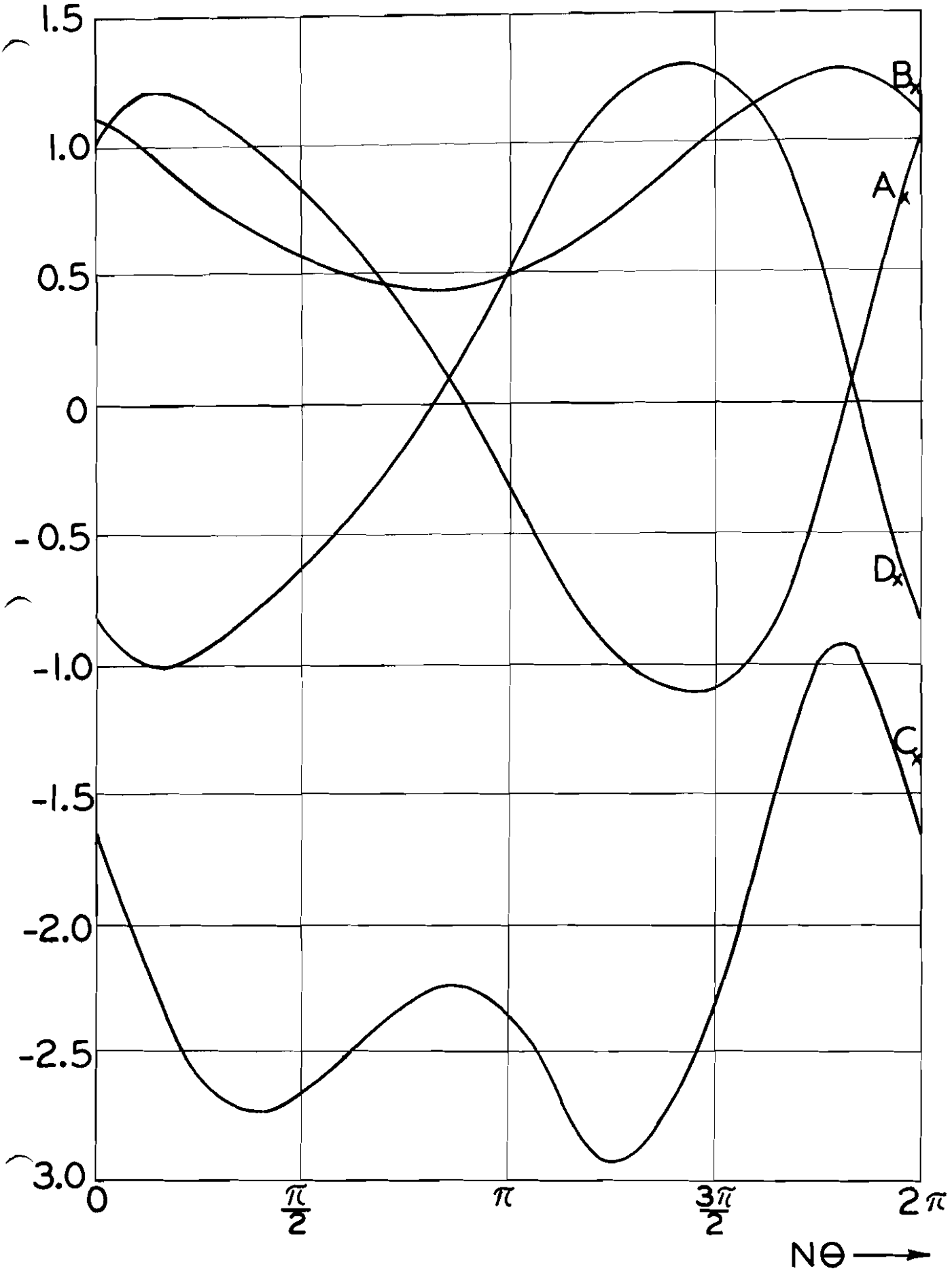
1.5
1.0
0.5
0
-0.5
-1.0
-1.5
-2.0
-2.5
-3.0
0
π/2
π
3π/2
2π
Nθ
B_x
A_x
D_x
C_x

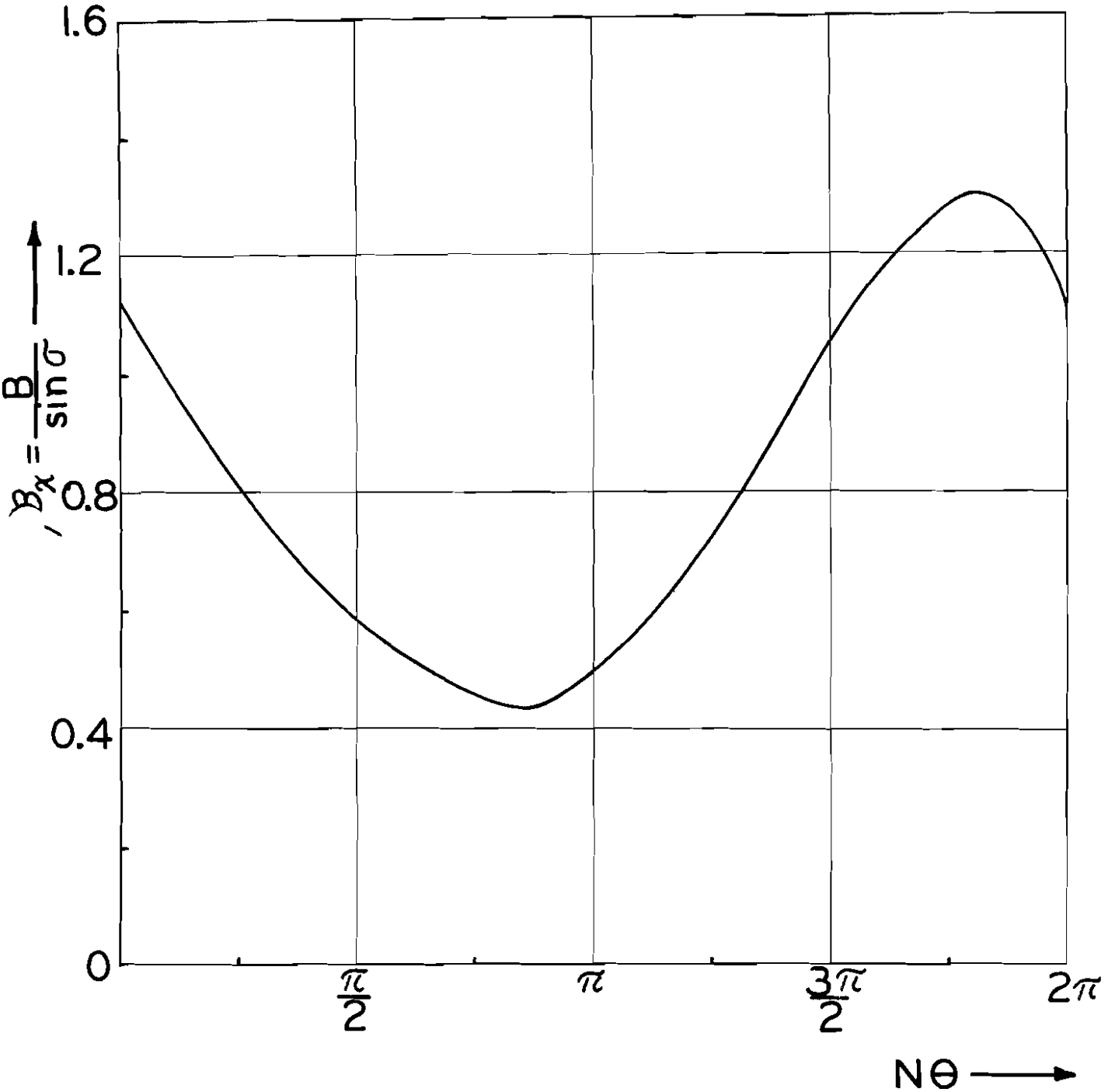
1.6
1.2
0.8
0.4
0
$B_x = \frac{B}{\sin\sigma}$
$\frac{\pi}{2}$
π
$\frac{3\pi}{2}$
2π
$N\theta$

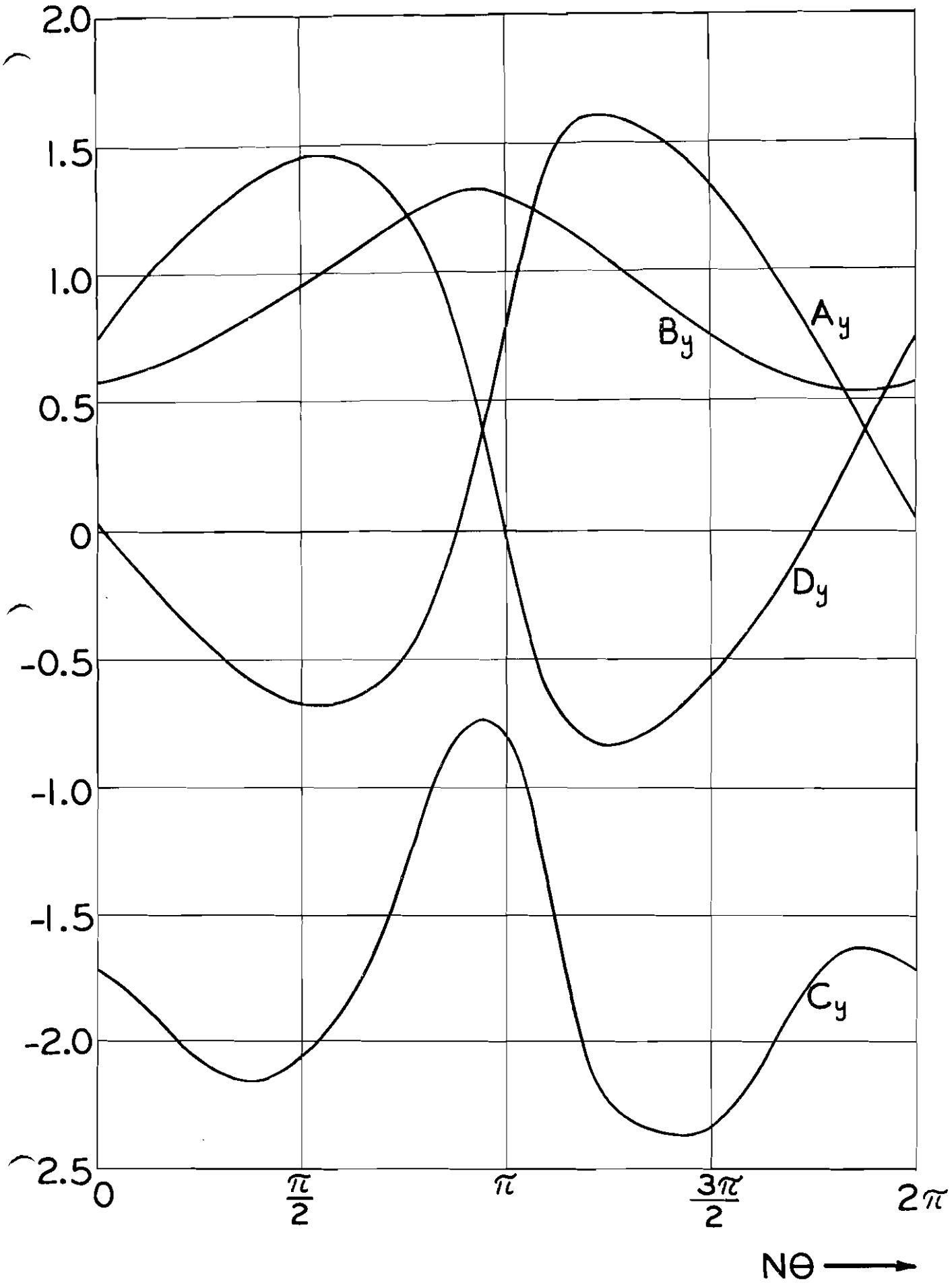
2.0
1.5
1.0
0.5
0
-0.5
-1.0
-1.5
-2.0
-2.5
0
π/2
π
3π/2
2π
Nθ
A_y
B_y
C_y
D_y

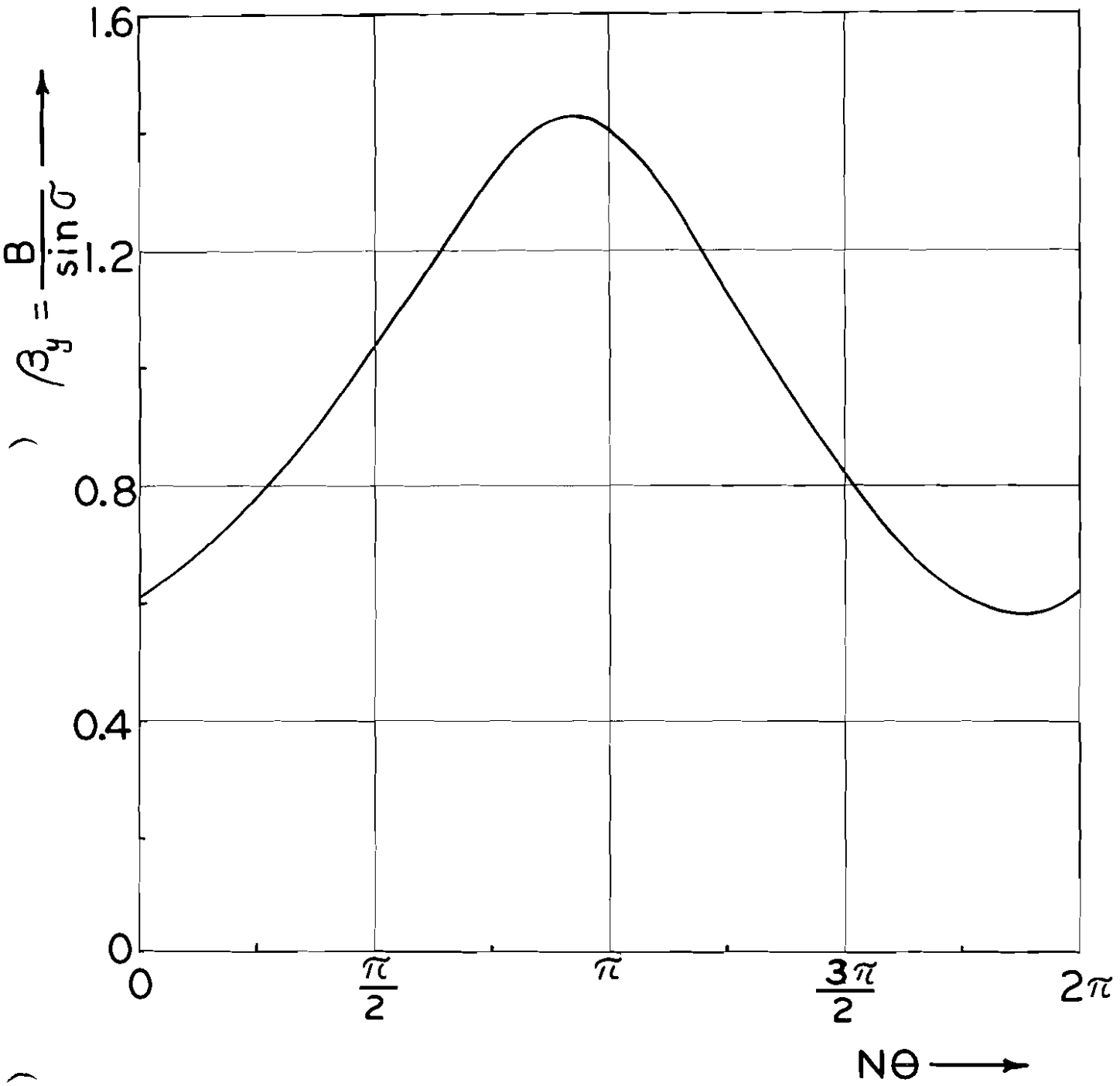
1.6
1.2
0.8
0.4
0
$\beta_y = \frac{B}{\sin\sigma}$
0
$\frac{\pi}{2}$
π
$\frac{3\pi}{2}$
2π
$N\theta$

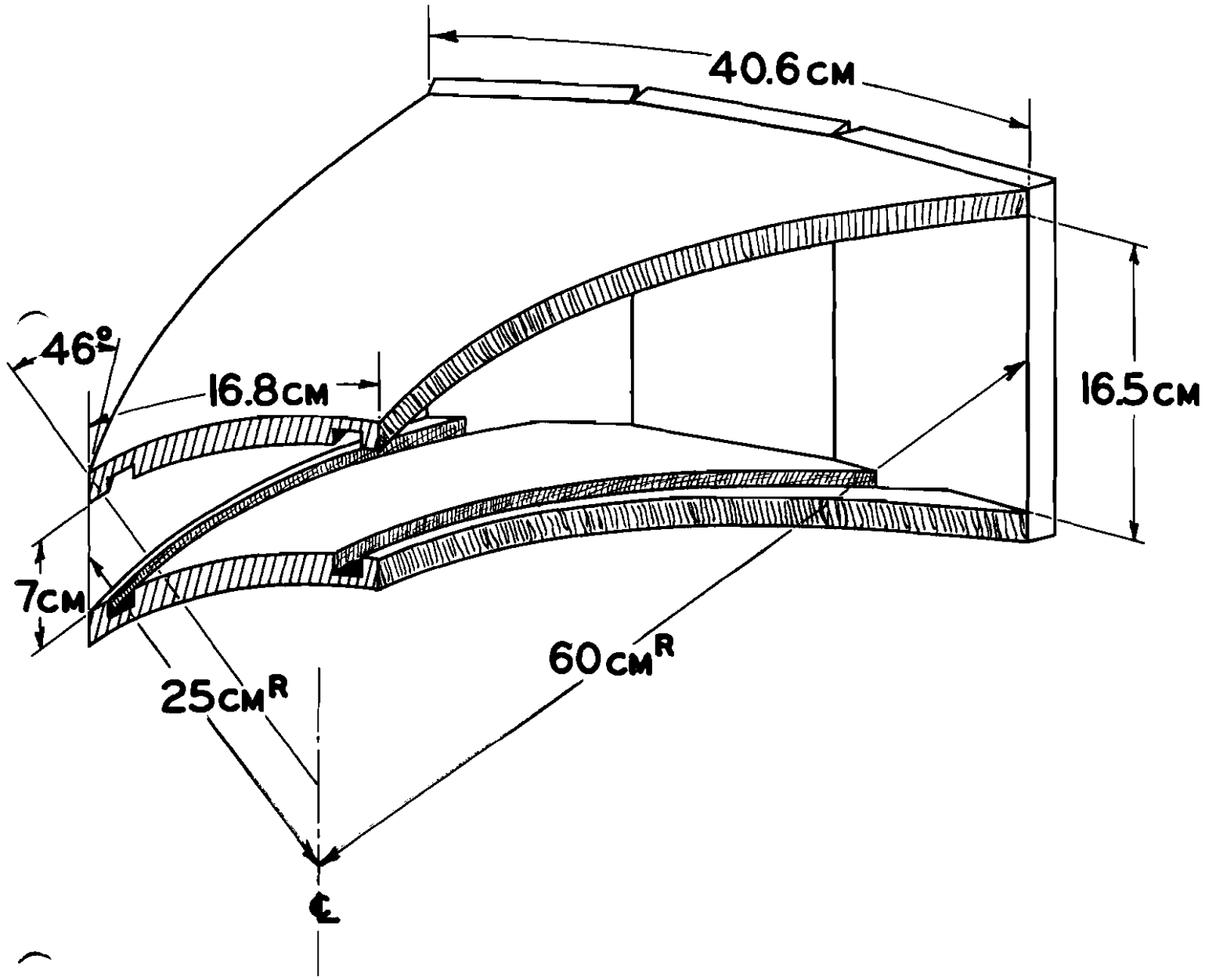
40.6 CM
46°
16.8 CM
16.5 CM
7 CM
60 CM R
25 CM R
℄

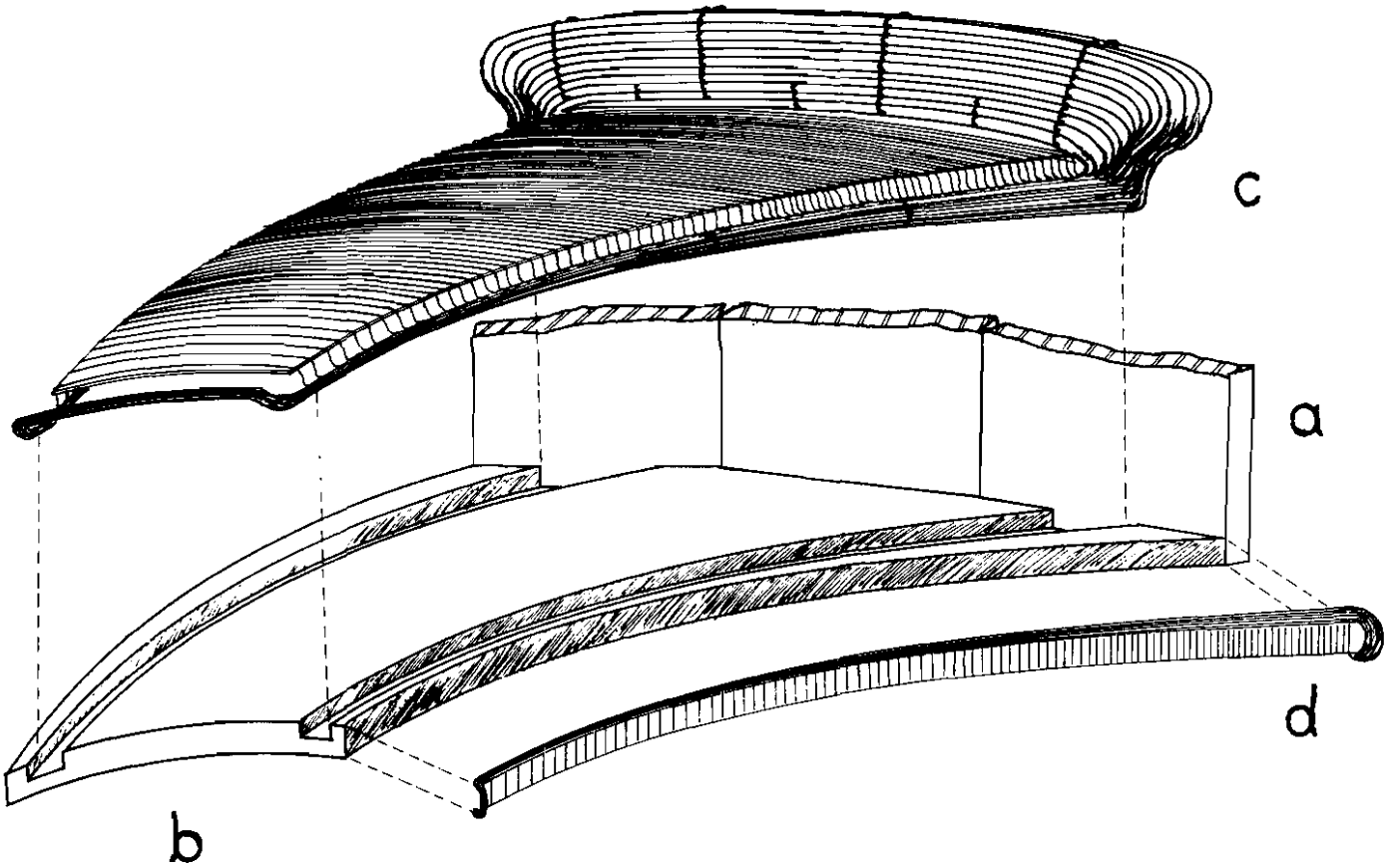
c
a
d
b

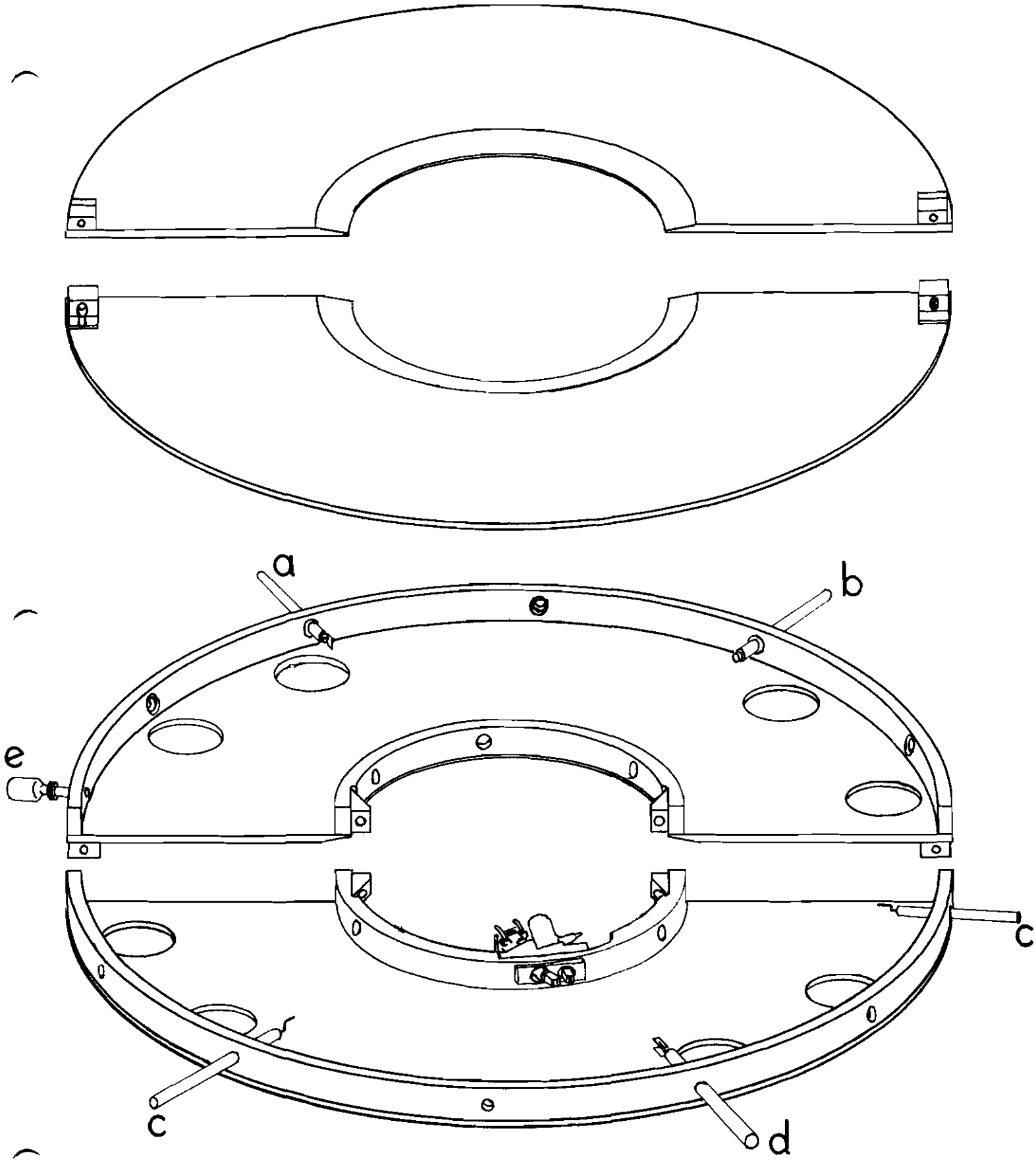
a
b
e
c
c
d

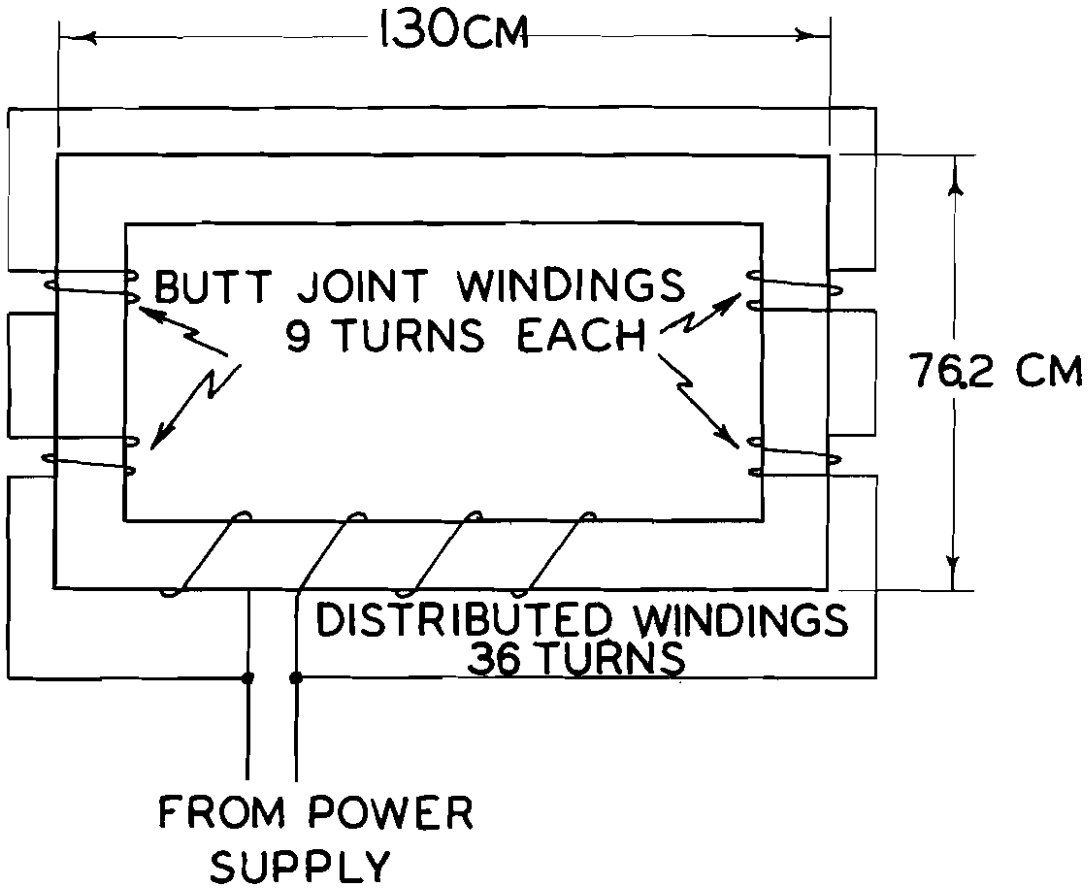
130CM
BUTT JOINT WINDINGS
9 TURNS EACH
76.2 CM
DISTRIBUTED WINDINGS
36 TURNS
FROM POWER
SUPPLY

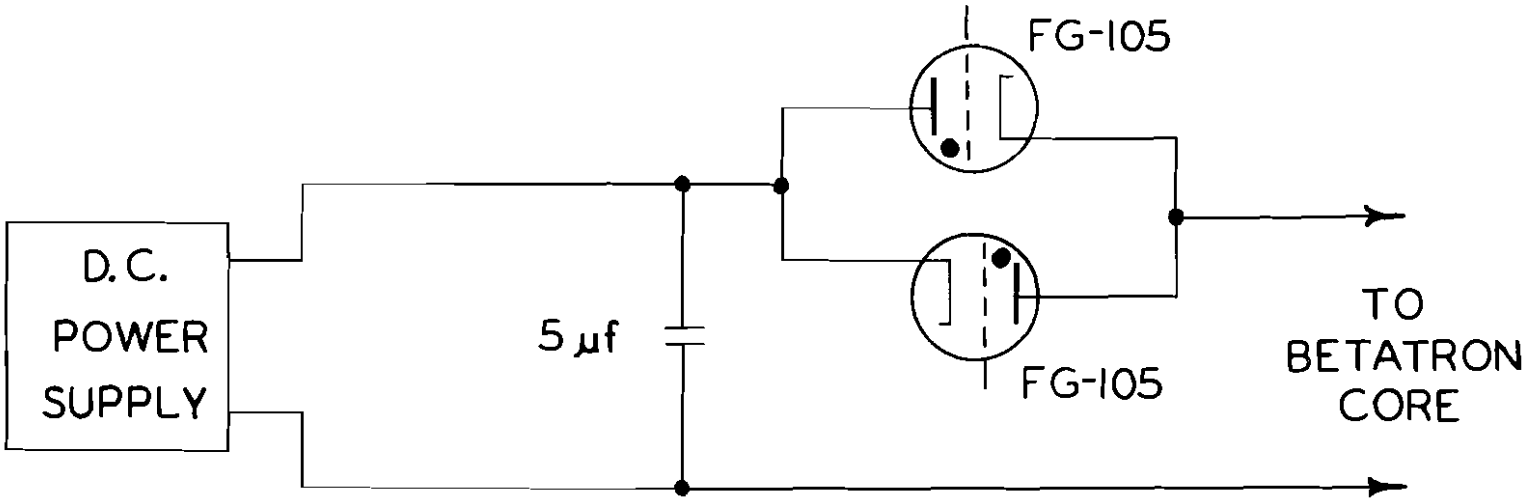
FG-105
D.C.
POWER
SUPPLY
5 μf
FG-105
TO
BETATRON
CORE

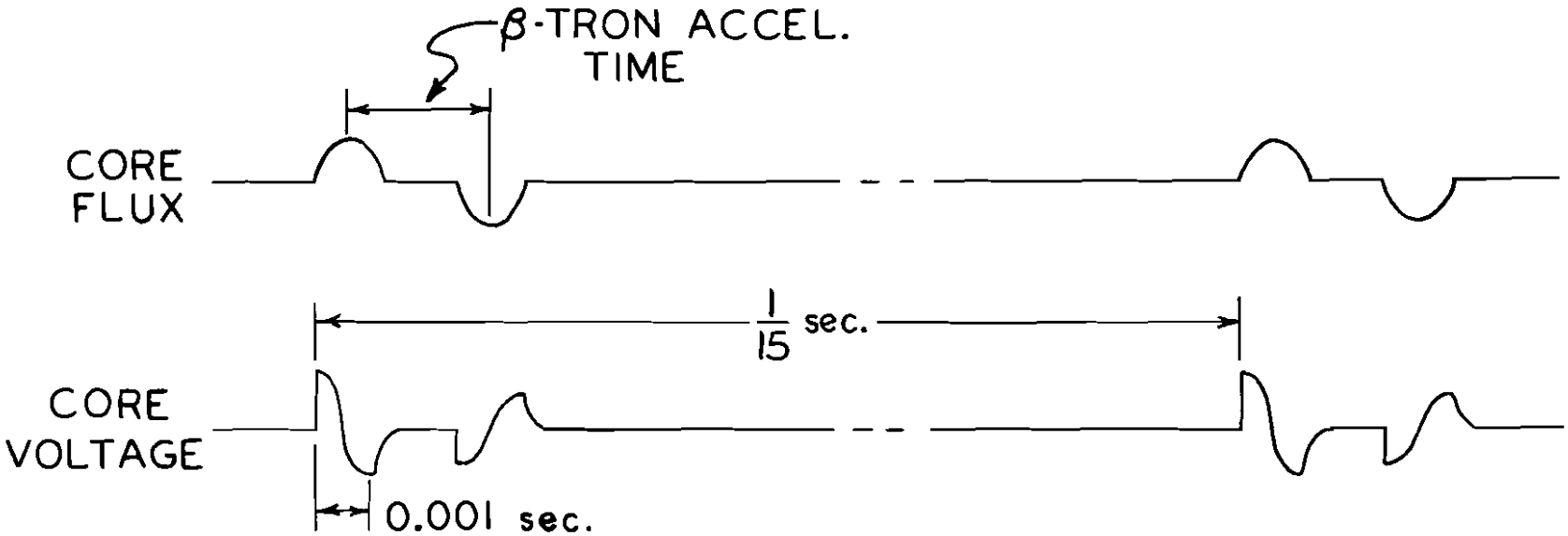
β-TRON ACCEL.
TIME
CORE
FLUX
1/15 sec.
CORE
VOLTAGE
0.001 sec.

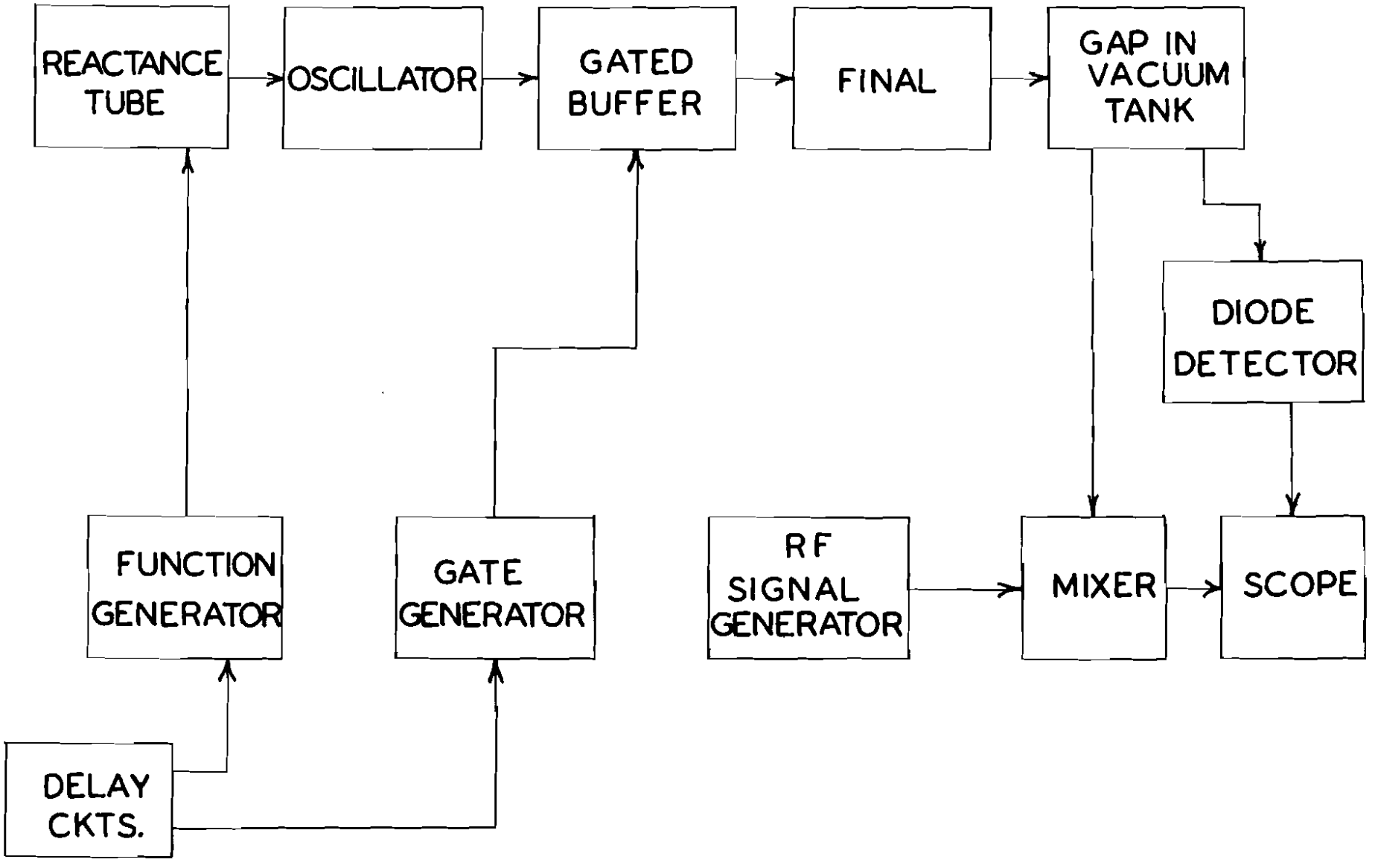
REACTANCE TUBE
OSCILLATOR
GATED BUFFER
FINAL
GAP IN VACUUM TANK
DIODE DETECTOR
FUNCTION GENERATOR
GATE GENERATOR
RF SIGNAL GENERATOR
MIXER
SCOPE
DELAY CKTS.

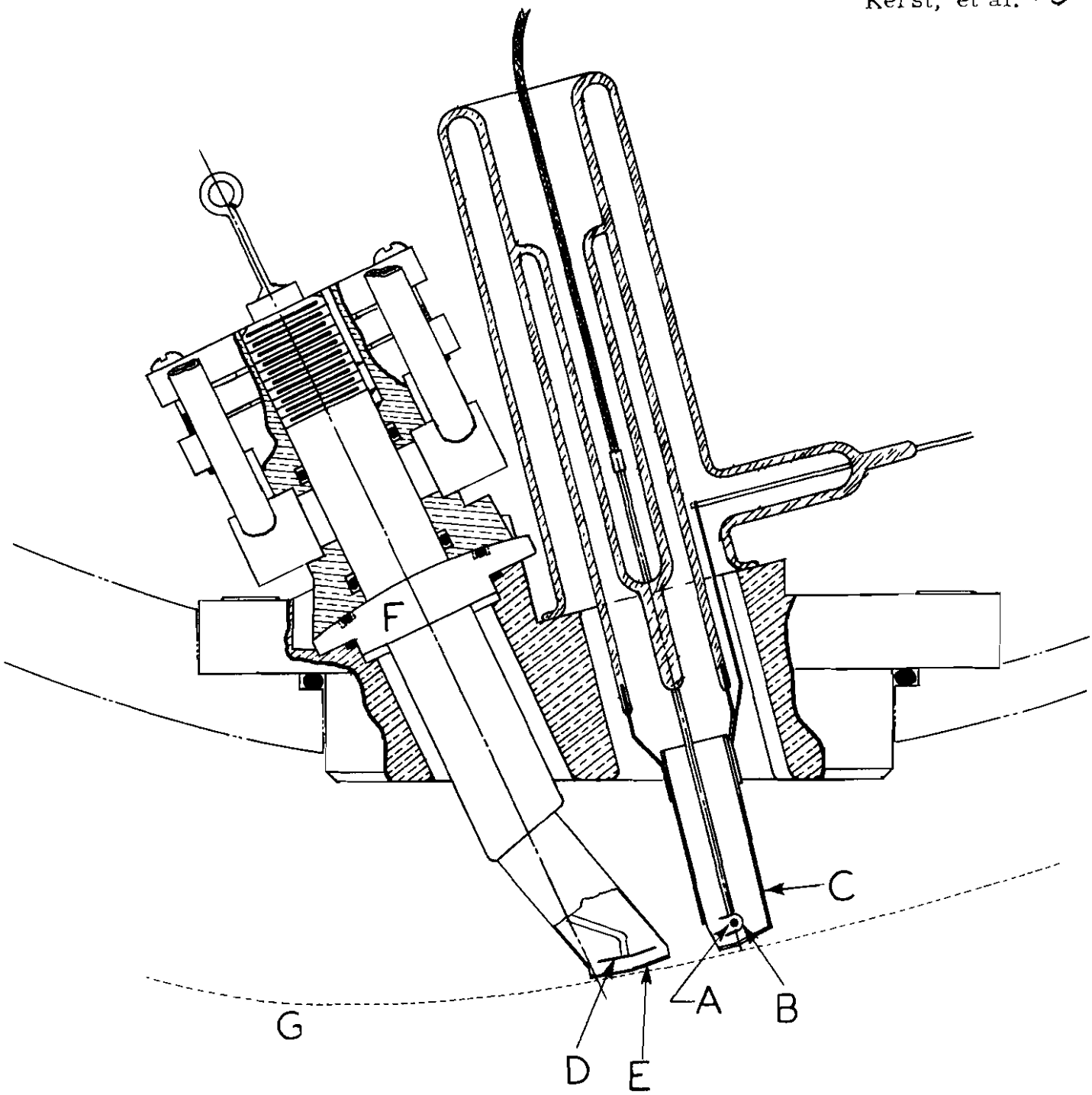
F
C
A
B
G
D
E

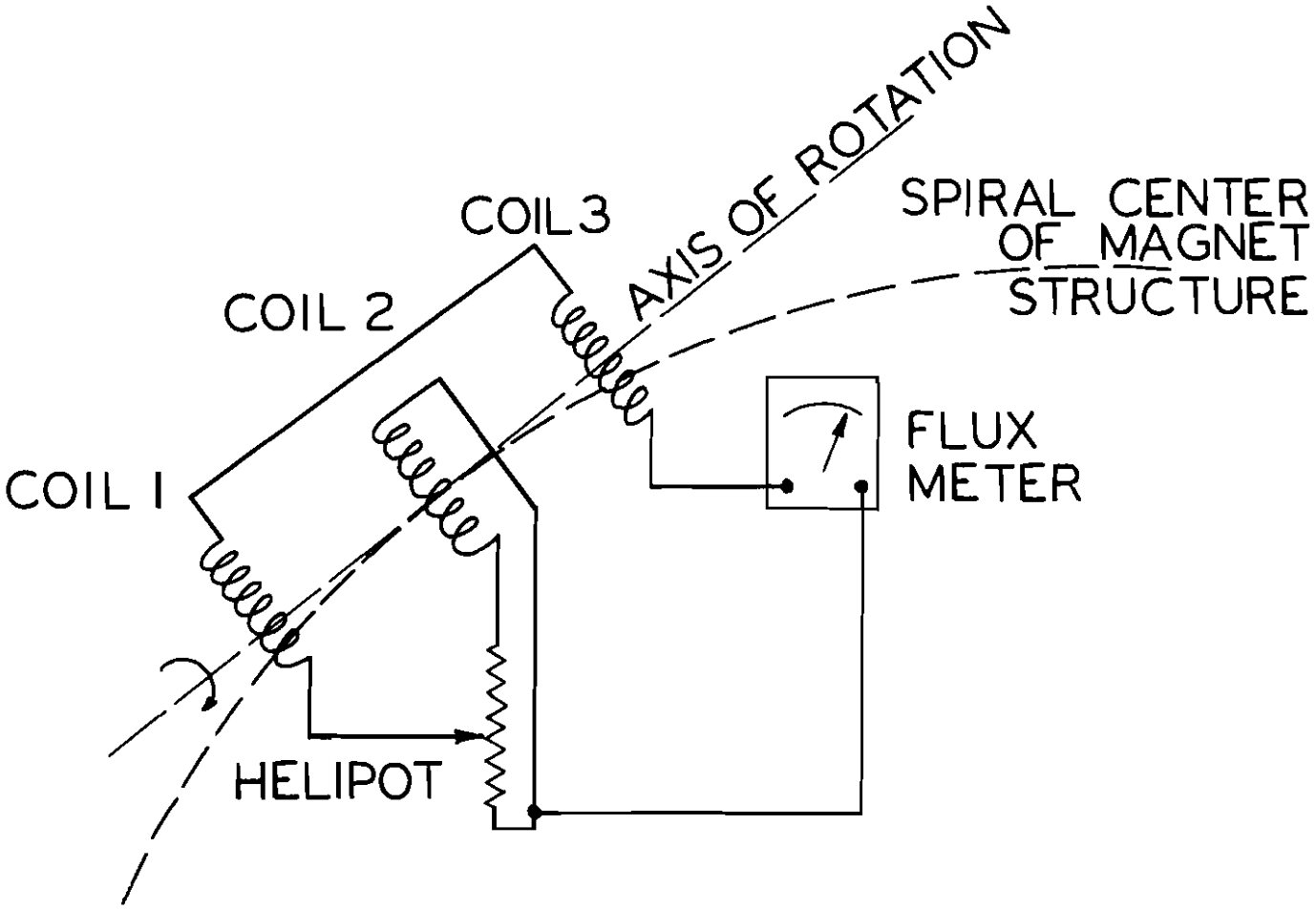
AXIS OF ROTATION
SPIRAL CENTER OF MAGNET STRUCTURE
COIL 3
COIL 2
COIL 1
FLUX METER
HELIPOT

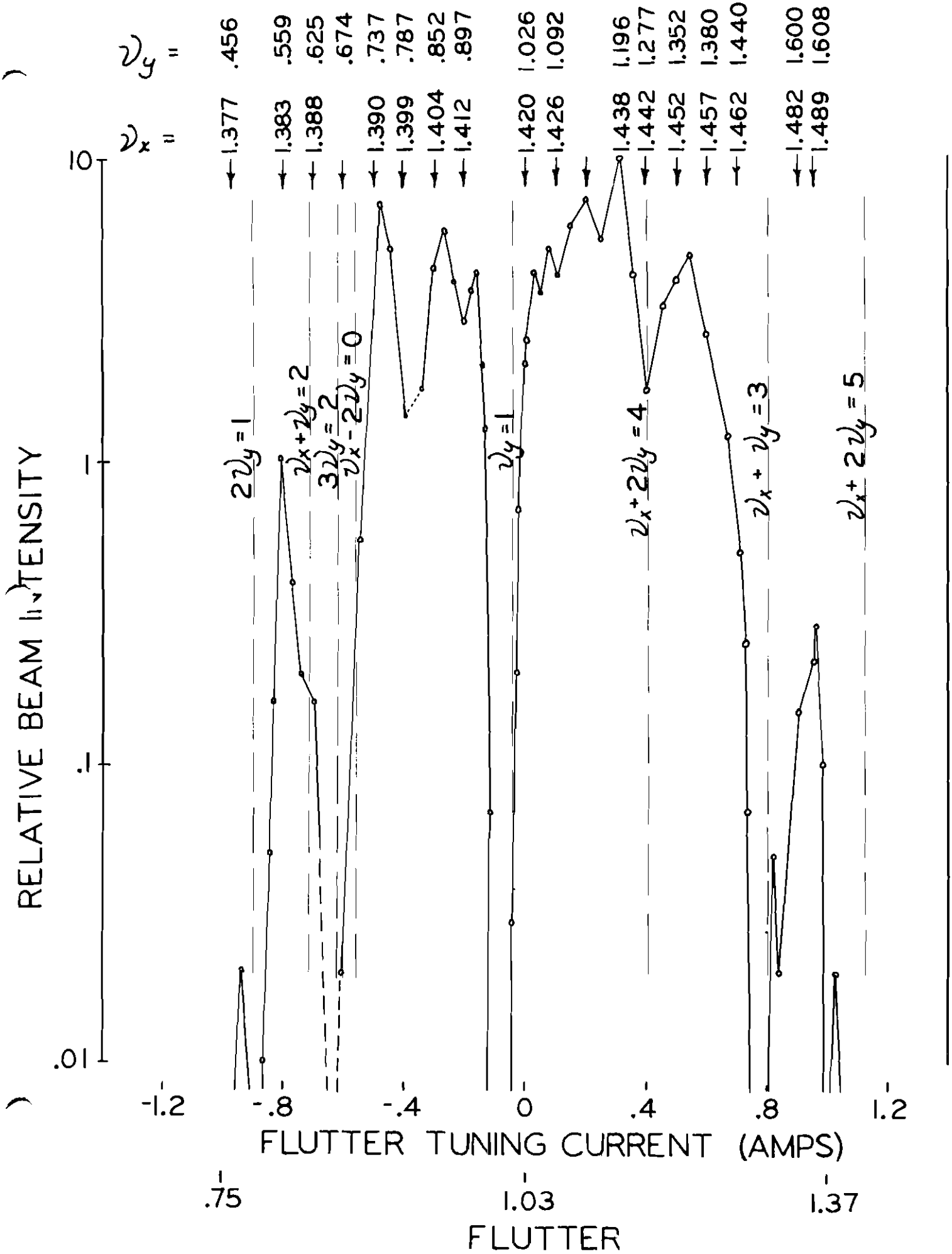
ν_y = .456 .559 .625 .674 .737 .787 .852 .897 1.026 1.092 1.196 1.277 1.352 1.380 1.440 1.600 1.608
ν_x = 1.377 1.383 1.388 1.390 1.399 1.404 1.412 1.420 1.426 1.438 1.442 1.452 1.457 1.462 1.482 1.489
$2\nu_y = 1$
$\nu_x + \nu_y = 2$
$3\nu_y = 2$
$\nu_x - 2\nu_y = 0$
$\nu_y = 1$
$\nu_x + 2\nu_y = 4$
$\nu_x + \nu_y = 3$
$\nu_x + 2\nu_y = 5$
RELATIVE BEAM INTENSITY
10
1
.1
.01
-1.2
-.8
-.4
0
.4
.8
1.2
FLUTTER TUNING CURRENT (AMPS)
.75
1.03
1.37
FLUTTER

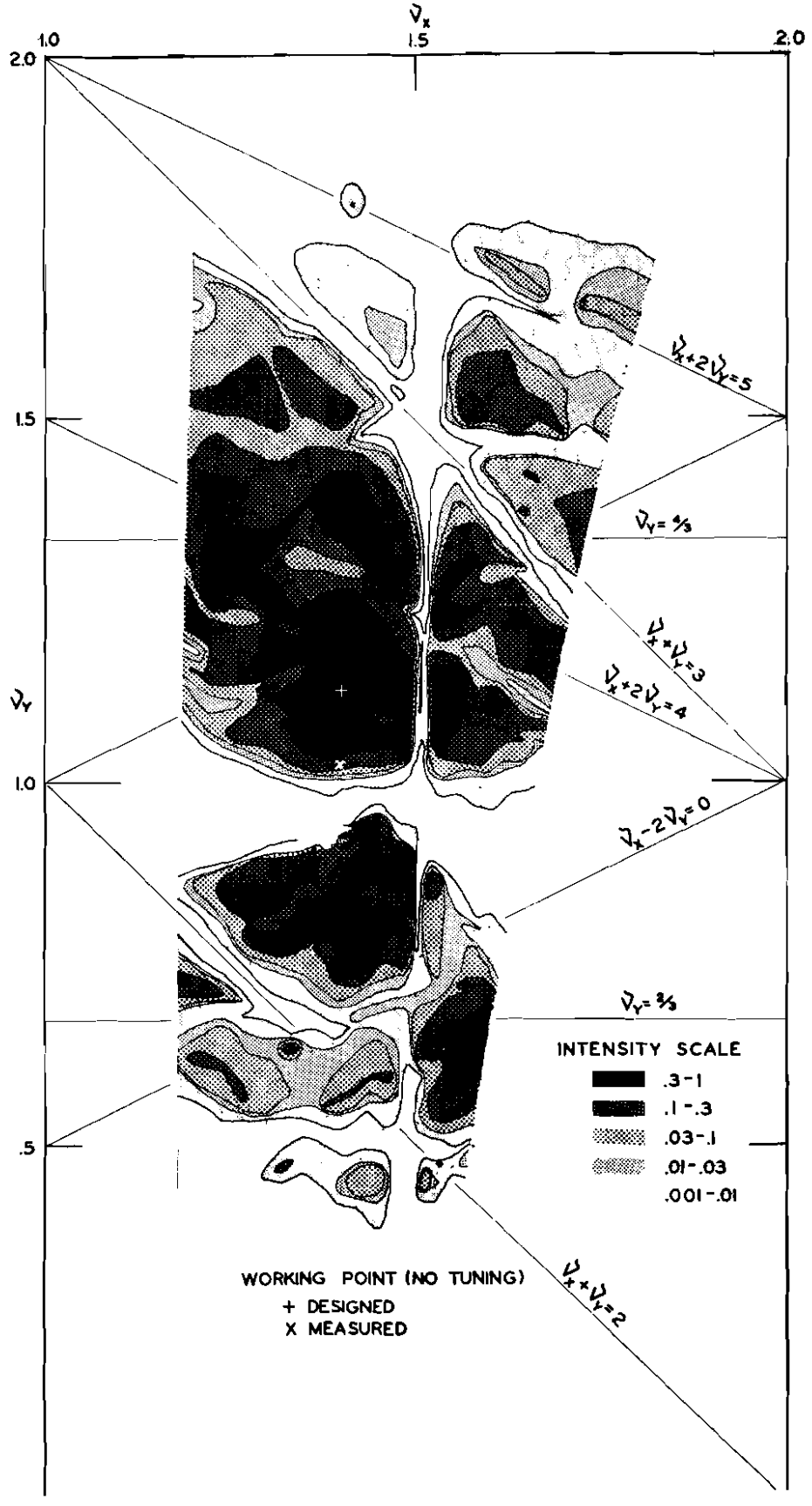
ν_x
1.0
1.5
2.0
2.0
1.5
1.0
.5
ν_y
$\nu_x+2\nu_y=5$
$\nu_y=4/3$
$\nu_x+\nu_y=3$
$\nu_x+2\nu_y=4$
$\nu_x-2\nu_y=0$
$\nu_y=2/3$
$\nu_x+\nu_y=2$
INTENSITY SCALE
.3-1
.1-.3
.03-.1
.01-.03
.001-.01
WORKING POINT (NO TUNING)
+ DESIGNED
X MEASURED

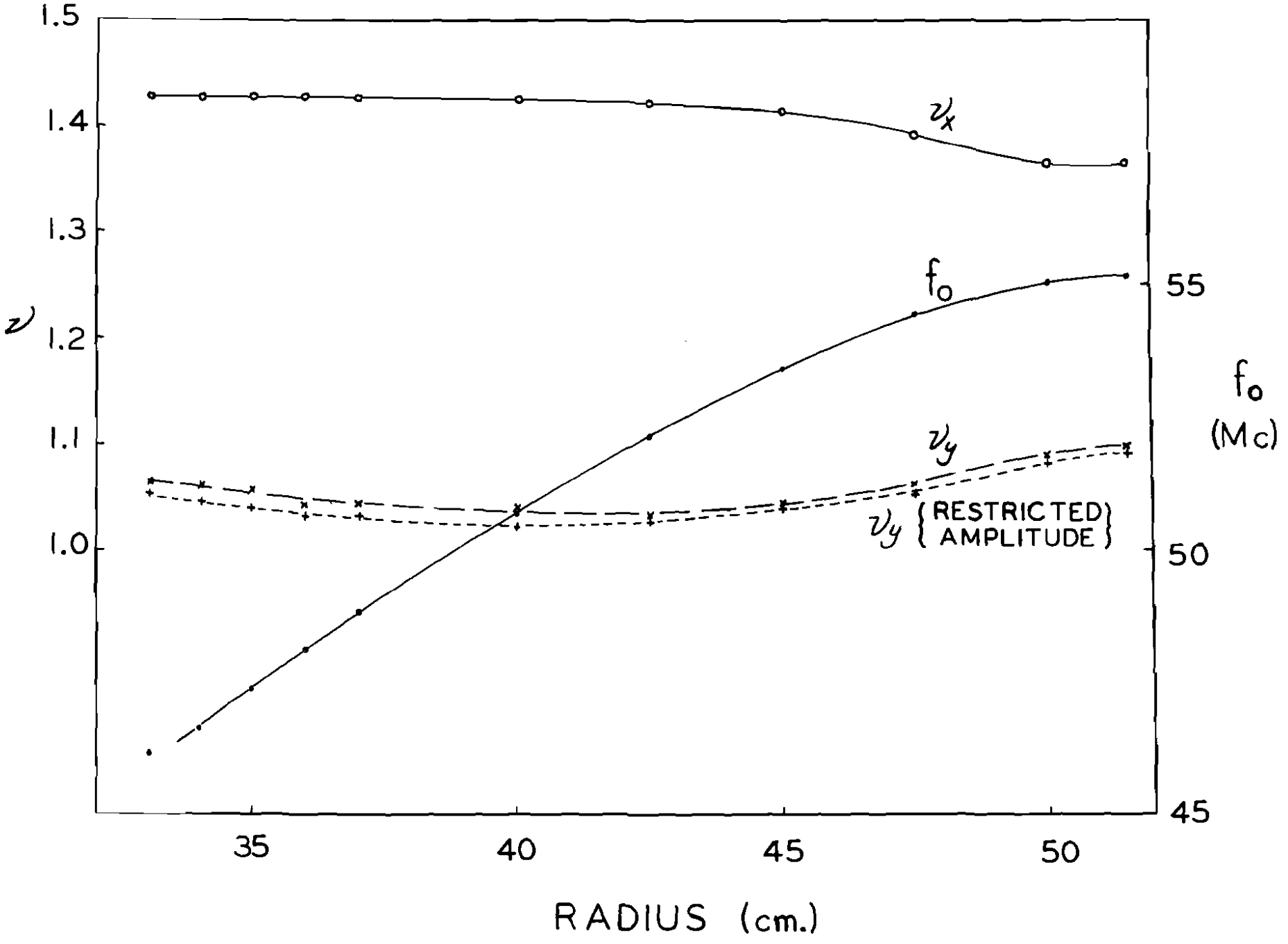
1.5
1.4
1.3
1.2
1.1
1.0
ν
35
40
45
50
RADIUS (cm.)
55
50
45
f₀
(Mc)
νx
f₀
νy
νy {RESTRICTED AMPLITUDE}

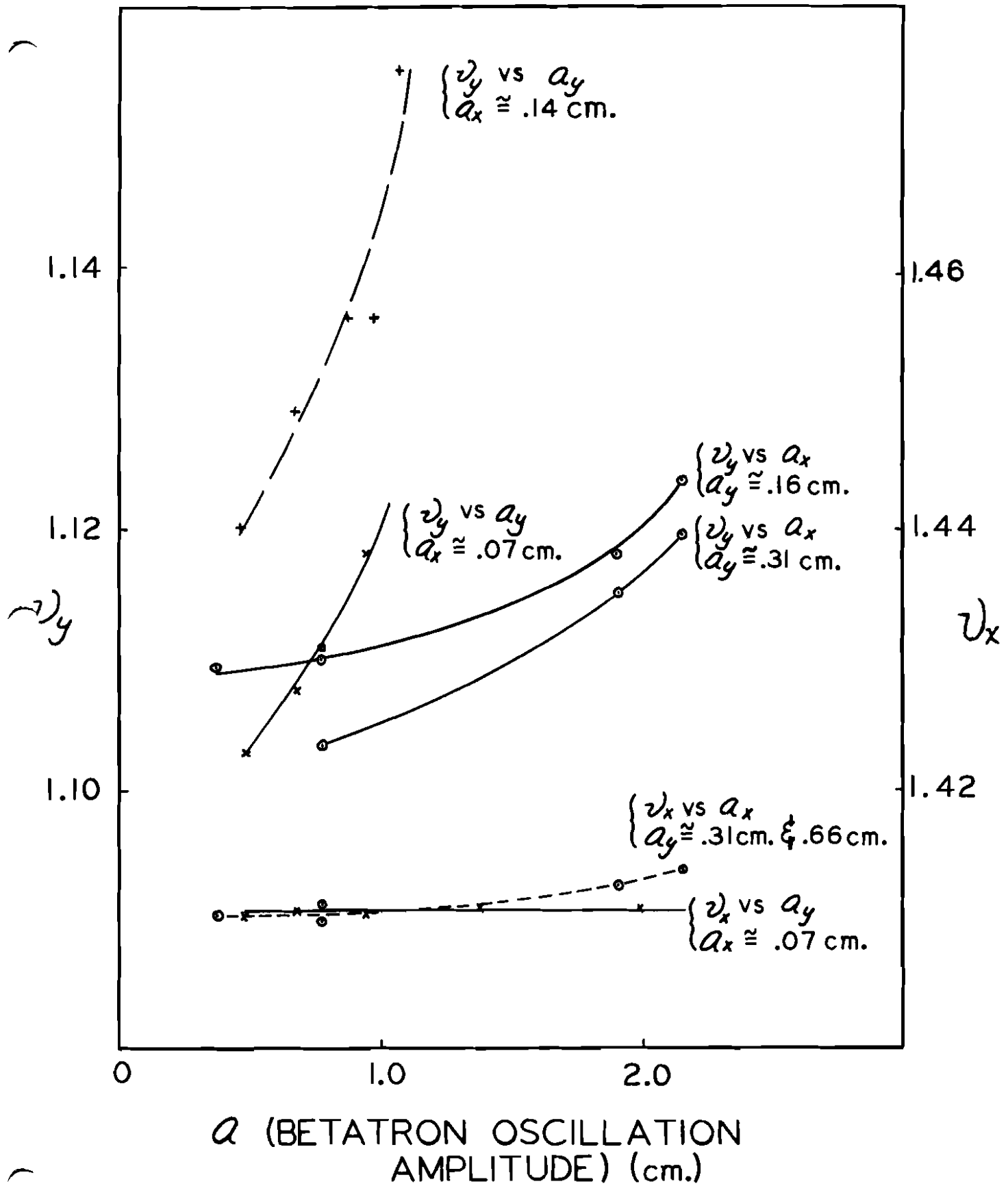
ν_y vs a_y
$a_x \cong .14$ cm.
ν_y vs a_x
$a_y \cong .16$ cm.
ν_y vs a_y
$a_x \cong .07$ cm.
ν_y vs a_x
$a_y \cong .31$ cm.
ν_x vs a_x
$a_y \cong .31$ cm. & .66 cm.
ν_x vs a_y
$a_x \cong .07$ cm.
1.14
1.12
1.10
1.46
1.44
1.42
ν_y
ν_x
0
1.0
2.0
a (BETATRON OSCILLATION AMPLITUDE) (cm.)

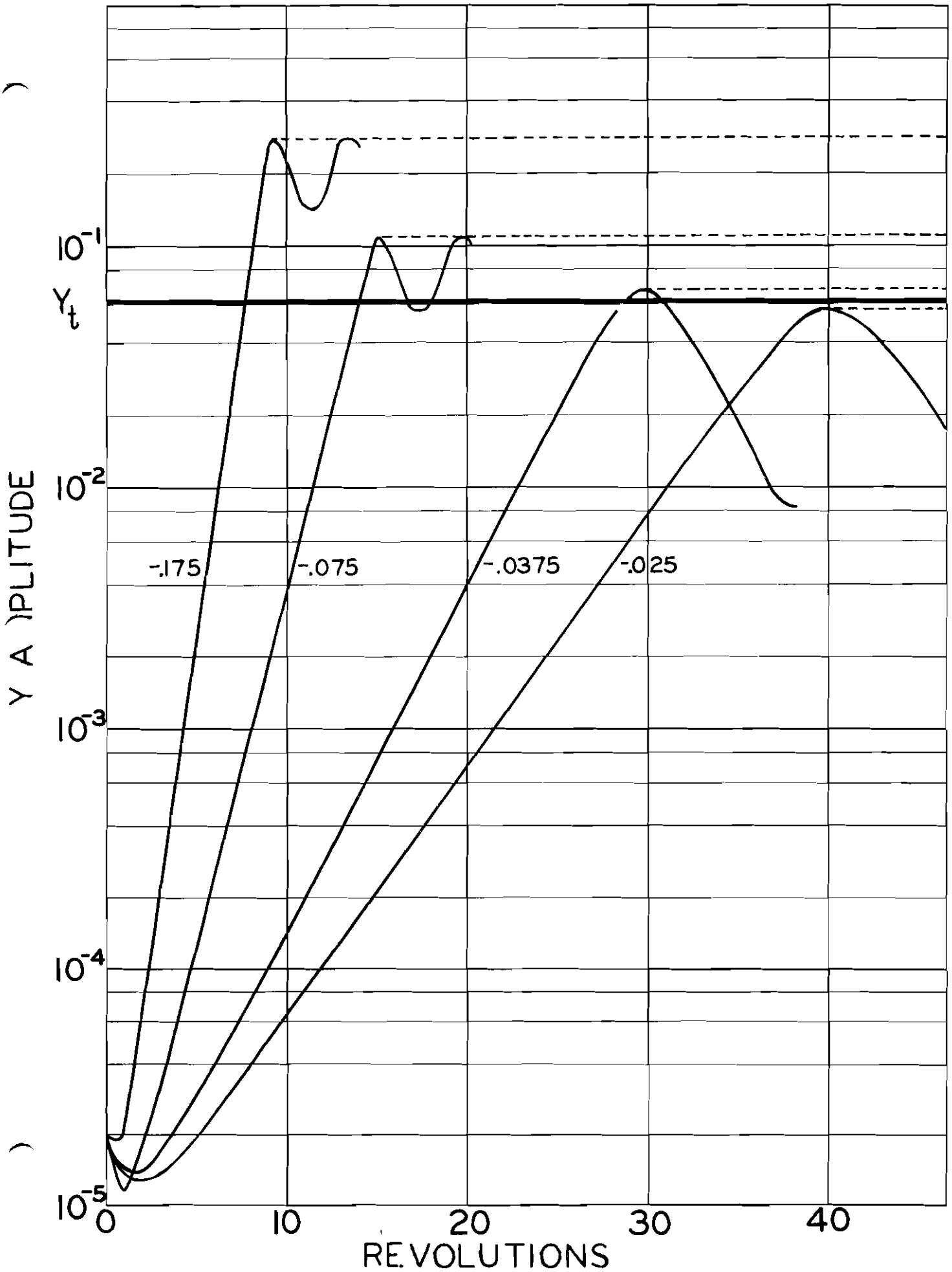
10^{-1}
Y_t
10^{-2}
10^{-3}
10^{-4}
10^{-5}
Y A)PLITUDE
-.175
-.075
-.0375
-.025
0
10
20
30
40
REVOLUTIONS

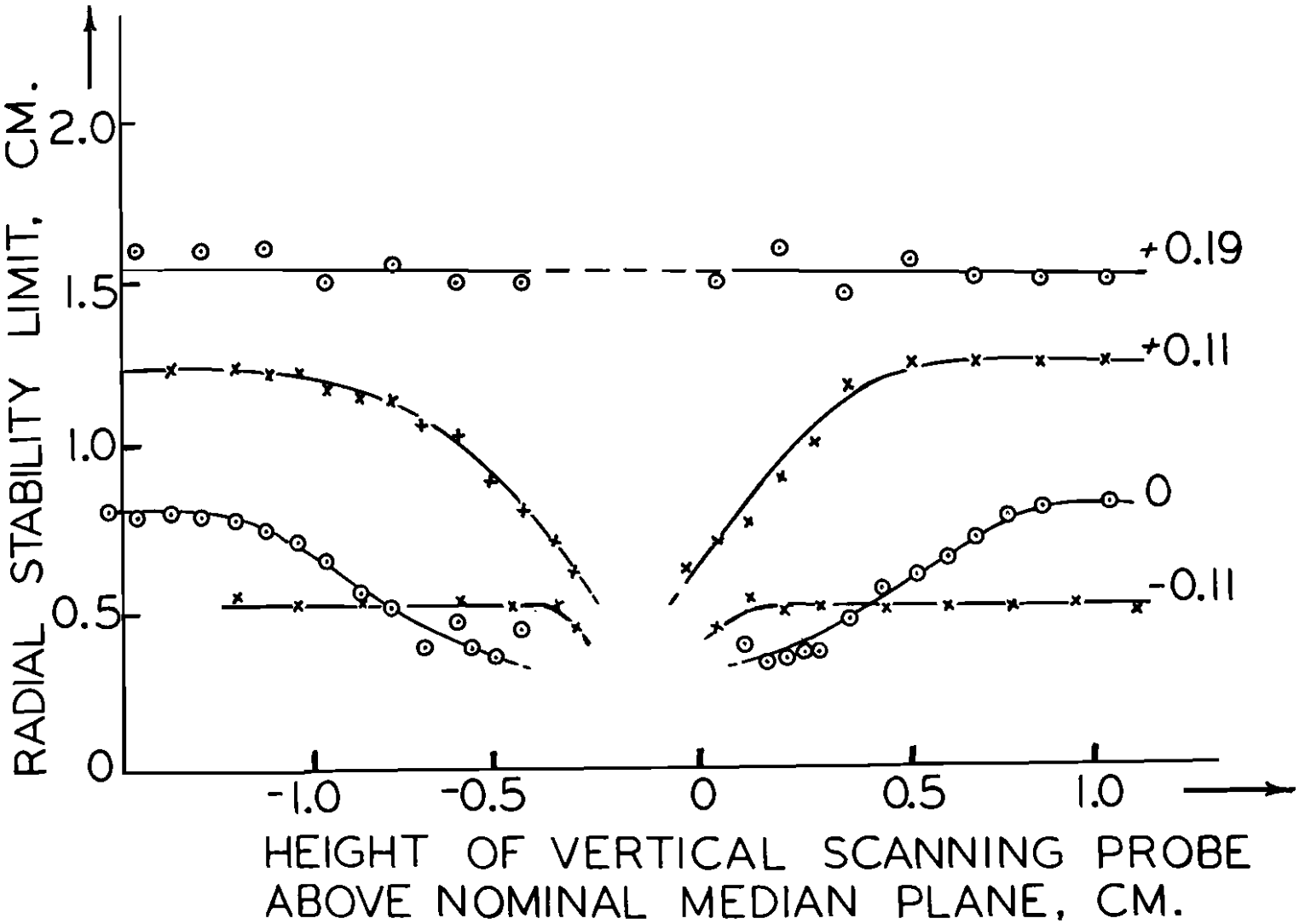
RADIAL STABILITY LIMIT, CM.
2.0
1.5
1.0
0.5
0
+0.19
+0.11
0
-0.11
-1.0
-0.5
0
0.5
1.0
HEIGHT OF VERTICAL SCANNING PROBE
ABOVE NOMINAL MEDIAN PLANE, CM.

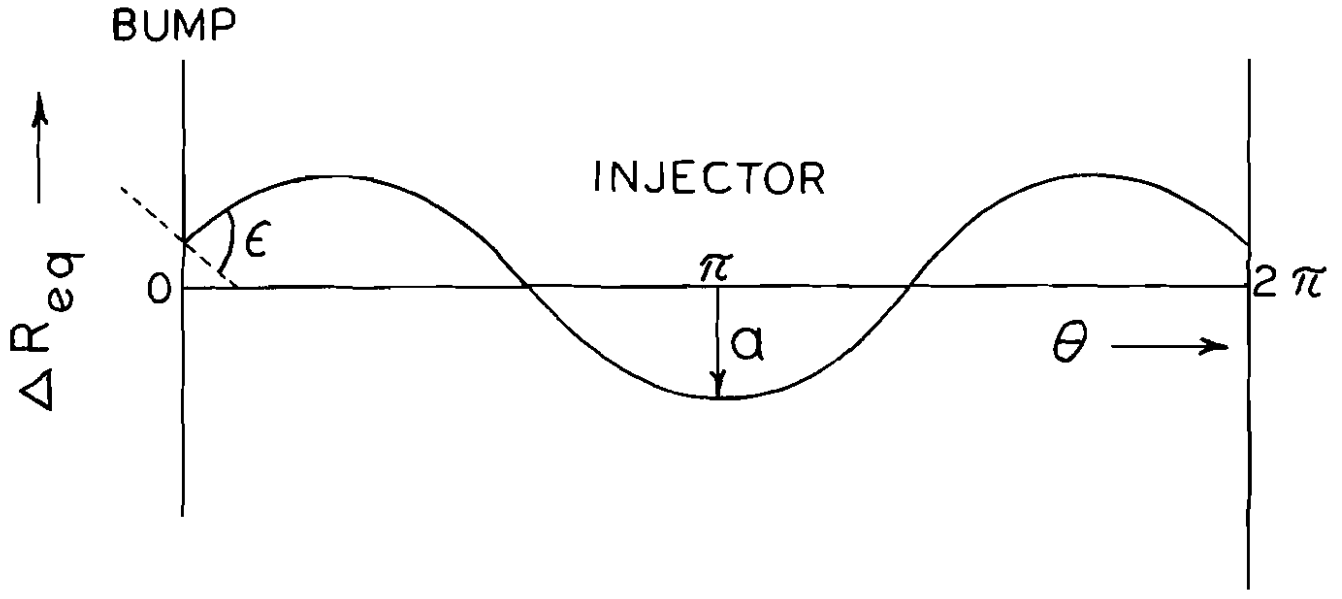
BUMP
INJECTOR
ΔR_{eq}
ϵ
0
π
2π
a
θ

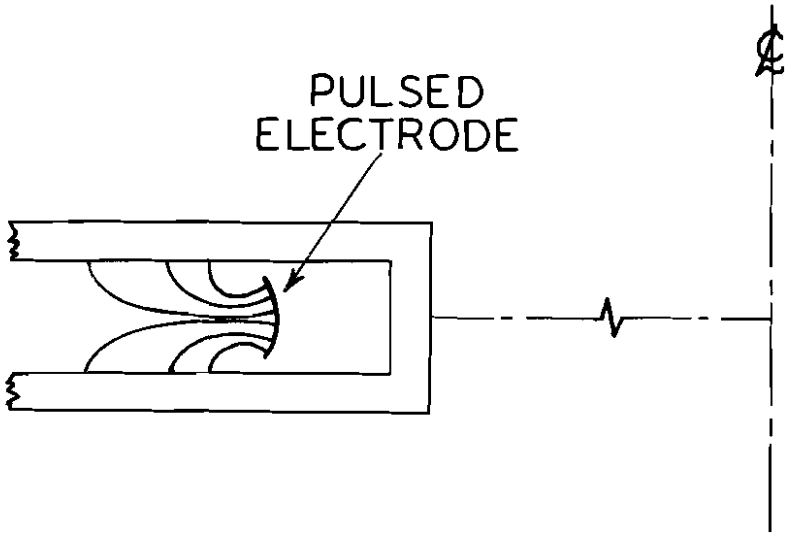
PULSED
ELECTRODE
℄

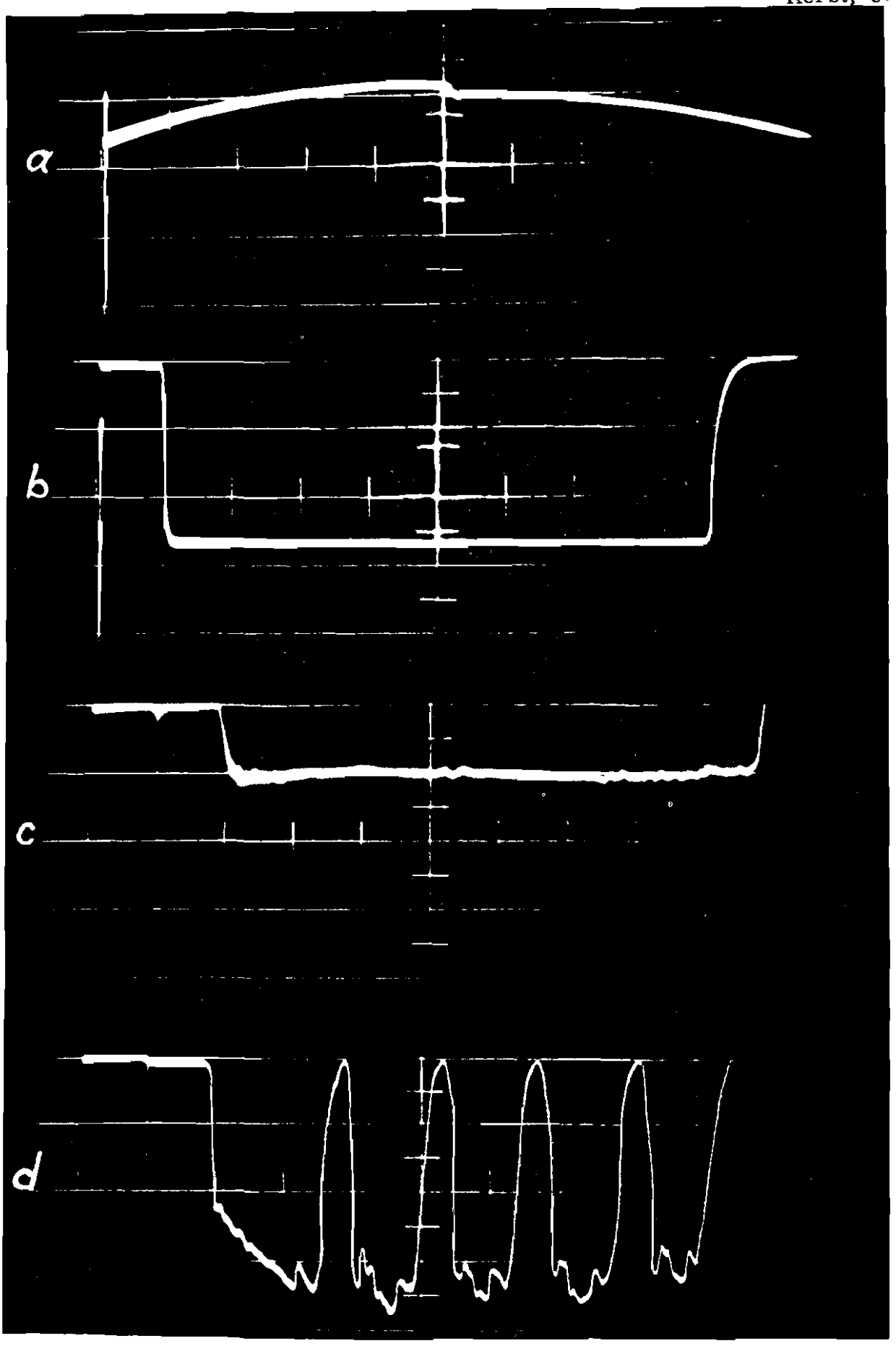
a
b
c
d

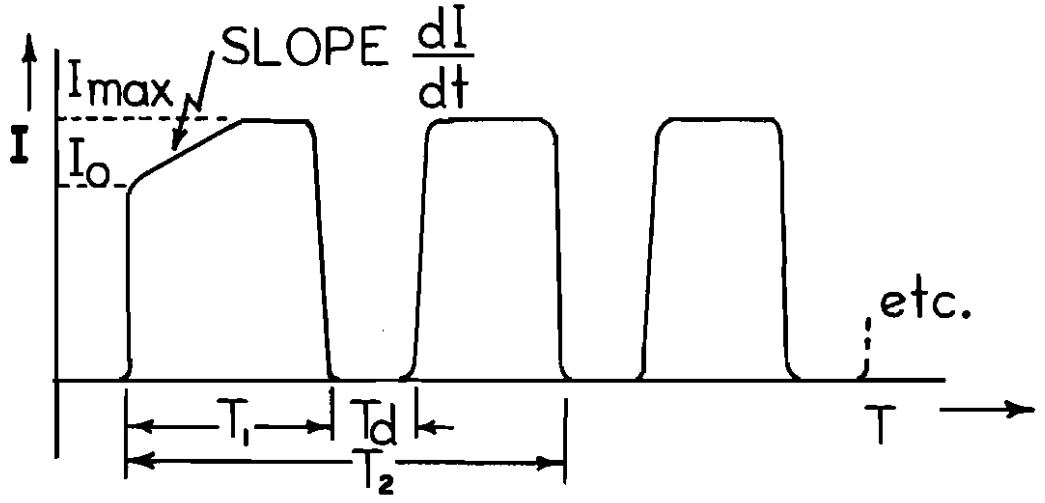
SLOPE $\frac{dI}{dt}$
Imax
I
Io
etc.
T1
Td
T2
T

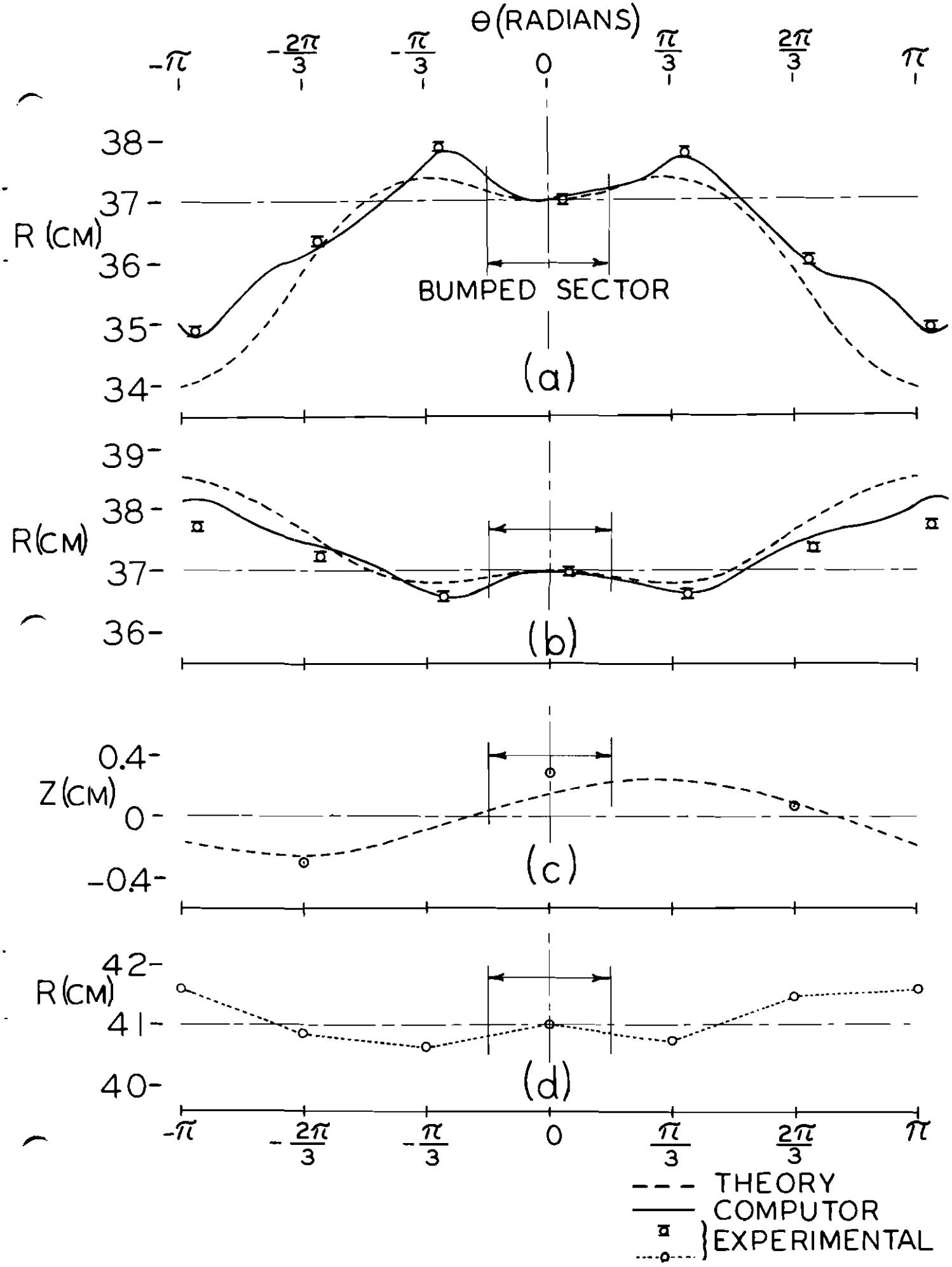
θ (RADIANS)
-π
-2π/3
-π/3
0
π/3
2π/3
π
R (CM)
38
37
36
35
34
BUMPED SECTOR
(a)
39
38
37
36
R(CM)
(b)
0.4
0
-0.4
Z(CM)
(c)
42
41
40
R(CM)
(d)
THEORY
COMPUTOR
EXPERIMENTAL

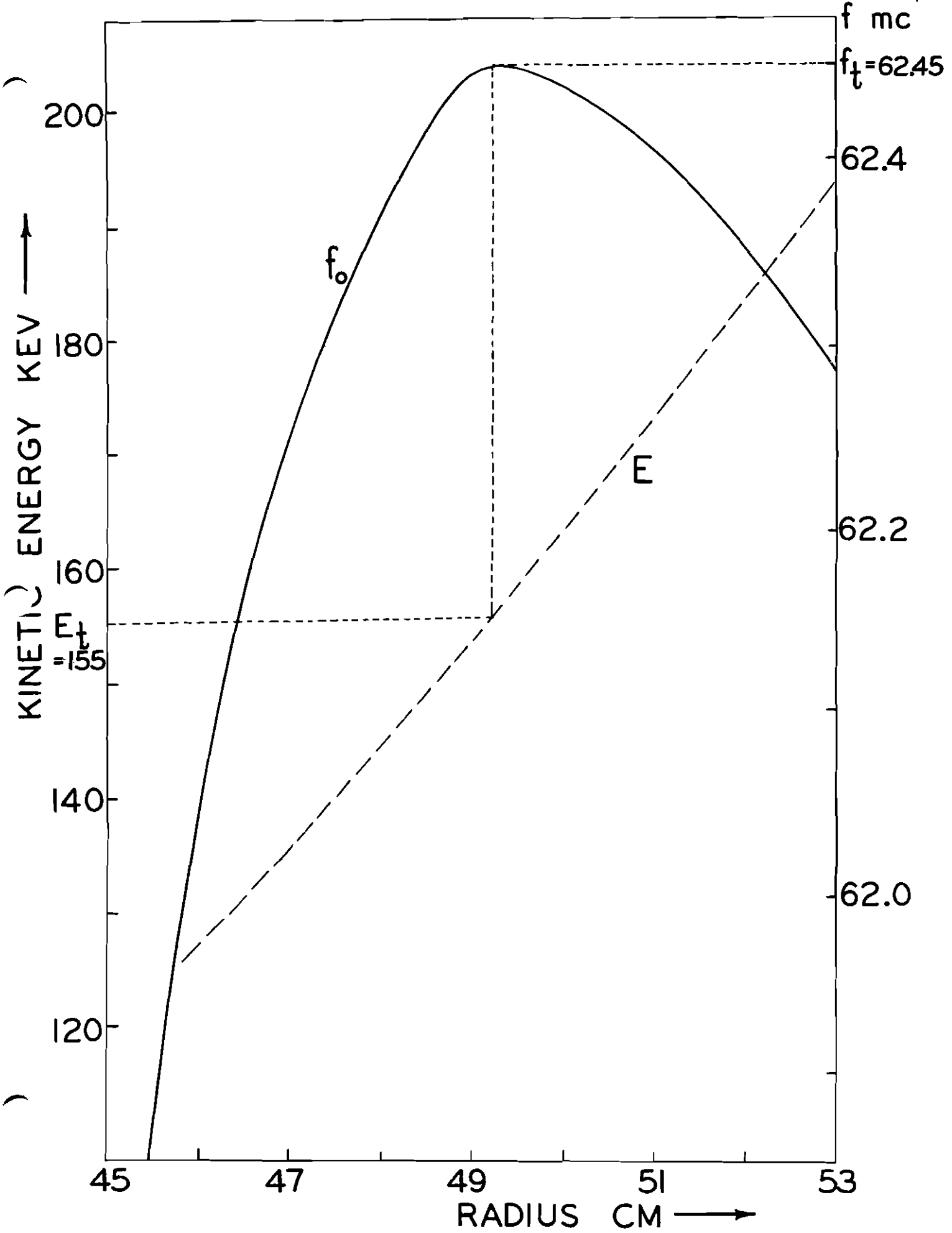
f mc
f_t=62.45
62.4
62.2
62.0
200
180
160
140
120
KINETIC ENERGY KEV
E_t
=155
f_o
E
45
47
49
51
53
RADIUS CM

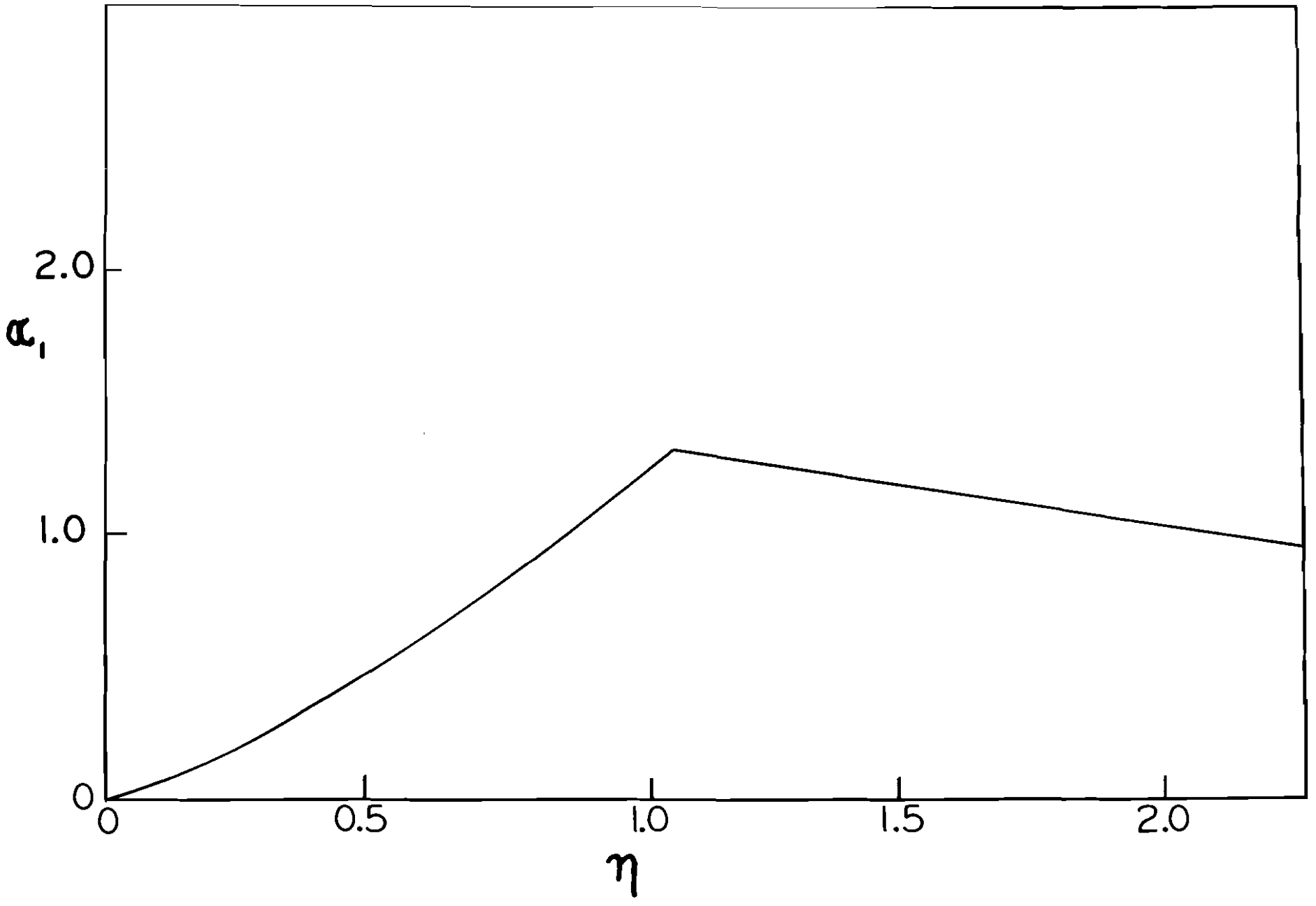
2.0
1.0
0
α_1
0
0.5
1.0
1.5
2.0
η

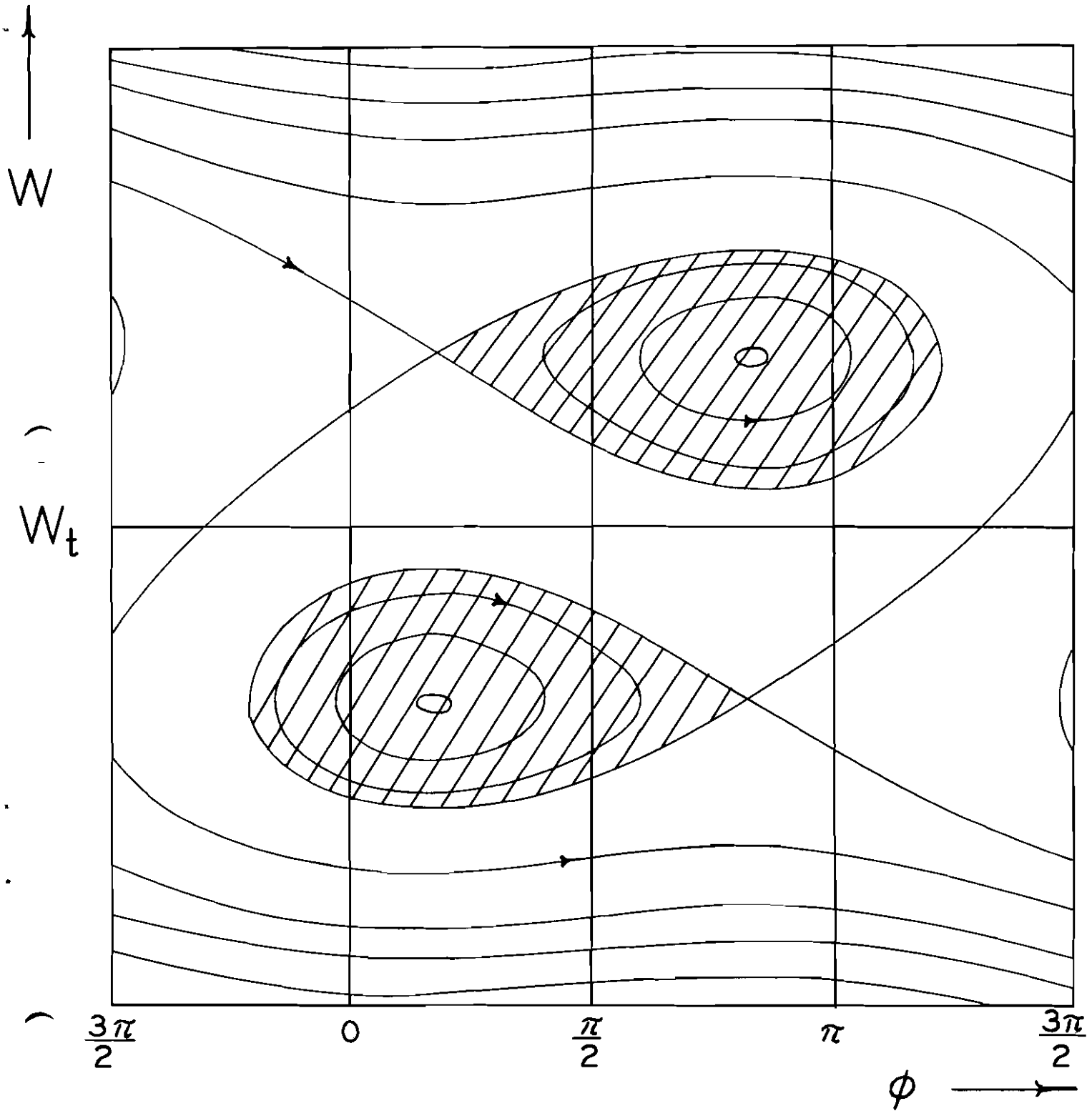
W
W_t
$\frac{3\pi}{2}$
0
$\frac{\pi}{2}$
π
$\frac{3\pi}{2}$
ϕ

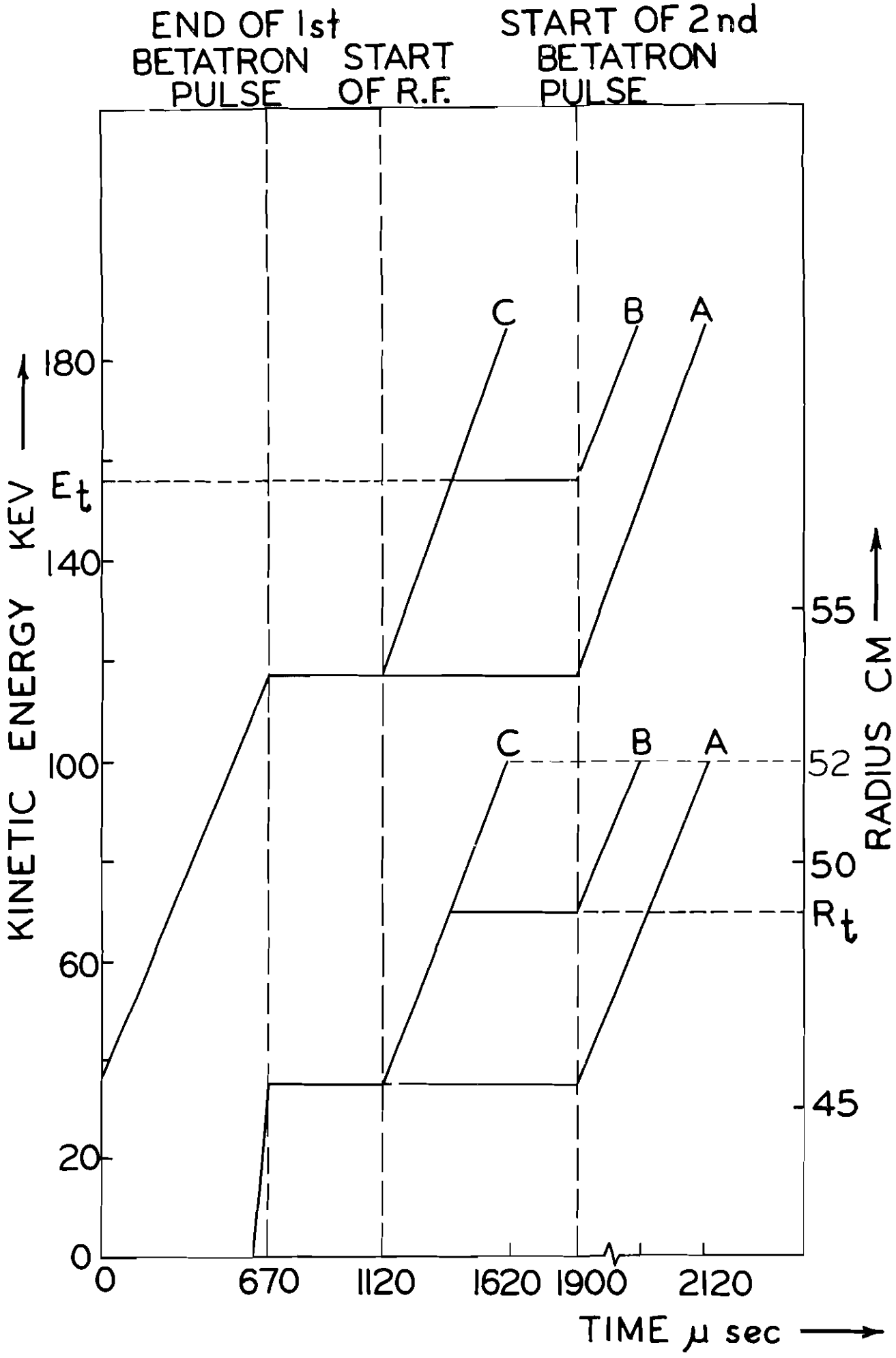
END OF 1st BETATRON PULSE
START OF R.F.
START OF 2nd BETATRON PULSE
C
B
A
C
B
A
180
E_t
140
100
60
20
0
KINETIC ENERGY KEV
55
52
50
R_t
45
RADIUS CM
0
670
1120
1620
1900
2120
TIME μ sec

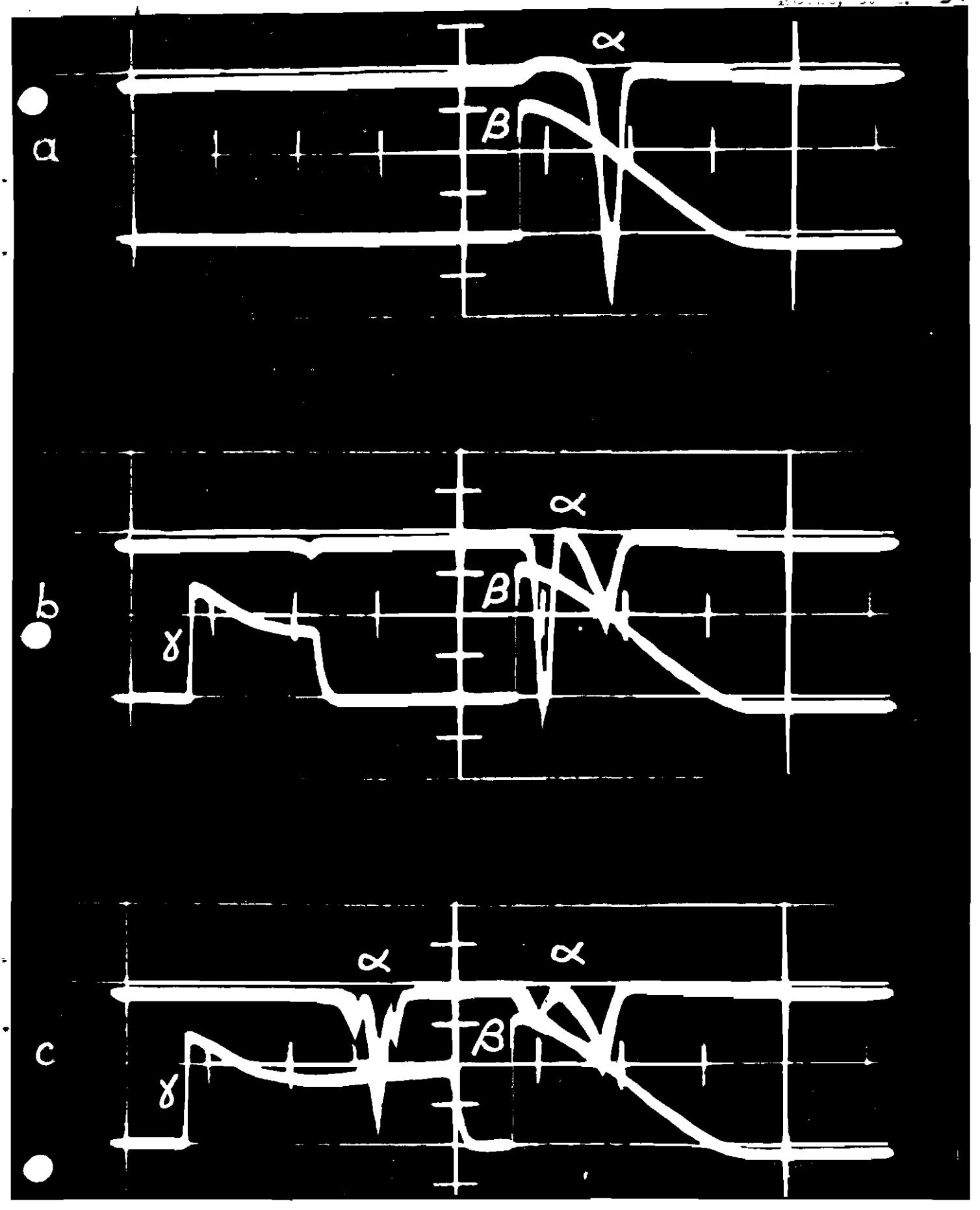
a
α
β
b
α
β
γ
c
α
α
β
γ

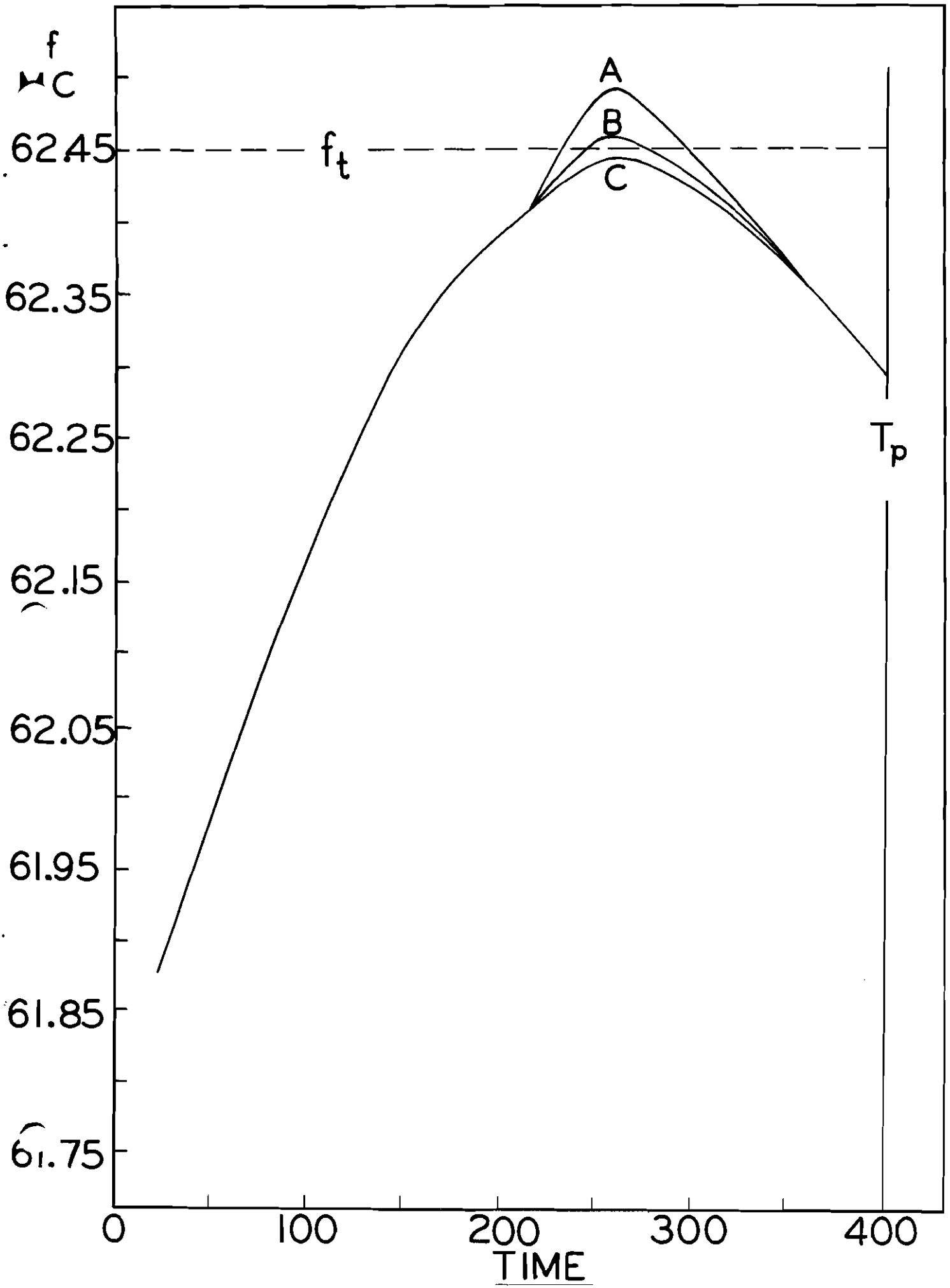
f
μC
62.45
62.35
62.25
62.15
62.05
61.95
61.85
61.75
f_t
A
B
C
T_p
0
100
200
300
400
TIME

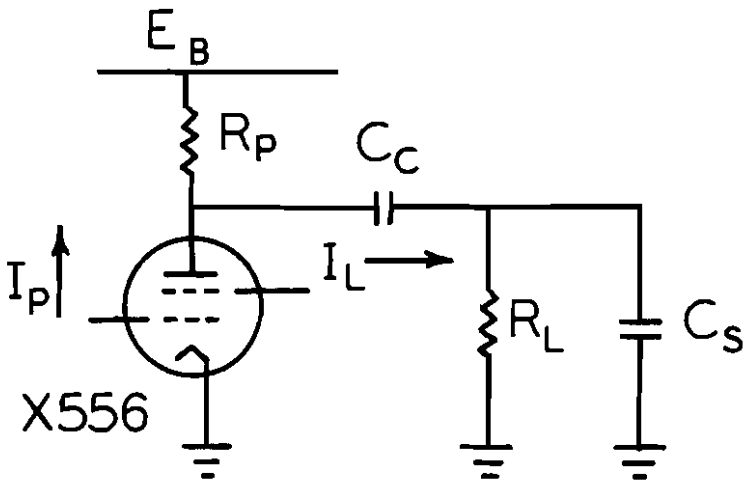
E B
Rp
Cc
Ip
IL
RL
Cs
X556

Kerst et al 34

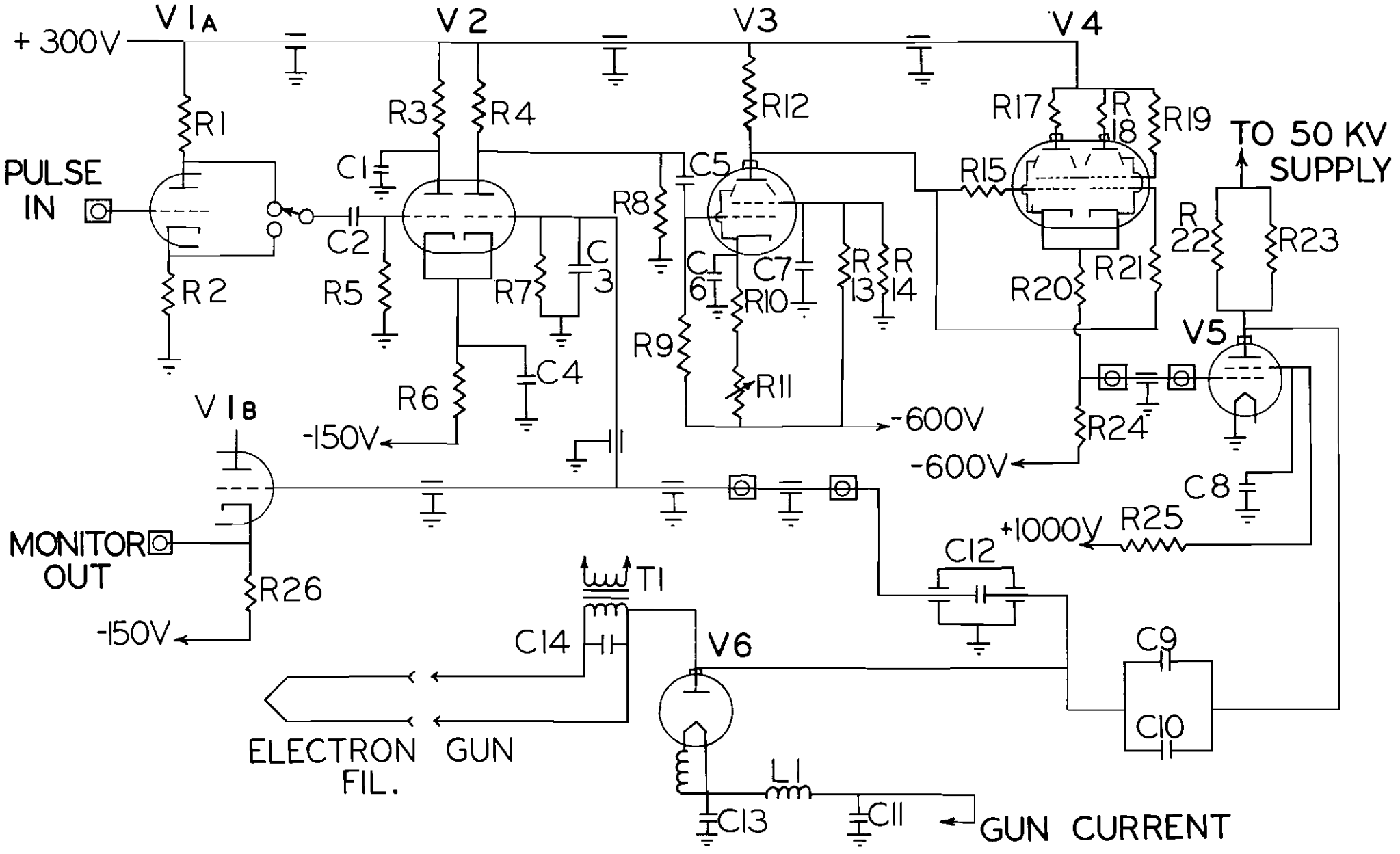

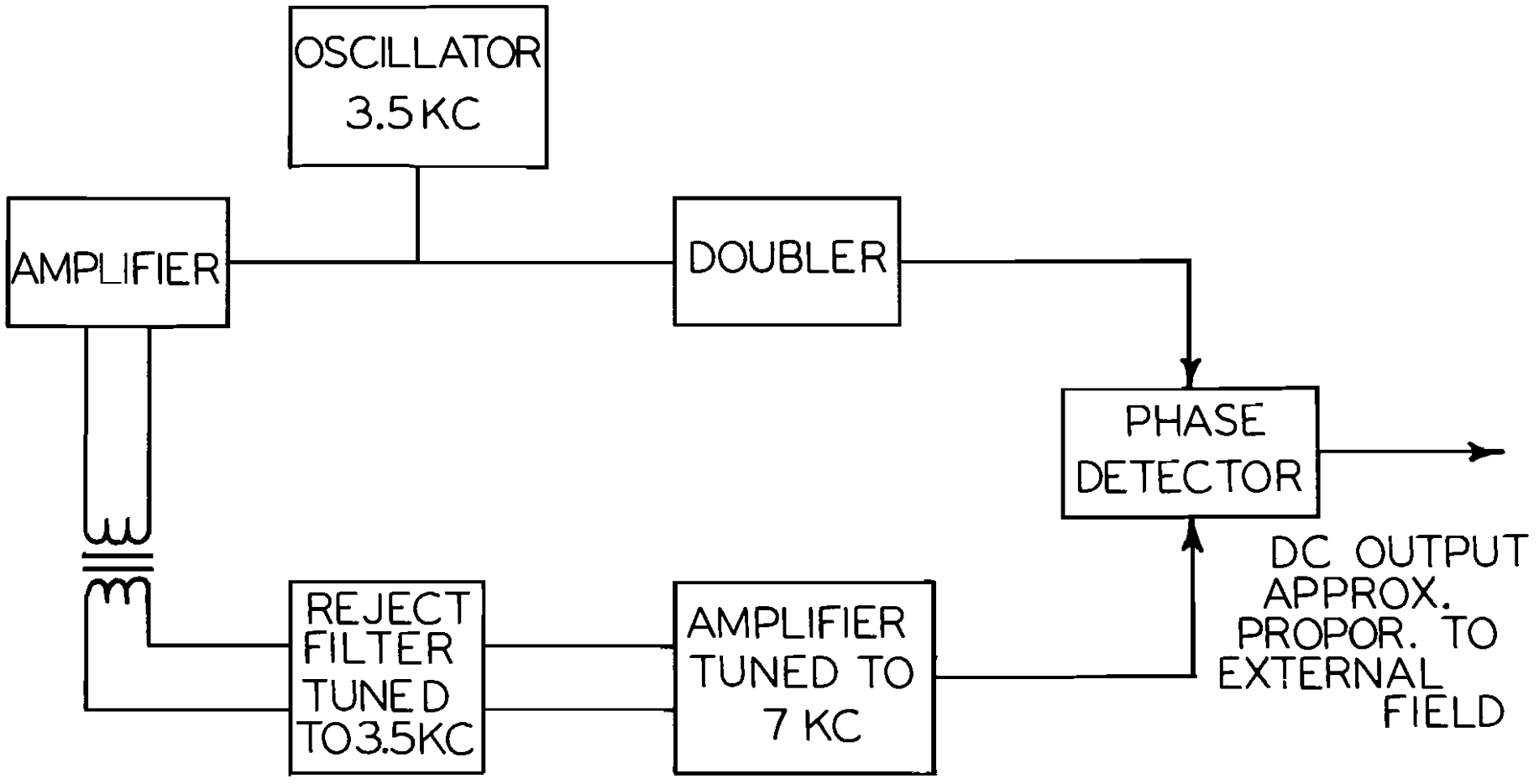
OSCILLATOR
3.5 KC
AMPLIFIER
DOUBLER
PHASE
DETECTOR
REJECT
FILTER
TUNED
TO 3.5KC
AMPLIFIER
TUNED TO
7 KC
DC OUTPUT
APPROX.
PROPOR. TO
EXTERNAL
FIELD

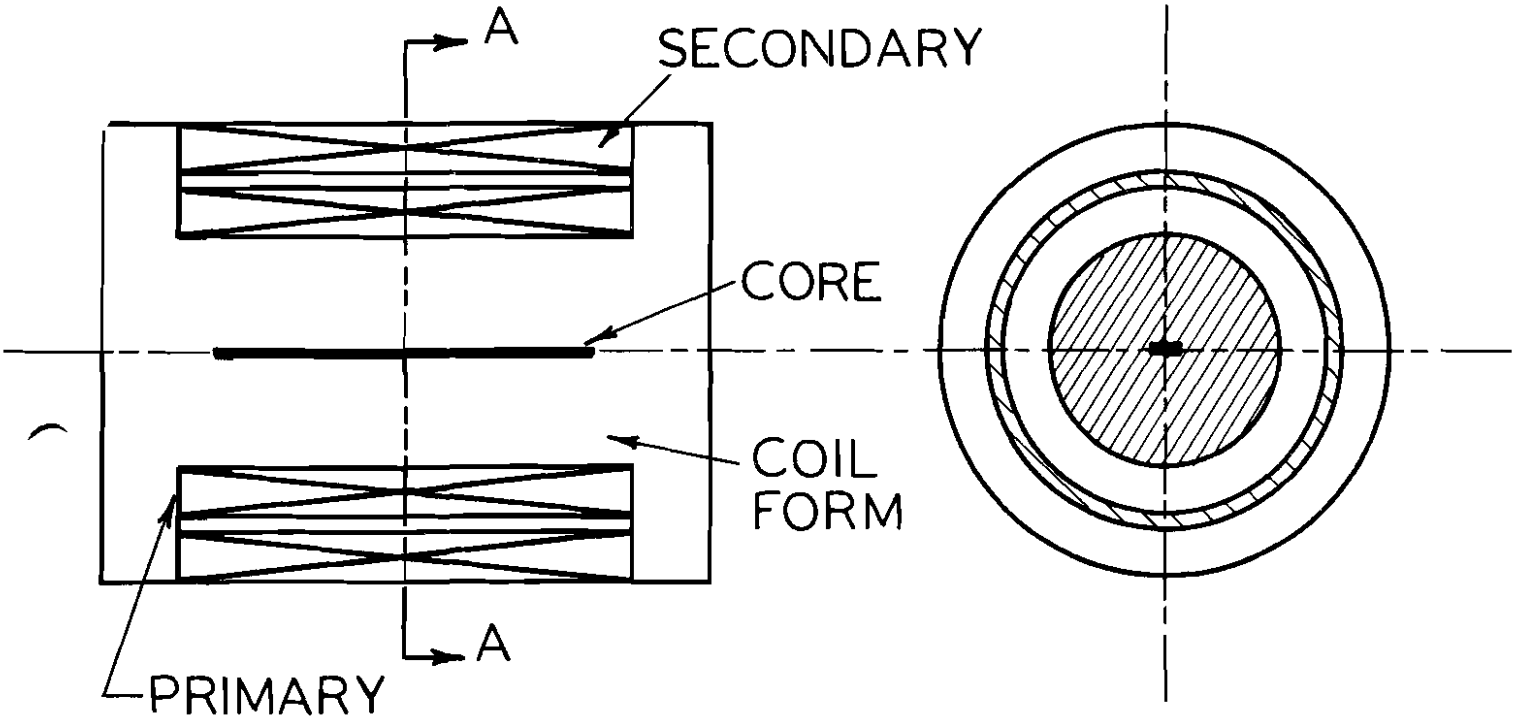
A
SECONDARY
CORE
COIL
FORM
A
PRIMARY

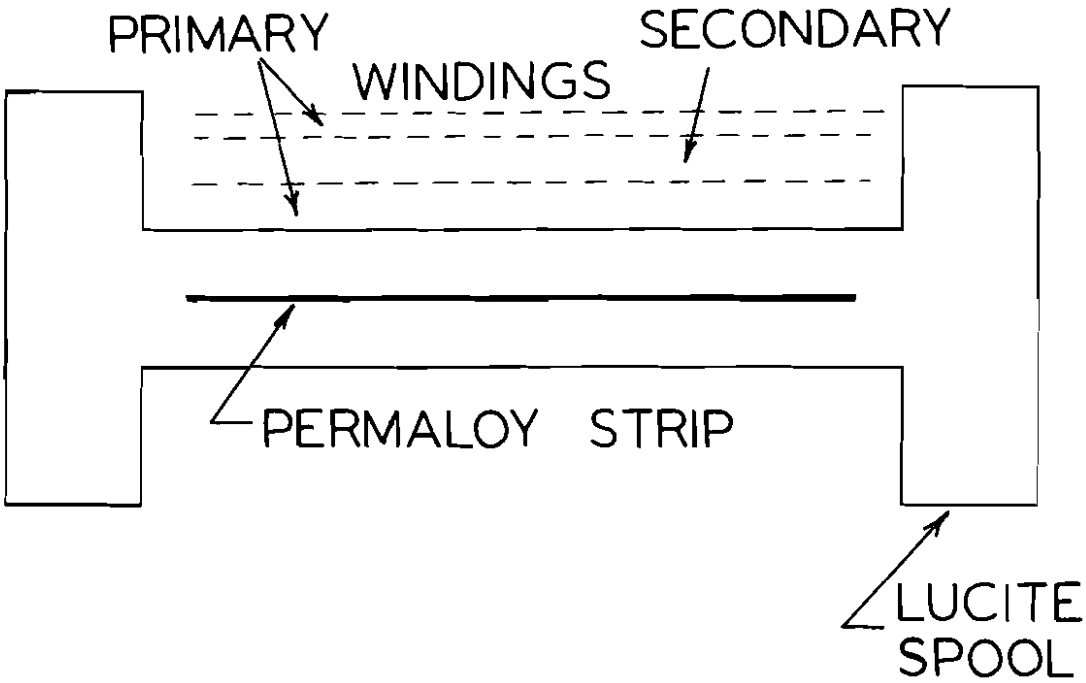
PRIMARY
SECONDARY
WINDINGS
PERMALOY STRIP
LUCITE
SPOOL

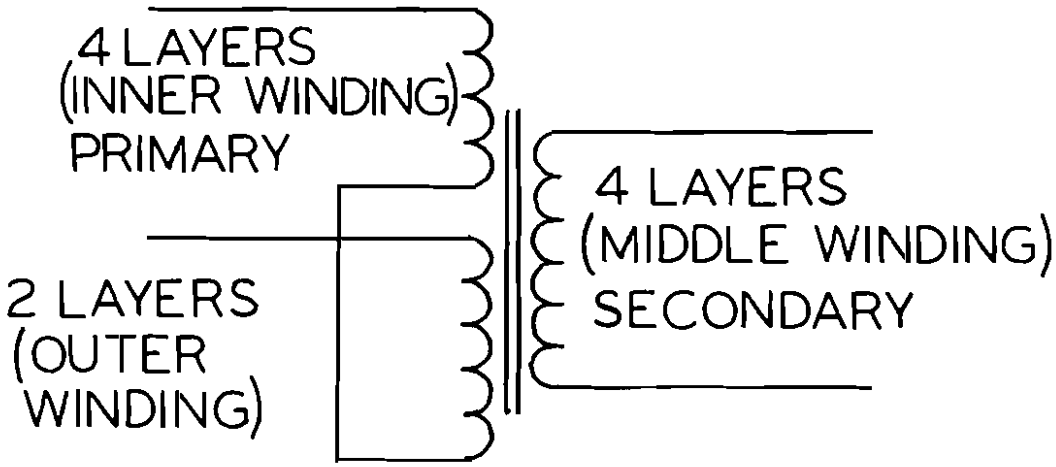
4 LAYERS
(INNER WINDING)
PRIMARY
2 LAYERS
(OUTER
WINDING)
4 LAYERS
(MIDDLE WINDING)
SECONDARY

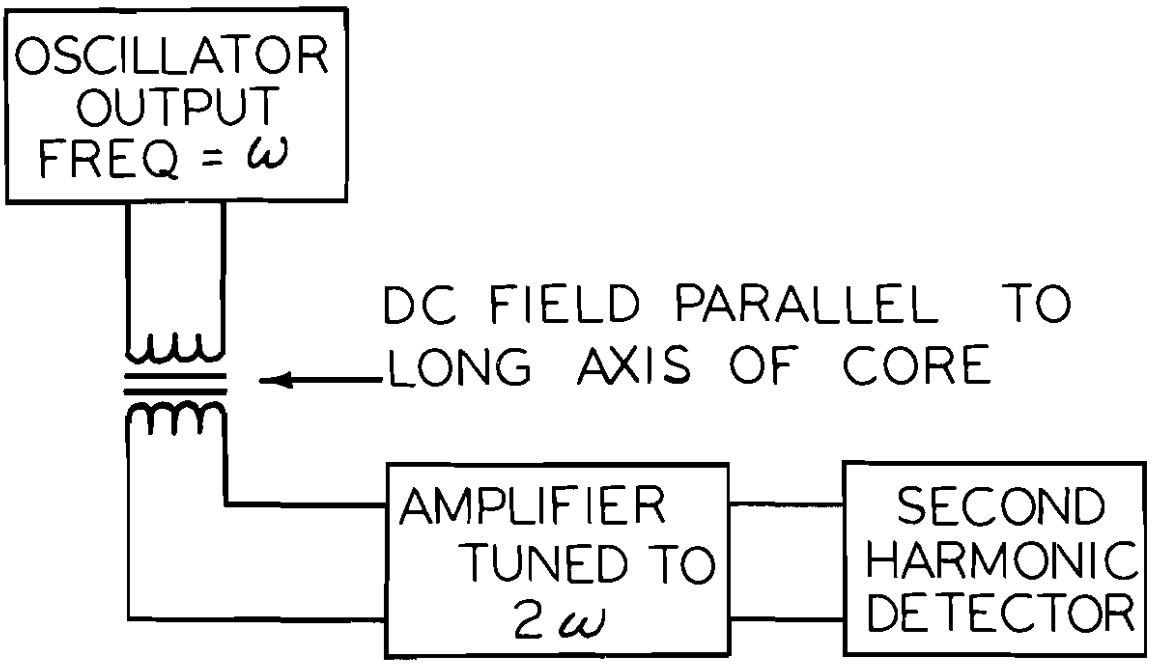
OSCILLATOR
OUTPUT
FREQ = ω
DC FIELD PARALLEL TO
LONG AXIS OF CORE
AMPLIFIER
TUNED TO
2ω
SECOND
HARMONIC
DETECTOR